Kinetics of phase segregation in a quenched alloy

Thesis

KINETICS OF PHASE SEGREGATION IN A QUENCHED ALLOY

by Anton Buhagiar B.Sc.,M.Sc.

The Open University

Milton Keynes

A Thesis in Statistical Mechanics

submitted for the Ph.D. degree at the Open University

May 1980

Date of submission : 30.5.80
Date of award : 25.3.81

Abstract.

We model the time evolution of a lattice gas or binary alloy quenched from infinite temperature ($T = \infty$) to $T < T_c$, the critical temperature. The alloy is represented on a simple cubic lattice of N sites by the Ising Model with Kawasaki dynamics assuming a nearest neighbour attraction. The basic kinetic process is the interchange of two unlike particles on adjacent sites, and is Markovian. The unit of time t is taken as one attempted interchange per lattice site.

The differential equation used is that of Becker-Döring which assumes the droplets of the new phase to grow or shrink by absorbing one particle at a time. For each size of droplet the equation contains two kinetic coefficients a_ℓ and b_ℓ which are related to the probability that an ℓ-droplet absorbs or emits one particle. The two coefficients are related by a detailed balance condition.

We first find the coefficient a_ℓ in the limit of zero density $a_\ell(0)$, assuming steady state diffusion as in the Lifshitz Slyozov theory. We express $a_\ell(0)$ as the solution of a lattice diffusion problem describing the motion of the other particles near a given ℓ-cluster with suitable boundary conditions at infinity and at the surface of the cluster.

The differential equation is solved numerically for densities $\rho = 0.05, 0.075, 0.10$. The solution compares well with histograms from real alloys (Ni - Al) and computer simulation of alloys, at the same value of ℓ^*, which characterizes the supersaturation.

To determine $\ell^*(t)$, we need to know the variation of a_ℓ with ℓ^*. We find a_ℓ is negative for small ℓ^* (or high supersaturation) indicating the presence of spinodal decomposition

initially. For $\ell^* > 26$, however, a_ℓ is approximately constant (2.0) for $0 < t < 7000$. Also ℓ^* is linear over most of this range and is well predicted by the differential equation over $0 < t < 5000$. For larger densities and for $7000 > t > 5000$, however, the differential equation underestimates ℓ^* because of coalescence.

Contents

Chapter IV: Calculation of $a_1(0)$ and $a_2(0)$ in terms of the parameter $\gamma \equiv \frac{P_{-1}}{P_0} - 1$ in the limit of zero density.

IV.1 The Green's function $G(\underline{r})$

IV.2 Calculation of $a_1(0)$ in terms of $\gamma = \frac{P_{-1}}{P_0} - 1$ using $G(\underline{r})$

IV.3 Calculation of $a_2(0)$ in terms of γ using $G(\underline{r})$.

Chapter V: Comparison of the Differential equations with the simulation of a quenched alloy at the same value of ℓ^*.

V.1 Numerical computation of differential equations

V.2 Empirical estimates for $\mu(\ell^*)$

V.3 Comparison of the Concentractions c_ℓ of the large clusters in the simulation and the differential equations at the same value of ℓ^*.

Chapter VI: Calculation of $\mu(\ell^*)$: comparison of ℓ^*_{sim} and ℓ^*_{de} at the same value of simulation time t.

VI.1 Statistical mechanics of a lattice gas on the Bethe lattice.

VI.2 Equilibrium distribution of small clusters on the Bethe lattice.

VI.3 The diffusion constant on the Bethe lattice as a function of ζ.

VI.4 Comparison of ℓ^*_{de} and ℓ^*_{sim} at the same value of simulation time t.

Chapter VII: Comparison of the Becker-Döring equations with the Lifshitz-Slyozov Theory and with real alloys.

VII.1 Reduction of the Becker-Döring equations to (I,12).

VII.2 Comparison of A,K, A/K for simulation and differential equations

VII.3 Comparison of the cluster size distribution predicted by our equations with that of real alloys.

Preface

This thesis is an account of an attempt to improve the theory of coarsening in quenched alloys due to Lifshitz and Slyozov.

We model the time evolution of a lattice gas or binary alloy quenched from infinite temperature ($T = \infty$) to $T < T_c$ where T_c is the critical temperature. The alloy is represented by the Ising Model with Kawasaki dynamics assuming a nearest neighbour attraction. The basic kinetic process is the interchange of two unlike particles on adjacent sites, and is Markovian. The time unit is one attempted interchange per lattice site. The model is described in Chapter I.

In Chapter II, we set up the system of differential equations of Becker-Döring which assumes the droplets of the new phase to grow or shrink by absorbing or emitting one particle at a time. For each size of droplet, the equation contains two kinetic coefficients a_ℓ and b_ℓ which are related to the probability that an ℓ-droplet absorbs or emits one particle. The coefficients are related by a detailed balance condition.

In Chapters III and IV, we calculate the coefficients $a_\ell(0)$, the value of a_ℓ in the limit of zero density. As in the Lifshitz-Slyozov theory, we assume the absorption of monomers by a central cluster to be diffusion-controlled. We then express $a_\ell(0)$ as the solution of a lattice diffusion problem describing the motion of the other particles near a specified ℓ-cluster with suitable boundary conditions at infinity and at the surface of the cluster. We also derive various empirical formulae for $a_\ell(0)$ as a function

of ℓ, and of temperature T. We also obtain a closed formula for $a_1(0)$ and $a_2(0)$ in terms of the transition probabilities. We compare these results with what classical diffusion theory predicts for spherical clusters.

The differential equations are solved numerically in Chapter V for densities $\rho = 0.05, 0.075, 0.10$. Its solution compares well with histograms from a computer simulation of a binary alloy (Marro, 1975), at the same value of ℓ^*, the characteristic cluster size, which grows linearly with time approximately.

In Chapter VI, we complete the comparison by finding ℓ^* as a function of t. Thus we need to know the variation of a_ℓ with ℓ^*. For small ℓ^*, a_ℓ is negative implying the existence of spinodal decomposition for high supersaturation, but for $200 > \ell^* > 30$, a_ℓ is approximately constant and equal to twice $a_\ell(0)$. We find that ℓ^* is linear in t over most of the range $0 \leq t \leq 7000$, as is to be expected during coarsening. Our equations predict ℓ^* well in the range $0 \leq t \leq 5000$, but underestimate ℓ^* for the higher densities $\rho = 0.075$ and 0.10 for $t > 5000$, because of the coalescence of large particles.

In Chapter VII we compare our solution with histograms of the cluster size distribution in real alloys (e.g. Ni - Al, Cd - Ag). Our theory seems to be an improvement on the Lifshitz - Slyozov theory in predicting the cluster size distribution in real alloys.

Original work is contained in Chapters III, IV, V, VII, Section VI.4, and parts of Section I.3 and I.4. The first three sections of Chapter VI are almost entirely due to my supervisor Professor O. Penrose. Chapters I and II are of an introductory nature. The simulation was done by Marro (1975).

The most important reference on which this work is based is the paper by Penrose et al (1978), and we follow the formulation in that paper throughout. Other important references are the review article by Penrose O. and Lebowitz J. (1978) which serves as a good introduction to the work contained in this thesis; the paper by Kalos et al where the steady state distribution formula (I.6) is given; and also the paper by Ardell and Nicholson (1966) which compares the distribution of Ni Aℓ alloys with the Lifshitz Slyozov theory. The paper by Lifshitz and Slyozov (1961) is also important.

I would like to thank my supervisor Professor Oliver Penrose, without whose guidance this work could not have been possible.

This thesis is not substantially the same as one which has already been submitted to any other university. This thesis can be made available or photocopied at the discretion of the Librarian at the Open University.

List of Figures

Chapter I

Fig (I,i): Illustration of a quench from Temperature $T_1 > T_c$ to $T < T_c$ on the spinodal curve of an alloy AB.

Fig (I,ii): A graph of W_s against $\frac{V}{KT}$ for $0.7 \leq \frac{V}{KT} \leq 2.0$

Fig (I,iii): A graph of C against $\frac{V}{KT}$ for $0.7 \leq \frac{V}{KT} \leq 2.0$. The constant W_s and C occur in the formula $\frac{Q_\ell}{Q_{\ell+1}} = W_s(1 + \frac{C}{(\ell-2)^{1/3}})$

Chapter III

Fig (III,i): Graphs of $a_\ell(0)^3$ against ℓ for the range $-0.8 \leq \gamma \equiv \frac{p_{-1}}{p_0} - 1 \leq 0.8$. The points lie on a straight line with a small intercept, for each value of γ, as predicted by (III,24).

Fig (III,ii): Graphs of $\frac{p_0}{a_\ell(0)}$ against $\frac{p_o}{p_{-1}}$ for $1 \leq \ell \leq 6$ over the range $0.2 \leq \frac{p_{-1}}{p_0} < 2$. The graphs for each integer ℓ are all straight lines meeting on the line $\frac{p_0}{p_{-1}} = -1$.

Chapter IV

Fig (IV,i): Illustration showing a monomer at the origin with its nearest neighbours and second nearest neightbours. The two symmetries of the second nearest neighbours with respect to the central cluster are also shown.

Fig (IV,ii) Illustration showing a dimer at (0,0,0) and (1,0,0) and its ten nearest neighbours. We also show the four symmetries of the second nearest neighbours with respect to the central dimer.

Chapter V

Fig (V,i) Graph of t_{de}, the time in the differential equations with coefficient $a_{\ell}(0)$, against simulation time t, when the value of ℓ^* is the same in the simulation and the differential equations. The slope of this graph gives an empirical estimate for $\mu(\ell^*)$. It is seen that $\mu(\ell^*)$ is practically constant for $t > 1000$. Densities $\rho = 0.05, 0.075, 0.10$

Fig (V,ii): Comparison of c_{ℓ} for $\ell > 20$ for the simulation and the differential equations for $0 < t < 7000$. Densities $\rho = 0.05, 0.075, 0.10$.

Chapter VI

Fig (VI,i): Graph of $\mu(\ell^*)$ against ℓ^* . The quantity $\mu(\ell^*)$ is effectively constant and approximately equal to 2 in the range $50 \leq \ell^* \leq 200$.

Fig (VI,ii): Graph of $\frac{1}{6D_c}$ against t_{de} . The area under this graph up to t_{de} gives the simulation time t according to the theory in this chapter.

Fig (VI,iii), (VI,iv), (VI,v): Graph of ℓ^* and ℓ^*_{de} against simul ation time t for densities $\rho = 0.05, 0.075, 0.10$ respectively.

Fig (VI,vi): Graph of t_{de} against t as predicted by the theory in this chapter for densities $\rho = 0.05, 0.075, 0.10$. The lines are approximately straight and their slopes are equal to $\mu(\ell^*)$. Compare this graph with that in Fig (V,i).

Chapter VII

Fig(VII,i): Graph of $g(\ell,\ell^*)$ against the argument $f = \ell n(\ell^*) + \phi(\frac{\ell}{\ell^*})$ for differential equations and simulation for various values of ℓ^*. The constant A/K is taken to be be 4.0. This is a 'universal' curve independent of the value of ℓ^*. Density $\rho = 0.075$.

Fig(VII,ii): Graph of the slope of the previous figure against f, for simulation and differential equations. For a given value of A/K, the concentration C_ℓ are proportional to the ordinates in this figure. Density $\rho = 0.075$.

Fig(VII,iii): Graph of $\ell^{*1/3}\ell^{2/3}c_\ell$ against $(\frac{\ell}{\ell^*})^{\frac{1}{3}}$ for our differential equations and for Ni Al alloys(Ardell and Nicholson, 1966). The predictions of Lifshitz and Slyozov are also given. The ordinates at $\ell = \ell^*$ are all scaled down to 1.

List of Tables

Chapter IV

Table (IV,i): Table of the Green's function $G(\underline{r})$ defined in (IV,2), the functions $H^i(\underline{r})$ for a_1 from (IV,5) and the functions $G^i(\underline{r})$ for a_2 from (IV,22) for relevant values of $\underline{r}$.

Table (IV,ii): The kinetic coefficient $a_1(0)$ and $a_2(0)$ in the limit of zero density calculated by the Green's function method, compared with S.O.R. calculations from Chapter III. The closed formulae are given in equations (IV,17) and (IV,29).

Chapter V

Table (V,i): Position of local maxima and minima in $c_\ell - \ell$ curves, and concentration at these two points for both differential equations and simulation. Densities $\rho = 0.075$ and 0.10.

Chapter VI

Table (VI,i): Equilibrium parameters for the Bethe lattice for coordination number $q = 6$. These are compared with corresponding values obtained from a simulation of a lattice gas on the simple cubic lattice (Kalos et al, 1978). Temperature $\frac{V}{KT} = 1.5, 1.0926, 0.99438$.

Table (VI,ii): Steady state parameters on the Bethe lattice calculated in terms of ξ at $\frac{V}{KT} = 1.5$. In particular we give c_1, ℓ^* and $\mu(\ell^*) = 6D_c$.

Table (VI,iii): Values of ℓ^*_{de} and ℓ^*_{sim} corresponding to the same simulation time t. Densities $\rho = 0.05, 0.075, 0.10$.

Chapter VII

Table (VII,i): Comparison of the prediction of formulae (VII,18) with simulation values of g obtained from Table VII of Penrose et al (1978).

Chapter I Introduction

I.1 Motivation of this work

A binary alloy, which we call AB, such as ZnAℓ or NiAℓ, is spatially homogeneous when it is in thermal equilibrium at a temperature $T_1 > T_c$ the critical temperature, that is it consists of one thermodynamic phase. If the system is suddenly quenched to a lower temperature $T < T_c$, it remains spatially homogeneous. Thermal equilibrium, however, requires the coexistence of two phases, one A-rich and one B-rich phase, whenever the fraction of A-atoms ρ is in the range $\rho_A < \rho < \rho_B$, where ρ_A and ρ_B are the concentration of the A and B phases at time $t \to \infty$. This quench is shown in Fig(I,i), which gives the densities ρ_A and ρ_B for temperatures T below T_c. The nature of the time evolution of a quenched alloy is very important in metallurgy.

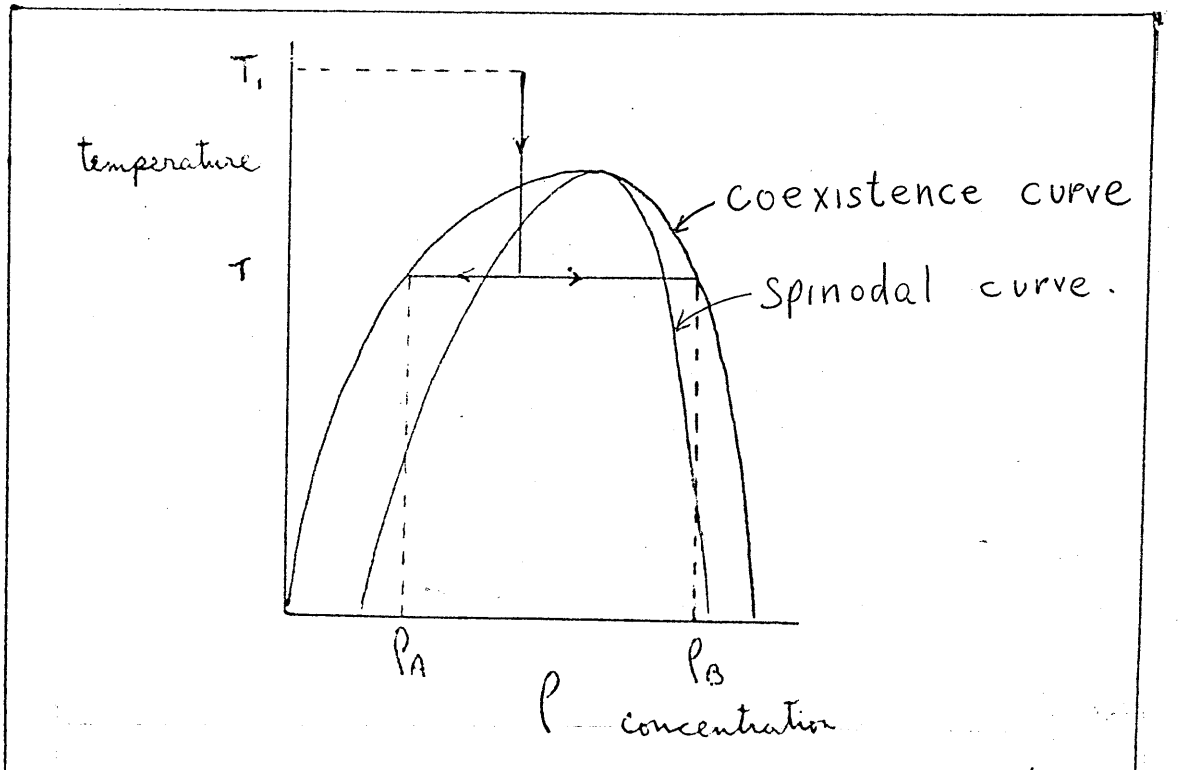

Fig (I,i): Illustration of a quench from Temperature $T_1 > T_c$ to $T < T_c$ on the phase diagram of an alloy AB.

The kinetics of this physical system can be studied by a set of kinetic equations put forward by Becker and Döring in 1935- these equations are well established as the basis for successful treatments of some topics in phase transition kinetics such as metastability and Ostwald ripening. The physical basis of these equations is that droplets of the new phase grow or shrink by absorbing or emitting particles one at a time. For each size of droplet, the equations contain two kinetic coefficients, one giving the probability per unit time that the droplet will emit a particle, the other giving the probability that it will absorb a particle. The normal methods for calculating these coefficients depend on treating the droplets as if they were spheres of the new phase. This assumption is, however, obviously invalid for 'droplets' consisting of only a few particles and is in any case difficult to relate quantitatively to the basic microscopic model. The difficulty of establishing such a relationship has already led to much controversy in the treatment of metastability. Refer for example to Lothe and Pound (1962).

It is the purpose of this work to describe, for a particular microscopic model, how the kinetic coefficients can be calculated directly from microscopic quantities. These kinetic coefficients, when used in the Becker-Döring theory, give a system of differential equations which can be integrated numerically to predict how the distribution of cluster signs varies with time. These predictions are then compared with the results of computer simulations of the same microscopic model carried out by Kalos et al (1978) and also with some experimental results.

The model to which our results apply is the Ising model with Kawasaki dynamics. This is a model of a binary alloy in which each lattice site is occupied by one atom and the state changes with time according to a Markov process where the allowed transitions are interchanges of the atoms on two neighbouring sites.

The model is mathematically equivalent to a lattice gas, with each site either empty or occupied by a particle, in which case the allowed transitions are jumps of any particle to any neighbouring empty site. In either case, a nearest-neighbour attractive law is assumed and the transition probabilities are chosen in accordance with a detailed balancing condition which includes a specification of the temperature.

The Becker-Döring theory assumes that the new phase consists of widely separated droplets or nuclei immersed in the old phase. This requires one of the components of the alloy (the one which predominates in the new phase) to have a relatively small concentration. At such concentrations it is convenient to use a lattice gas picture regarding the minority atoms as 'particles' and the majority atoms as 'empty sites'. We can then describe the configurations in terms of clusters, a cluster being defined as a maximal connected set of particles i.e. of minority atoms, and to identify the clusters with the 'droplets' in the Becker-Döring theory. It was pointed out by Lifshitz and Slyozov (1961), and

by Wagner (1961) that the rate of change of the average number of particles in a large spherical cluster can be found by treating the motion of the other particles nearby as a diffusion problem. We therefore apply a similar idea to the motion of the particles near a cluster of any size or shape: we express the Becker-Döring Kinetic coefficients in terms of the solution of a lattice diffusion problem describing the motion of the other particles near a specified cluster with suitable boundary conditions at infinity and at the surface of the cluster. The Kinetic coefficients are first found in the limit of zero density, i.e. when there are very few monomers round the central cluster; we then calculate these coefficients for non-zero densities.

Finally we compare the solution of the Becker-Döring system of equations using these coefficients, with experimental results on real alloys and with computer simulation of real alloys. We also see to what extent our results agree with the prediction of the theory of Lifshtiz and Slyozov (1961), which has been widely used in metallurgy to explain the kinetics of coarsening in quenched alloys.

I.2 The Kinetic Ising Model of a lattice gas

Most works on the time evolution of phase transitions in statistical mechanics has been done on dynamical models based on the Ising model (Ising, 1925). The reader is referred to the article "Towards a rigorous theory of metastability" (Penrose and Lebowitz, 1978) for a review of these models.

The Kinetic model relevant to the lattice gas (or binary alloy) is that of Kawasaki (1966,1972). The simplest dynamical assumption is that the configuration of the lattice gas changes by a random movement of particles to a neighbouring empty site. In binary alloy language this is interpreted as a random interchange of atoms on neighbouring sites.

Kawasaki's Kinetic model of the lattice gas was simulated on the computer (Marro 1975). The lattice was taken to be simple cubic with N sites (N = 125,000). The basic dynamic process in the simulation was as follows: a site is picked at random, and then a nearest neighbour is picked at random, and if exactly one of these two sites is full, the particle moves to the other site with a transition probability p_n defined by

$$p_n = \frac{1}{y^n + 1} \qquad (I,1)$$

where n, positive or negative, is the net decrease or increase respectively in the number of nearest neighbours the particle will have after the proposed move, and y is the Boltzman factor defined by

$$y = e^{\frac{V}{KT}} \qquad (I,2)$$

where $V > 0$ is the attraction between two particles of the lattice gas which are nearest neighbours, K is Boltmann's constant, and T is the absolute temperature. Equation (I,1) satisfies detailed balancing (Glauber 1963).

In the simulation, the duration Δt_{sim} of one such attempted interchange was defined to be $\frac{1}{N}$ units of time. Therefore, the probability $p(\underline{x},y)$ of moving a particle from a site $\underline{x}$ to a neighbouring site $\underline{y}$ in time $\frac{1}{N}$ given $\underline{x}$ is full and $\underline{y}$ empty can be written as

$$p(\underline{x},\underline{y}) =$$

[prob (site $\underline{x}$ is chosen from N sites) × prob(choosing nearest neighbour $\underline{y}$) + prob(site $\underline{y}$ is chosen from N sites) × prob(choosing nearest neighbour $\underline{x}$)] × transitional probability that the interchange between $\underline{x}$ and $\underline{y}$ takes place

$$= [\frac{1}{N} \times \frac{1}{6} + \frac{1}{N} \times \frac{1}{6}] \times p_n = \frac{p_n}{3} \times \frac{1}{N}$$

$$= \frac{p_n}{3} \quad \Delta t_{sim} \qquad (I,3)$$

since $\frac{1}{N}$ is the duration of one attempted interchange in the simulation. The probability that a molecule at site $\underline{x}$ goes to a neighbouring empty site $\underline{y}$ is therefore $\frac{p_n}{3}$ per unit time.

Such a model,however, is a simplification of real alloys where lattice misfit of the two kinds of atoms and resulting elastic distortion have to be taken into account. Also exchange in most real alloys take place indirectly via vacancies (the 'hole' mechanism) rather than by the 'ring' mechanism used in the Kawasaki model. The ring mechanism is observed only in Cu - Mo and some pure metals like copper and gold. Marro et al, however, noticed that the simulation results did not depend crucially on the number of vacancies.

I.3 Equilibrium properties of the Kawasaki model.

Each configuration of the lattice gas can be partitioned into subsets which we call 'clusters'. A cluster is a collection of occupied sites such that no such site is a nearest neighbour of an occupied site outside the cluster, but if a cluster is subdivided into subsets, then at least one member of one subset is the nearest neighbour of a member of another subset. The number per lattice site of clusters consisting of exactly ℓ particles is denoted by C_ℓ.

The equilibrium values of C_ℓ can be found in terms of the partition function Q_ℓ for clusters of size ℓ (Lebowitz and Penrose, 1978). The quantities Q_ℓ are given by

$$Q_\ell = \sum_\lambda{}' y^{n(\lambda)} \qquad (I,4)$$

where y is the Boltzmann factor $e^{\frac{V}{KT}}$ defined in (I,2), and $\sum'$ runs over the set of translationally inequivalent clusters λ of size ℓ, and $n(\lambda)$ is the number of pairs of nearest neighbours in cluster λ. The partition functions Q_ℓ are polynomials in the Boltzmann factor y and have been found exactly by Sykes (1976) for the simple cubic lattice for ℓ = 1 to 10:

$$Q_1 = 1$$

$$Q_2 = 3y$$

$$Q_3 = 15y^2$$

$$Q_4 = 83y^3 + 3y^4$$

$$Q_5 = 486y^4 + 48y^5$$

$$Q_6 = 2967y^5 + 496y^6 + 18y^7$$

$$Q_7 = 18748y^6 + 4368y^7 + 378y^8 + 8y^9$$

$$Q_8 = 121725y^7 + 36027y^8 + 4854y^9 + 306y^{10} + y^{12}$$

$$Q_9 = 807381y^8 + 288732y^9 + 51030y^{10} + 5544y^{11} + 159y^{12} + 24y^{13}$$

$$Q_{10} = 5447203y^9 + 2280792y^{10} + 488976y^{11} + 72244y^{12} + 5103y^{13} + 396y^{14} + 24y^{15}$$

The importance of these Q_ℓ's lies in the fact that the equilibrium value of C_ℓ can be obtained in terms of these Q_ℓ's. For low densities, we have (Penrose and Lebowitz,1978)

$$c_\ell = Q_\ell \, z^\ell \qquad \text{(I,5)}$$

where z is the fugacity of the system for given temperature T and density ρ.

Equation (I,5) has to be modified to hold for higher values of the fugacity z or density ρ. The empirical law corresponding to (I,5) for higher densities has been observed in computer simulations

of a binary alloy (Sur 1977). The results have been analysed by Kalos et al.(1978). They found that the distribution of sizes of small clusters at equilibrium and also at low supersaturation when the system appeared to be in a metastable state could be represented by the empirical formula

$$c_1 \simeq (1 - \rho)^3 W$$

$$c_\ell \simeq (1 - \rho)^4 Q_\ell W^\ell \qquad \ell \geq 2 \tag{I,6}$$

where ρ is the density in lattice gas language or fractional concentration of minority phase in alloy language. The empirical formula (I,6) reduces to (I,5) in the limit of zero density, when $W \to z$. Equation (I,6) is very important, and the extent of its validity will be discussed in the next section.

For $\ell \geq 11$, the coefficient Q_ℓ are obtained from the extrapolation formula for $Q_\ell / Q_{\ell+1}$ given by (Penrose et al, 1978).

$$W_\ell = \frac{Q_\ell}{Q_{\ell+1}} = W_s \left(1 + \frac{C}{(\ell - 2)^{1/3}}\right) \tag{I,7}$$

The physical basis of this equation is that the excess pressure of a spherical droplet of radius r (proportional to $\ell^{1/3}$) is proportional to $1/r$. The quantity W_s is the saturation value of W in equation (I,6) and the constant C acts like a surface tension. The presence of $(\ell - 2)$ rather than ℓ in (I,7) was explained by Frenkel (1946). The reason for this is that for a

system of ℓ molecules, the total number of internal degrees of freedom is $3(\ell - 2)$ and not 3ℓ, as it is assumed to be, to a good approximation, in classical thermodynamics. This distinction becomes important only for small ℓ. (I,7) is related to the Capillarity approximation (Abraham 1974) whereby small clusters are treated as macroscopic drops.

Table (I,i): The constant W_S and C in (I.7) for various temperatures

$\frac{V}{KT}$	W_S	C
.7	.04152	1.044
.8	.03624	1.104
.9	.03143	1.180
1.0	.02704 (.03525)	1.275
1.094	.0235 (.0298)	1.38
1.2	0.01942	1.555
1.3	0.01613	1.764
1.4	0.01315	2.046
1.5	0.01046 (0.010526)	2.440 (2.415)
1.6	.00849	3.019
1.7	.005897	3.932
1.8	.003989	5.556
1.9	.002316	9.157
2.0	.008660	23.45

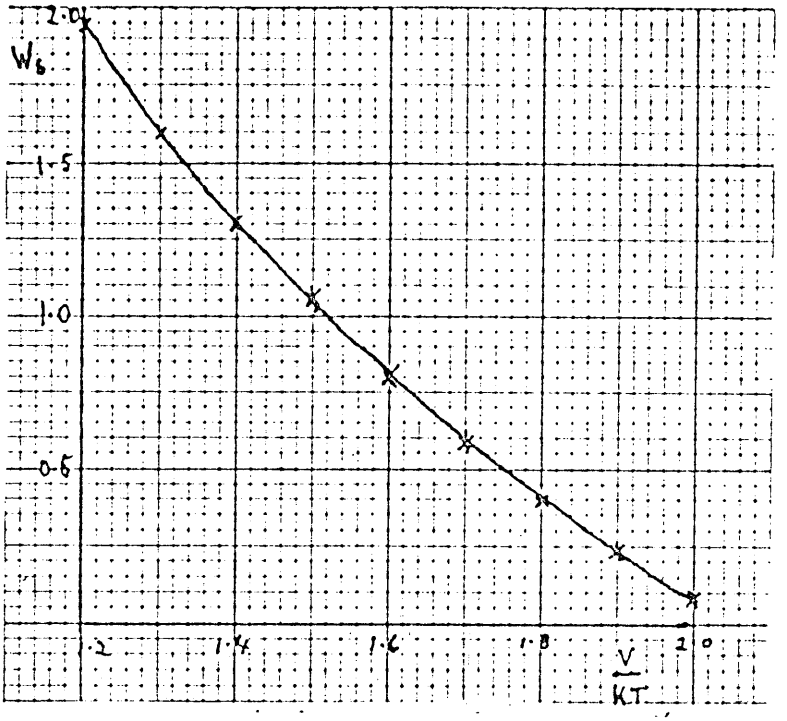

Fig (I,ii): A graph of W_s against $\frac{V}{KT}$ for $0.7 \leq \frac{V}{KT} \leq 2.0$

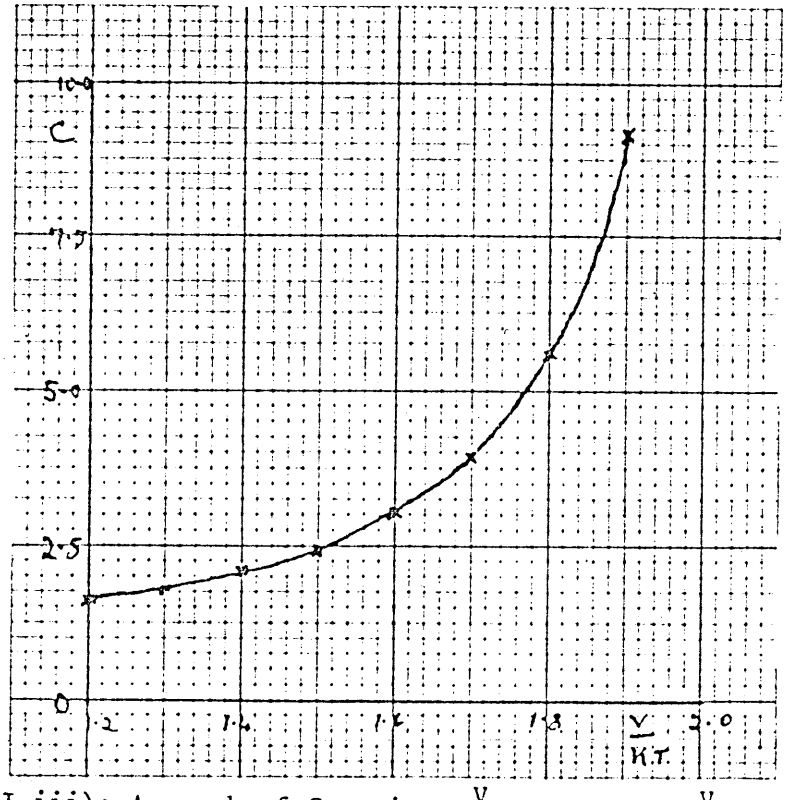

Fig (I,iii): A graph of C against $\frac{V}{KT}$ for $0.7 \leq \frac{V}{KT} \leq 2.0$. The constant W_s and C occur in the formula $\frac{Q_\ell}{Q_{\ell+1}} = W_s\left(1 + \frac{C}{(\ell-2)^{1/3}}\right)$

We have performed a least square analysis of (I,7) for different temperatures for ℓ = 4 to 9. We give W_S and C in Table (I,i) for different values of $\frac{V}{KT}$. The accuracy of (I,7) for $1 \leq \ell \leq 9$ with these values of W_S and C is always better than 0.2% for the range $0.7 \leq \frac{V}{KT} \leq 2.0$. We compare three values of W_S for different temperatures with values of W_S observed in ~~the~~ simulations at the coexistence density at these temperatures (Kalos,1978). These are given in brackets in Table (I,i). At $\frac{V}{KT} = 1.5$, the values of W_S differ by only $\frac{1}{2}$% but are considerably lower at $\frac{V}{KT} = 1.0$ and 1.09. A possible reason for this is that for these higher temperatures, for given ℓ, there are relatively fewer compact clusters and so the clusters tend to deviate more from the compactness of spherical clusters at higher temperatures. In Fig (I,ii) and (I,iii) we plot C and W_S against V/KT for V/KT > 1.2.

I.4 Validity of the distribution (I,6) for small clusters under condition of steady state for various temperatures and densities.

The distribution (I,6) holds for small clusters under equilibrium conditions (Kalos et al 1978). To find the parameter w in (I,6), for a given density ρ and temperature T we define ρ_L as the total number of particles per site in clusters of size L or less. Assuming (I,6) is valid

$$\rho_L = \sum_{1}^{L} \ell c_\ell = (1-\rho)^3 W + (1-\rho)^4 \cdot \sum_{2}^{L} \ell Q_\ell W^\ell \qquad (I,8)$$

where L is a suitable integer such as 10 or 20, such that clusters less than L are considered 'small', and clusters bigger than L are considered 'big'. The quantity ρ_L signifies the number of particles in the small clusters.

To find the equilibrium distribution of the small clusters at infinite temperature, we can put $\rho_L = \rho$ in (I,8) because C_{L+1} is very small under these conditions. One can then solve for W in (I,8) and get the distribution of small clusters from (I,6), with Q_ℓ evaluated at $T = \infty$ ($y = 1$). We compare C_ℓ predicted by the W-formula (I,6) with concentration C_ℓ of small clusters obtained from a simulation (Marro 1975) with the particles distributed at random on the lattice, corresponding to infinite temperature. In Table (I,ii) we give this comparison for $\rho = 0.075$ using a value L = 10. We can see that the agreement is quite good. This method works for densities ρ less than about 10%.

ℓ	$125{,}000 \times C_\ell$ simulation	$125{,}000 \times C_\ell$ solving (I,9)
1	5790	5866
2	965	965
3	310	286
4	88	97
5	35	36
6	21	14
7	11	6
8	4	2
9	1	1
10	0	0
> 10	1	0

Table (I,ii): Comparison of simulation concentration C_ℓ with C_ℓ as obtained from solving for W in (I,9).

Density $\rho = 0.075$, temperature $T = \infty$.

The equation (I,6) can also be shown to hold under approximately steady state conditions, if one considers W to be a parameter which decreases slowly with time while nucleation is taking place until it reaches W_S at equilibrium. Thus given ρ_L, ρ and T, one can solve for W from (I,8) and use (I,6) to give us the steady state distribution for small clusters. In Table (I,iii), we compare, for $T = 0.59T_C$ ($y = 4.482$) and $\rho = 0.10$, the predictions of the W-formula (I,7) with the distribution of small clusters from a simulation done by Marro et al (unpublished). We compare them for various times. The parameter W was obtained by finding ρ_{10} from the simulation, and then solving (I,8) with L = 10. The agreement again is quite good over the range $1.4 \leq \frac{W}{W_S} \leq 2$, so (I,6) is valid even for quasi-equilibrium conditions. We give also the predictions of a differential equation, described in Chapter II, for the evolution of C_ℓ with time. We give C_ℓ for ℓ = 1 to 10 in the differential equation, for a value of time when the value of C_1 is approximately the same as that in the W-formula (I,6). The differential equation distribution is quite near to the W-formula and to the simulation distribution, and it predicts ρ_{10} accurately.

t_{sim}	W/W_S	ℓ^*		C_1	C_2	C_3	C_4	C_5	C_6	C_7	C_8	C_9	C_{10}	ρ_{10}
75.67	2.0160	15.43	sim	2134	546	248	145	97	69	53	44	34	29	6764
			W-formula	1934	497	237	144	100	75	60	50	44	39	6771
			de	1923	497	241	152	110	85	69	59	51	45	7172
550.88	1.7007	42.94		1621	368	139	71	39	27	18	14	9	9	3818
				1631	353	142	73	43	27	18	13	9	7	3813
				1631	354	142	74	44	29	20	14	11	9	3896
1105.72	1.6211	60.78		1545	333	123	59	32	18	13	9	6	5	3358
				1554	321	123	60	34	20	13	9	6	4	3352
				1555	322	123	61	34	21	14	10	7	5	3399
2358.4	1.5063	110.51		1465	282	100	42	23	12	8	4	3	2	2813
				1445	277	98	45	23	13	8	5	3	2	2809
				1443	277	98	45	23	13	8	5	3	2	2807
4118.24	1.4292	180.18		1397	260	83	33	16	8	5	3	2	1	2508
				1371	250	84	36	18	10	5	3	2	1	2504
				1371	250	84	36	18	10	5	3	2	1	2504
5570.5	1.4310	177.90		1420	266	77	32	16	9	4	3	2	1	2515
				1373	250	84	37	18	10	5	3	2	1	2510
				1373	250	84	37	18	10	5	3	2	1	2510

Table(I,iii): Steady state distribution of small clusters at $T = 0.59T_C$ and density $\rho = 0.10$ which is considerably higher than the coexistence density 0.146 at this temperature. We give this distribution (a) for a simulation of a lattice gas, (b) for the W-formula (I,6) using ρ_{10} found in (a), and finally (c) from a differential equation, described in Chapter II, using (I,6) for its equilibrium properties, when the value of C_1 is the same as in (b). The agreement is good in all three cases. The factor W_S is the equilibrium value of W, and is equal to 0.010526; ℓ^* is defined in (I.9).

Equation (I,7) can be used to relate W, which is a measure of the supersaturation, to a characteristic cluster size ℓ^*, which we define by

$$W = W_s\left(1 + \frac{C}{(\ell^* - 2)^{1/3}}\right) \qquad (I,9)$$

When ℓ^* is defined in this way, it can be shown (Penrose et al, 1978) that ℓ^* is a critical size such that clusters larger than ℓ^* grow at the expense of those less than ℓ^*, which tend to shrink. While nucleation is taking place, W decreases slowly to W_S, and ℓ^* increases by (I,9). The basic assumption in the theory of coarsening (Lifshitz and Slyozov 1961, and Wagner 1961) is that ℓ^* increases linearly with time during the coarsening of quenched alloys.

The quantity ℓ^*, or W, characterizes the distribution of the small clusters via (I,9) and (I,6). We have shown in this section that the important formula (I,6) holds not only for equilibrium but also under conditons which are approximately steady state. It holds for a considerable range of temperatures T above and below T_C and for densities ρ at least as high as 0.10.

I.5 Fundamental equations of the Lifshitz-Slyozov theory

In a supersaturated solution diffusion effects may bring about the formation of grains of the new phase. Two stages of this process may be distinguished. In the first concentration fluctuations produce nuclei of the new phase which grow directly from the supersaturated medium. The second stage may be considered to begin when the grains thus formed have reached an appreciable size and the degree of supersaturation is small. The rate of formation of these

larger droplets is most often controlled (Greenwood 1969) by the rate at which the solute diffuses between particles. The second stage is often called coarsening or Ostwald ripening.

To obtain the fundamental equation of Lifshitz and Slyozov we solve the diffusion equation for the monomer concentration

$$\frac{\partial c(\underline{r},t)}{\partial t} = D \nabla^2 c(\underline{r},t)$$

given a spherical cluster of radius R at the origin. D is the diffusion constant of monomers. Assuming steady state and using spherical symmetry, this equation reduces to $\frac{\partial^2}{\partial r^2}(rc) = 0$, that is

$$c(r) = A + B/r \qquad (I,10).$$

where A and B are constants determined by two boundary conditions. As $r \to \infty$, $c(r)$ tends to the overall monomer concentration c_1, and so $A = c_1$. Kelvin's equation now gives $c(R)$, the monomer concentration at the surface of the cluster, as

$$c(R) = c_{1,eq} + \frac{\alpha}{R}$$

where c_{1eq} is the equilibrium concentration of monomers and α is a positive constant. This equation holds for small supersaturations $\Delta \equiv c_1 - c_{1,eq} << 1$ With these boundary conditions, (I,10) then gives

$$c(r) = c_1 + \frac{\alpha - R\Delta}{r} \qquad (I,11).$$

The rate at which monomers flow towards the central cluster per unit area is given by $j = D \frac{\partial c}{\partial r}\Big|_{r=R}$, and this is equal to the rate of growth of the radius of the cluster $\frac{dR}{dt} = j$. Using (I,11) we obtain

$$\frac{dR}{dt} = \frac{D}{R}\left(\Delta - \frac{\alpha}{R}\right)$$

Thus for every value Δ of the supersaturation there exists a critical radius $R_C = \frac{\alpha}{\Delta}$ such that a cluster of this size is in equilibrium with the solution. If $R > R_C$ the grain grows, if $R < R_C$ it dissolves. This is the basic mechanism for coarsening. Both Δ and R_C themselves vary with time.

Assuming a spherical cluster, if we define volume of grain to be $\ell = \frac{4}{3}\pi R^3$ and define $\bar{\ell} = \frac{4}{3}\pi R_C^3$ as the critical size, we can then write

$$\frac{d\ell}{dt} = 4\pi D\alpha \left[\left(\frac{\ell}{\bar{\ell}}\right)^{1/3} - 1\right] \qquad (I,12)$$

This formula is the basic for the Lifshitz-Slyozov theory. From (I,12) we see that particles of size greater than $\bar{\ell}$ tend to grow at the expense of particles of size less than $\bar{\ell}$ which tend to disappear. The critical size $\bar{\ell}$ is predicted to grow linearly with time in the case of diffusion controlled growth. It has been shown (Penrose et al, 1978) that for large ℓ, the equations of Becker and Döring can be reduced to an equation similar to (I,12) with $\bar{\ell} = \ell^*$, defined in (I,9). We will set up the Becker-Döring equations in the next chapter, and we will compare their predictions with those of Lifshitz and Slyozov in Chapter VII.

Chapter II The Becker-Döring Equation

It is the purpose of this chapter to set up a system of differential equations of the Becker Döring type (Becker-Döring 1935) to predict the kinetics of the growth of clusters in the Kawasaki model.

The basic assumption of the Becker-Döring theory is that a drop or cluster of one phase can increase or decrease in size by at most one particle at a time. So the Becker-Döring model neglects processes like the coagulation of two large clusters to form an even larger one, or its inverse - the breaking up of a large cluster into two large parts. Rough estimates, however, indicate that processes involving more than one large cluster are relatively unimportant for sufficiently small times and for low densities of minority phase (e.g. 10%) (Penrose et al 1978). Coalescence effects have been studied by Smoluchowski (1916) in connection with formation of raindrops, and also by Binder (1974,1976) and by Mirold and Binder (1977).

We will follow closely the paper 'Growth of clusters in a First Order Phase Transition' by Penrose et al (1978), in the formulation of the Becker-Döring equations in this chapter.

II.1 The Kinetic Equations

We define c_ℓ as the number of clusters of size ℓ per site of the lattice. If the only processes considered are the absorption and emission of a monomer by a cluster of arbitrary size, we can write the Becker-Döring equations as

$$\frac{dc_\ell}{dt} = J_{\ell-1} - J_\ell \qquad \ell \geq 2 \qquad (II,1)$$

where J_ℓ is the net rate of conversion per site of ℓ-particle clusters into $(\ell + 1)$-particle clusters, and is given by

$$J_\ell = a_\ell \, c_\ell \, c_1 - b_{\ell+1} \, c_{\ell+1} \qquad \ell \geq 1 \qquad (II,2)$$

Here a_ℓ and $b_{\ell+1}$ are kinetic coefficients: a_ℓ describes the rate at which ℓ-particle clusters absorb monomers and $b_{\ell+1}$ is a coefficient describing the rate at which $(\ell+1)$-particle clusters emit monomers. To complete the system of equations we also need one for c_1. The condition determining c_1 is the conservation of matter, which can be written as

$$\sum_{\ell=1}^{\infty} \ell c_\ell = \rho = \text{a constant} \qquad (II,3)$$

when ρ is the total number of particles divided by the total number of lattice sites. We call ρ the density, which is a constant independent of time.

The coefficients a_ℓ and $b_{\ell+1}$ in formula (II,2) are related through the fact that by detailed balancing argument, $J_\ell = 0$ at equilibrium. If the density is small enough for the equilibrium state to have only one phase, it is reasonable to assume that the cluster concentration at equilibrium c_ℓ^{eq} are given approximately by equation (I,6) for all ℓ:

$$c_1^{eq} = (1 - \rho)^3 W \quad \text{and} \quad c_\ell^{eq} = (1 - \rho)^4 Q_\ell W \quad \ell \geq 2 \qquad (I,6)$$

where Q_ℓ is the partition function for ℓ-sized clusters on the simple cubic lattice. Substituting (I,6) into (II,2) and setting $J_\ell = 0$, we obtain for the ratio $b_{\ell+1}/a_\ell$ at density ρ a formula depending weakly on the density through the factor $(1 - \rho)^3$:

$$\frac{b_{\ell+1}}{a_\ell} = \frac{c_1^{eq} c_\ell^{eq}}{c_{\ell+1}^{eq}} = \begin{cases} W_\ell (1 - \rho)^3 & \text{for } \ell \geq 2 \\ W_1 (1 - \rho)^2 & \ell = 1 \end{cases} \qquad (II,4)$$

where W_ℓ is defined by

$$W_\ell = Q_\ell / Q_{\ell+1} \qquad (II,5)$$

The asymptotic nature of W_ℓ has already been discussed in equation (I,7). If we let $\rho \to 0$ in (II,4) we obtain

$$b_{\ell+1}(0) = a_\ell(0)\, W_\ell \qquad (II,6)$$

where $b_{\ell+1}(0)$ and $a_\ell(0)$ are the values of $b_{\ell+1}$ and a_ℓ in the limit of zero density.

Equation (II,4) shows the dependence of the ratio $b_{\ell+1}/a_\ell$ on density. In Chapter V, we will show that a_ℓ can be written as

$$a_\ell = \mu(\ell^*)\, a_\ell(0) \qquad (II,7)$$

where $a_\ell(0)$ is thevalue of a_ℓ in the limit of zero density, and $\mu(\ell^*)$ gives the variation of a_ℓ with ℓ^* or equivalently with the size distribution of the small clusters, these being most mobile.

In Chapter III we will describe a method of calculating $a_\ell(0)$ and we will derive an asymptotic formula for the form $a_\ell(0) \propto \ell^{1/3}$ i.e. that a_ℓ increases as the radius of an ℓ-cluster approximately in the case of diffusion controlled growth (Penrose et al 1978, and Lifshitz and Slyozov 1961). The equations (II,4), (II,6) and (II,7) imply that the variation with density of $b_{\ell+1}$ is given by

$$b_{\ell+1} = \mu(\ell^*)\, b_{\ell+1}(0) \times \begin{cases} (1-\rho)^3 & \ell \geq 2 \\ (1-\rho)^2 & \ell = 1 \end{cases} \qquad \text{(II, 8)}$$

where $b_{\ell+1}(0)$ is the value of $b_{\ell+1}$ in the limit of zero density.

The factor $(1 - \rho)^3$ in (II,8) represents the reduction in the probability of evaporation of a monomer from an $(\ell+1)$-particle cluster caused by the possibility that a monomer cannot by definition form on any site next to a site that is already occupied. In (II,8) we assumed for simplicity that (II,4) is valid also at higher densities for which the equilibrium has two phases although the size distribution formula (I,6) is not valid for large ℓ either in the true equilibrium state or even in the quasistationary state with a time dependent W (Penrose et al, 1978).

For numerical purposes, one has to take a finite system of equations in (II,1). This is done by letting $c_\ell = 0$ for $\ell > L$. This L is different from the L in equation (I,8). We then define the derivative of C_L by

$$\frac{dC_L}{dt} = J_{L-1} \qquad \text{(II, 9)}$$

Provided L is big enough the solution does not depend on the actual value of L. We took L to be 800. The choice of L will be discussed in more detail in Chapter V.

Equations based on the Decker-Döring[11] theory were used by others including Courtney (1962), Abraham (1969), Bauer et al (1978). Their differential equationswere considerably different from ours. The coefficient a_ℓ in their theory was taken to be proportional to $\ell^{2/3}$ for surface controlled growth. In this work (see Chapter III and IV) we will take a_ℓ proportional to $\ell^{1/3}$ for diffusion controlled growth, which is the more common mechanism of growth in the coarsening of quenched alloys. Another important distinction is that in our system of equations we have determined the time variation of c_1 using conservation of mass, whereas c_1, the concentration of monomers, is assumed to be constant with time in the cited works. With our equations, c_1 decreases monotonically with time for the initial conditions described in section I.5.

The three authors mentioned above also used very small values for L namely 110, 110, and 25. By comparsion, we have to take $L \simeq 800$ to describe what happens in the simulations

(Marro 1975) since there was a considerable number of clusters of size 600 in the simulation for the later times.

II.2 Existence of a Phase Transition for $\rho > \rho_s$, $T < T_c$

When in equation (I,8) we let $L \to \infty$, we obtain an infinite series for the density in terms of W. The function $\rho(W)$ is the number of particles in the 'vapour phase' for a given value of W. The radius of convergence of the series for $\rho(W)$ is given by $\lim \left(\frac{Q_\ell}{Q_{\ell+1}}\right) = W_s$ from equation (I,7). For $T < T_c$, the value $\rho(W_s) = \rho_s$, the critical density, which is finite (Fisher, I967). For $\rho \leq \rho_s$ one can find a value of W in $(0, W_s]$ so that $\rho(W) = \rho$. In this case therefore no new phase is nucleated. For $\rho > \rho_s$, however, no such W can be found since the density in the vapour phase cannot exceed ρ_s. Therefore $\rho - \rho_s$ is the density of the nucleated phase. The quantity ρ_s is the saturated vapour pressure in lattice gas language, or the equilibrium concentration of one metal in a binary alloy.

For $T > T_c$, however, Fisher's theory would require $C \to 0$ in (I,7) as $T \to T_c$ from below. This is not confirmed by our data in Table (I,i), where for $\frac{V}{KT_c} (\approx 0.89)$, C is about 1.18. This suggests that (I,7) is not accurate for large ℓ for temperatures T near to or larger than T_c.

II.3 The free energy

The system of Becker-Döring equations has a free energy, whose derivative with respect to time is always negative. We define the free-energy per site f by (Penrose, unpublished):

$$\frac{-f}{KT} = C_1\left[\log \frac{(1-\rho)^3}{C_1} + 1\right] + \sum_2^\infty C_\ell \log\left[1 + \frac{(1-\rho)^4 Q_\ell}{C_\ell}\right] \qquad (II, 11)$$

Differentiating with respect to t, using (II,1) and (II,3) for $\frac{dc_\ell}{dt}$, we have

$$\frac{d}{dt}\left(-\frac{f}{KT}\right) = \left(-J_1 - \sum_1^\infty J_\ell\right) \log\left[\frac{(1-\rho)^3}{C_1}\right] + \sum_2^\infty (J_{\ell-1}-J_\ell)\log\left[\frac{(1-\rho)^4 Q_\ell}{C_\ell}\right]$$

We now group the terms with coefficient J_ℓ together and the expression is equal to

$$= J_1 \log \frac{C_1^{\,2}}{(1-\rho)^6}\frac{(1-\rho)^4 Q_2}{C_2} + \sum_2^\infty J_\ell \log\left[\frac{C_1}{(1-\rho)^3}\frac{C_\ell}{Q_\ell}\frac{Q_{\ell+1}}{C_{\ell+1}}\right]$$

Then using equation (II,4) for all $\ell \geq 1$ and using (II,2) for the definition of J_ℓ, we can express the above expression as

$$\frac{d}{dt}\left(-\frac{f}{KT}\right) = \sum_1^\infty J_\ell \log\left(1 + \frac{J_\ell}{b_{\ell+1}\, C_{\ell+1}}\right) \geq 0 \qquad \text{(II, 12)}$$

The term on the right hand side is always positive whatever the value of J_ℓ since $b_{\ell+1}\ \ c_{\ell+1} \geq 0$. This means that the free energy is monotonically decreasing for all time whatever the initial conditions.

One can also find the equilibrium distribution of clusters by minimizing the free energy subject to this condition that $\sum_{1}^{\infty} \ell C_\ell = \rho$ using Lagrangian multipliers. This gives the same concentration distributions for equilibrium as given by the distribution (I,6), and the same relation for ρ in terms of w as in (I,8).

Chapter III : The Kinetic Coefficients $a_\ell(0)$ in the Limit of Zero Density.

In this chapter, we will calculate the coefficients $a_\ell(0)$ for $\ell = 1$ to 6. Assuming a concentration c_1 of monomers and c_ℓ of clusters of size ℓ, the quantity $a_\ell c_\ell c_1$ is the rate (Becker and Döring, 1935) at which clusters of size ℓ absorb monomers to become clusters of size $\ell + 1$. Thus a_ℓ is the rate at which clusters of size ℓ absorb monomers to become clusters of size $\ell + 1$, per unit concentration of ℓ-clusters c_ℓ and per unit monomer concentration c_1. The coefficients $a_\ell(0)$ are then defined as the value of a_ℓ when the density ρ tends to zero.

First we will give some definitions which we will use later on throughout this chapter. We define

Σ = the infinite cubic latice.

λ = an equivalence class of translationally equivalent clusters in Σ.

ϵ = set of points in Σ which are occupied by a given cluster in λ.
The origin belongs to ϵ.

$N_1(\epsilon)$ = set of all the nearest neighbours of C not themselves in ϵ.

$N_2(\epsilon)$ = set of all the nearest neighbours of N_1 not themselves in ϵ or N_1 .

B = a closed cubic boundary with faces perpendicular to the three coordinate axis of the lattice Σ. The boundary B completely encloses ϵ, N_1, N_2 and is disjoint from them.

By these definitions ϵ, N_1, N_2, B are all disjoint and all subsets of Σ. We also define the vectors $\underset{\sim}{e}_i$, i = 1, ..., 6 to be equal to the six vectors (1, 0, 0), (-1, 0, 0), etc.

III.1 Microscopic formulation.

In this section we formulate the problem of finding $a_\ell(0)$. Given a class of translationally equivalent clusters λ of size ℓ, we define C_λ to be the concentration of clusters in λ. A cluster in λ can be transformed to a cluster of size $(\ell + 1)$ by absorbing a monomer at a lattice site in N_1. Conversely a cluster of size $\ell + 1$ occupying the lattice sites of λ and any one site in N_1, can be converted to a cluster in λ by emitting the particle at N_1. The union of the equivalence classes of such $(\ell + 1)$ - clusters is $\{\underset{\sim}{\epsilon} \cup \underset{\sim}{x} : \underset{\sim}{\epsilon} \in \lambda \text{ and } \underset{\sim}{x} \in N_1(\underset{\sim}{\epsilon})\}$, denoted by λ^+ for brevity. We also denote by $C_\lambda +$ the total concentrations of such $(\ell + 1)$-clusters on Σ which are in λ^+. Therefore λ^+ can contain clusters of different shape and orientation.

We now define J_{λ,λ^+} to be the net probability per unit time that the clusters in Σ isomorphic to λ absorb monomers to become some $(\ell + 1)$- cluster in λ^+. Following Becker and Döring (1935) we can write J_{λ,λ^+} as

$$J_{\lambda,\lambda^+} = a_{\lambda\,\lambda^+} C_1 C_\lambda - b_{\lambda^+\lambda} C_{\lambda^+} \qquad \text{(III,1)}$$

where $a_{\lambda\ \lambda^+}$ is the probability per unit time that the clusters in λ absorb a monomer to form an $(\ell + 1)$-cluster per unit C_1 and per unit C_λ. Then $b_{\lambda^+\lambda}$ is the probability per unit time, per unit C_{λ^+} that any cluster in λ^+ breaks up into a monomer and an ℓ-cluster in λ. This equation is analogous to equation (II, 2) in our formulation of the Becker - Döring equations. We can then divide (III, 1) by C_λ:

$$J_{\lambda,\lambda^+}/C_\lambda = a_{\lambda\ \lambda^+} C_1 - b_{\lambda^+\lambda} C_{\lambda^+}/C_\lambda \qquad \text{(III,2)}$$

This gives the net probability per unit time that the given cluster ϵ in λ becomes an $(\ell + 1)$-cluster. We assume that the cluster ϵ is at the origin.

The size distribution of clusters on the lattice Σ can be assumed to be a canonical Gibbs distribution given by the equation (I, 5) in the limit of zero density. A simple generalization of (I, 5) can be made to obtain C_λ and C_{λ^+} under conditions of steady state. Let $n(\lambda)$ be the number of pairs of nearest neighbours in the cluster ϵ in λ, and $n(\epsilon \cup \underline{x})$ be the number of pairs of nearest neighbours in the $(\ell+1)$ cluster formed by adding a monomer at a site $\underline{x} \in N_1$. Then the steady state values of C_λ and C_{λ^+} are given by

$$C_\lambda = y^{n(\lambda)} C_1^{\ \ell} \text{ and } C_{\lambda^+} = \sum y^{n(\epsilon \cup \underline{x})} C_1^{\ \ell+1} \qquad \text{(III, 3)}$$

where y is the Boltzmann factor $e^{V/KT}$, and where the sum is only over translationally inequivalent clusters in λ^+. The quantity C_1 is obtained from the conservation of mass condition $\sum_1^\infty \ell C_\ell = \rho$ as explained near (I, 5). The density ρ is assumed to be arbitrarily small, so our analysis is done in the limit of zero density.

in λ

For any $\underline{x} \in \Sigma - \mathcal{C}$, i.e. outside the central cluster λ we can define a steady state probability $f(\underline{x})$ by

$$f(\underline{x}) = \text{prob}\{\text{site } \underline{x} \text{ is occupied by a monomer given that sites in } \mathcal{C} \text{ are full}\}.$$

When $\underline{x}$ is an immediate neighbour of the central cluster $\mathcal{C}$, i.e. $\underline{x} \in N_1$, $f(\underline{x})$ is related to the probability that an $(\ell + 1)$-cluster is present; otherwise $f(\underline{x})$ will be related to the probability that there is a monomer in the vicinity of the cluster $\mathcal{C}$.

The probability $f(\underline{x})$ is related to $f(\underline{x} + \underline{e}_i)$, that is f evaluated at the nearest neighbour of $\underline{x}$, via the transition probabilities $p(\underline{x}, \underline{x} + \underline{e}_i)$ which we defined in (I, 1), (I, 2) and (I, 3). We will now get a difference equation for $f(\underline{x})$ with suitable boundary conditions, and $a_{\lambda\lambda^+}$ can then be obtained in terms of $f(\underline{x})$.

In the low density limit, we can consider only reactions between a monomer and the given cluster $\mathcal{C}$ at the origin, and ignore all other reactions, say between the monomers themselves. If we also neglect the possibility of the cluster λ breaking up, we obtain from the Kawasaki dynamical assumption (Kawasaki 1966) the condition

$$\frac{df(\underline{x})}{dt} = \sum_{i=1}^{6} [f(\underline{x}+\underline{e}_i)\, p(\underline{x}+\underline{e}_i\,,\, \underline{x}) - f(\underline{x})\, p(\underline{x}\,,\, \underline{x}+\underline{e}_i)]$$

$$\text{for } \underline{x} \in \Sigma - (\mathcal{C} \cup N_1) \qquad \text{(III, 4)}$$

where the sum is over the neighbours of $\underline{x}$.

Provided that the cluster size distribution changes slowly enough with time, an assumption which we will examine later, we can put df/dt = 0 in this equation. We then obtain the steady state condition

$$\sum_{1}^{6} [f(\underline{x}+\underline{e}_i)\, p(\underline{x}+\underline{e}_i\ ,\ \underline{x}) - f(\underline{x})\, p(\underline{x}\ ,\ \underline{x}+\underline{e}_i)] = 0$$

$$\text{for } \underline{x} \in \Sigma - (\mathcal{C} \cup N_1) \qquad \text{(III, 5)}$$

For away from cluster C, $p(\underline{x}, \underline{y})$ will all be equal to $p_0/3$ and the difference equation (III, 5) reduces to the finite difference analogue of Laplace's equation:

$$\sum_{i=1}^{6} [f(\underline{x}+\underline{e}_i) - f(\underline{x})] = 0 \quad \text{for } \underline{x} \in \Sigma - (\mathcal{C} \cup N_1 \cup N_2) \qquad \text{(III, 6)}$$

For the second nearest neighbouring sites, $\underline{x} \in N_2$, however, the more general equation (III, 5) must be used, since some of the possible transitions change the energy.

One can then relate $J_{\lambda,\lambda^+}/C_\lambda$ to the function f and the transition probabilities. The cluster $\mathcal{C}$ can only become an $(\ell + 1)$-cluster in one move by monomers moving from N_2, the set of nearest neighbours of $\mathcal{C}$. The net rate $J_{\lambda,\lambda^+}/C_\lambda$ at which cluster $\mathcal{C}$ becomes an $\ell + 1$ cluster is therefore given by

$$\frac{J_{\lambda,\lambda^+}}{C_\lambda} = \sum_{\substack{\underline{n}_2 \in N_2 \\ \underline{n}_1 \in N_1}} [p(\underline{n}_2\ ,\ \underline{n}_1)\, f(\underline{n}_2) - p(\underline{n}_1\ \underline{n}_2)\, f(\underline{n}_1)] \qquad \text{(III, 7)}$$

The equation (III, 7) will be used in the next section to specify numerically the boundary conditions for the difference equation (III, 5).

III.2 Boundary Conditions

The boundary conditions for the difference equation (III, 5) describe what happens at infinity and at the sites $\underline{x} \in N_1$, that is the sites adjacent to the cluster λ. At infinity we have assuming widely separated parts of the system to be statistically independent,

$$f(\underline{x}) \longrightarrow C_1 \quad \text{as } \underline{x} \longrightarrow \infty \tag{III, 8}$$

For adjacent sites, $\underline{x} \in N_1$, the relevant condition describes the fact that if $\underline{x} \in N_1$, then we have an $(\ell + 1)$-cluster. In fact, remembering the definition of λ^+ and C_{λ^+}, we have

$$\begin{aligned} C_{\lambda^+} &= \text{prob}\{\text{there is a cluster } \lambda^+ \text{ of size } \ell + 1\} \\ &= \sum_{x \in N_1} \text{prob}\{\text{there is an } \ell\text{-cluster } \lambda \text{ at the origin}\} \\ &\quad \times \text{prob}\{\text{site } \underline{x} \text{ is full} \mid \text{cluster } \lambda \text{ at origin}\} \\ &= \sum_{\underline{x} \in N_1} C_\lambda \, f(\underline{x}) \end{aligned}$$

where the sum runs over all sites $\underline{x}$ in N_1.
This can be written as

$$\sum_{\underline{x} \in N_1} f(\underline{x}) = \frac{C_{\lambda^+}}{C_\lambda} \tag{III, 9}$$

To complete equation (III, 9) we need to know the $f(\underline{x})$ individually. We can assume for simplicity that the concentration of the $(\ell + 1)$-clusters of various shapes are at the same ratio as at equilibrium. So $f(\underline{x})$ can be assumed to satisfy a Gibbs distribution over N_1.

$$f(\underline{x}) = \text{constant} \times y^{n(\epsilon \cup \underline{x})} \quad \text{for } \underline{x} \in N_1 \qquad \text{(III, 10)}$$

where $y = \exp\left(\frac{V}{KT}\right)$ and $n(\epsilon \cup \underline{x})$ is the number of pairs of nearest neighbours in the $(\ell + 1)$-cluster $\epsilon \cup \underline{x}$. Equation (III, 10) holds at equilibrium and we will discuss its validity for steady state conditions later on in this section.

The difference equation (III, 5) together with boundary conditions (III, 8), (III, 9) and (III, 10) gives a system of linear equations which can be shown to have a unique solution (Isaacson and Keller, 1966). By the superposition principle this solution depends linearly on the parameters C_1 and $C_\lambda+/C_\lambda$. The part of the solution which is proportional to C_1 can be found by solving the difference equation under the conditions

$$\begin{aligned} &f(\underline{x}) \longrightarrow 1 \qquad \underline{x} \longrightarrow \infty \\ &f(\underline{x}) = 0 \qquad \underline{x} \in N_1 \end{aligned} \qquad \text{(III, 11)}$$

The part which is proportional to $C_\lambda+/C_\lambda$ can be found by solving the difference equation under the conditions

$$\begin{aligned} &f(\underline{x}) \longrightarrow 0 \qquad \text{as } \underline{x} \longrightarrow \infty \\ &f(\underline{x}) = y^{n(\epsilon \cup \underline{x})} / \sum_{\underline{x} \in N_1} y^{n(\epsilon \cup \underline{x})} \quad \text{for } \underline{x} \in N_1 \end{aligned} \qquad \text{(III, 12)}$$

In fact only one of these problems need be solved because by detailed balancing, $J_{\lambda\lambda}+ = 0$ at equilibrium which implies that $b_\lambda+_\lambda = a_{\lambda\lambda}+ \frac{C_1 C_\lambda}{C_\lambda+}$ with C_λ and $C_\lambda+$ given by (III, 3). We now

show how to obtain $a_{\lambda\lambda}{}^{+}$ from the problem (III, 11). In our numerical work we only solved (III, 11).

Once the solution of the difference equation (III, 5) with boundary conditons (III, 8) and (III, 11) is known, we can calculate $J_{\lambda\lambda}{}^{+}/C_{\lambda}$. In (III, 7), this was shown to be equal to the net rate of flow of monomers from N_2, the set of second nearest neighbours of cluster $\mathcal{C}$, to N_1, the set of nearest neighbours of the central cluster. By conservation of matter, the flow of clusters from N_2 to N_1 has to be equal to the total monomer flow towards $\mathcal{C}$ at large distances from $\mathcal{C}$. This flow is equal to the sum over any closed surface, which encloses the central cluster and does not pass through any of the lattice sites, of all the probability flows

$$p(\underline{x}\ ,\ \underline{x} + \underline{e}_i)\ f(\underline{x} + \underline{e}_i) - p(\underline{x} + \underline{e}_i\ ,\ \underline{x})\ f(\underline{x}) \qquad \text{(III, 13)}$$

along bonds which cross the surface, using a sign convention in which an inward flow counts as positive. By (III, 5) and the finite difference analogue of the divergence theorem, the quantity so defined is the same for all such surfaces, so we may calculate it using a large sphere. At large distances from cluster $\mathcal{C}$, our difference equation (III, 5) becomes approximately Laplace's equation (III, 6). So the probability flow along a bond in the $\underline{x}$ direction is given by $-(\frac{p_0}{3})\ \frac{\partial f}{\partial x}$, since $p(\underline{x}, \underline{y}) = \frac{p_0}{3}$ for $\underline{x}$ far from cluster $\mathcal{C}$, from equation (I, 3). Consequently, the total flow across a surface S is given approximately by a surface integral

$$\frac{J_{\lambda,\lambda}{}^{+}}{C_{\lambda}} = (\frac{p_0}{3})\int \frac{\partial f}{\partial n}\, dS \qquad \text{(III,14)}$$

where $\frac{\partial}{\partial n}$ denotes the outward normal derivative. At large distances, the solution of the difference equation (III,5) with boundary condition (III,8) has the same asymptotic form as that of Laplace's equation, namely

$$f(\underline{x}) = C_1 - \frac{K}{r} + 0(\frac{1}{r^2}) \qquad \text{(III,15)}$$

where K is independent of $\underline{x}$, but depends linearly on C_1 and $\frac{C_\lambda^+}{C_\lambda}$ and r is the Euclidean distance of the position vector $\underline{x}$ to the centre of gravity of the cluster $\mathcal{C}$.

We can assume that S is the surface of a large sphere with radius R and centre the origin. Then substituting (III,15) into (III,14) using spherical coordinates, the integral in (III,14) becomes equal to $4\pi r^2 \times \frac{\partial f}{\partial r} = 4\pi K$. We therefore have the equation

$$\frac{J_{\lambda\lambda^+}}{C_\lambda} = 4\pi(\frac{P_0}{3})K$$

combining this equation with (III,7) gives us

$$\frac{J_{\lambda\lambda^+}}{C_\lambda} = 4\pi(\frac{P_0}{3})K = \sum_{\substack{\underline{n}_2\in N_2 \\ \underline{n}_1\in N_1}} [p(\underline{n}_2,\underline{n}_1)f(\underline{n}_2) - p(\underline{n}_1,\underline{n}_2)f(\underline{n}_1)] \qquad \text{(III,16)}$$

We solved the difference equation (III,5) under boundary condition (III,11). Since those boundary condition are equivalent to formally putting $C_1 = 1$ and $C_\lambda^+/C_\lambda = 0$ in (III,2), we then obtain $a_{\lambda\lambda^+}$ as being equal to any one of the three quantities in (III,16). Remembering that in (III,11), $f(\underline{n}_1) = 0$ for all $\underline{n}_1\in N_1$, we can write for K and $a_{\lambda\lambda^+}$

$$a_{\lambda\lambda^+} = 4\pi(\frac{P_0}{3})K = \sum_{\substack{\underline{n}_2\in N_2 \\ \underline{n}_1\in N_1}} p(\underline{n}_2,\underline{n}_1)f(\underline{n}_2) \qquad \text{(III,17)}$$

This equation gives $a_{\lambda\lambda^+}$ and K in terms of the probabilities f(x).

III.3 Calculation of the Kinetic Coefficient $a_\ell(0)$

To solve numerically the difference equation (III,5) with boundary condition (III,11) we take a finite boundary B which completely contains the cluster $\mathcal{C}$, N_1 and N_2. For $\underline{x}$ on this boundary we take $f(\underline{x})$ to satisfy (III,15) to the first order in $\frac{1}{r}$.

$$f(\underline{x}) = 1 - \frac{K}{r} \qquad \underline{x}\epsilon B \tag{III,18}$$

This equation strictly speaking holds only when the boundary B recedes to infinity. In the case of $\ell = 1$ and 2, however, we found that when B is a cube of size 8, 9, 10, and using (III,18) as boundary condition, a_ℓ is the same to 0.1% for these three differently sized boundaries. Therefore we have omitted higher order terms like $\frac{1}{r^2}$ from the boundary condition (III,18) for $\underline{x}\epsilon B$. The constant K can be expressed numerically in terms of $f(\underline{x})$ using (III,17). One can then solve the difference equation for $f(\underline{x})$ by an S.O.R. method. We then obtain $a_{\lambda\lambda^+}$ from (III,17).

So far we have obtained $a_{\lambda\lambda^+}$, the probability that a given ℓ-cluster λ becomes an $(\ell+1)$-cluster. In our set of Becker Döring equations however, we have the average Kinetic constant a_ℓ for clusters of size ℓ. This is found by adding (III,1) over all the translationally inequivalent clusters λ of size ℓ. This gives us

$$J_{\ell} = \sum_{\lambda} J_{\lambda\lambda^+} = \sum_{\lambda} a_{\lambda\lambda^+} c_{\lambda} c_1 - \sum_{\lambda} b_{\lambda\lambda^+} c_{\lambda^+}$$

$$= \frac{\sum_{\lambda,\lambda^+} a_{\lambda,\lambda^+} c_{\lambda}}{\sum_{\lambda} c_{\lambda}} \times \sum_{\lambda} c_{\lambda} c_1 - \text{etc.}$$

Since $\sum_{\lambda} c_{\lambda} = c_{\ell}$, the total concentration of ℓ-clusters, comparing the coefficients of $c_{\ell} c_1$ in this equation with the definition (III,2) of $J_{\lambda\lambda^+}$ we have

$$a_{\ell} = \sum_{\lambda} a_{\lambda,\lambda^+} C_{\lambda} / \Sigma C_{\lambda} \qquad \text{(III,19)}$$

To simplify matters, we can assume that the ℓ-clusters of different shapes are in the same ratio as at equilibrium. This is a reasonable assumption for small ℓ because in the simulation, the non-equilibrium distribution of the size of the small clusters was found to be very close to an equilibrium distribution. This will therefore be probably true also of their shapes. Besides the Kinetic coefficient for a cluster of given size varies by at most 20% with a change in shape for sizes $\ell \leq 6$. Therefore assuming we have a canonical ensemble of ℓ-clusters at all times c_{λ} is proportional to $y^{n(\lambda)}$ where $y = e^{V/KT}$, and $n(\lambda)$ is the number of pairs of nearest neighbours in cluster λ. The mean value $a_{\ell}(0)$ of $a_{\lambda\lambda^+}$ for clusters λ of size ℓ in the limit of zero density is therefore:

$$a_{\ell}(0) = \frac{\sum_{\lambda,\lambda^+} a_{\lambda,\lambda^+} y^{n(\lambda)}}{\sum_{\lambda} y^{n(\lambda)}} \qquad \text{(III,20)}$$

where λ runs over all the translationally inequivalent clusters of size ℓ. In the first column of Table (III,i) we list a_{ℓ} for ℓ=1 to 6 calculated from the canonical average (III,20) with simulation parameters $\frac{V}{KT} = 1.5$, and transitional probabilities $p(\underline{x},\underline{y}) = \frac{p_i}{3}$ given by (I,1) and (I,3). To see the effect of

different averaging on the values of a_ℓ we also took a_ℓ to be the arithmetic mean of the $a_{\lambda\lambda^+}$, and the resulting value agreed to better than 1% for $\ell = 1$ to 6 with the canonical average given by (III,20).

In Table (III,ii) we also give values for $a_\ell(0)$, $\ell = 1$ to 6 for values of $\frac{V}{KT}$ in the range $-2.2 \leq \frac{V}{KT} \leq 2.2$. The range when $\frac{V}{KT}$ is less than zero corresponds to the situation when $p_0 > p_{-1}$, by equations (I,1) and (I,2). The situation $p_0 > p_{-1}$ can occur when both types of particles in a binary alloy are large compared with the lattice in which they are embedded, but in this case equation (I,1) does not hold.

Table (III,i) Kinetic Coefficients $a_\ell(0)$ in the limit of zero density for simulation parameters $\frac{V}{KT} = 1.5$, and $p_0 = \frac{1}{2}$. Transition probabilities $p(\underline{x},\underline{y}) = \frac{p_i}{3}$ with p_i given by (I,1) and (I,2).

ℓ	$a_\ell(0)$		
	by S.O.R. method canonical average (III,20)	from empirical equations (III,24) and (III,25)	Green's function (IV,17) and (IV,29)
1	2.29	2.34	2.30
2	2.81	2.78	2.80
3	3.17	3.12	
4	3.34	3.39	
5	3.63	3.63	
6	3.78	3.84	

Table (III,ii) Table of $a_\ell(0)$ the Kinetic coefficients in the limit of zero density for $\ell = 1$ to 6, for various temperatures. Constants M and N in the equation (III,24) $a_\ell(0)/D = (M+N\ell)^{1/3}$ are obtained by least squares for each temperature. $D = \frac{P_0}{3} = \frac{1}{6}$ is the diffusion constant of monomers.

$\gamma \equiv \frac{P_{-1}}{P_0} - 1$	$a_\ell(0)$ 1	2	3	4	5	6	M	N
-0.8	0.758	1.010	1.165	1.251	1.412	1.493	-35	125
-0.6	1.221	1.583	1.833	1.944	2.171	2.283	-38	435
-0.4	1.536	1.957	2.240	2.387	2.653	2.778	37	771
-0.2	1.764	2.217	2.534	2.699	2.976	3.118	169	1072
0.0	1.937	2.415	2.750	2.924	3.208	3.360	341	1324
0.2	2.077	2.567	2.922	3.086	3.383	3.533	558	1519
0.4	2.187	2.691	3.046	3.223	3.509	3.663	799	1663
0.6	2.279	2.792	3.149	3.325	3.609	3.761	1040	1776
0.8	2.359	2.876	3.233	3.405	3.671	3.826	1341	1837

III.4 Comparison of $a_\ell(0)$ with the diffusion theory of a spherical cluster.

We now relate the coefficient $a_\ell(0)$ found in the previous section with the prediction of classical diffusion theory for a spherical cluster. If we assume a large cluster of size ℓ to be spherical, we can then relate $a_\ell(0)$ to the diffusion constant D of monomers and the radius R_ℓ of the cluster

$$a_\ell(0) = 4\pi D R_\ell \qquad \text{(III,21)}$$

This formula holds for large ℓ. In the derivation of (III,21) (Chandrasekhar, 1954), (Penrose and Lebowitz 1978) it is assumed that all the small clusters are monomers.

The diffusion constant D for monomers can be easily obtained from equation (I,3). The equation (I,3) implies that in the limit of zero density, a monomer has a probability of $\frac{p_0}{3} = \frac{1}{6}$ per unit time of moving to each neighbouring site. Since there are six possible directions, the mean square displacement Δx^2 of a monomer per unit time $= \frac{p_0}{3} \times 6 = 1$. Einstein's relation then gives

$$D = \frac{\Delta x^2}{6\Delta t} = \frac{\frac{p_0}{3} \times 6}{6} = \frac{p_0}{3} = \frac{1}{6} \qquad \text{(III,22)}$$

This is twice the estimated value of D in Penrose et al (1978), which is incorrect.

Therefore to get $a_\ell(0)$ for a spherical cluster we substitute (III,22) into (III,21). Assuming the cluster to be a sphere of volume ℓ, we obtain

$$a_\ell(0) = 4\pi \times \frac{1}{6} \times \left(\frac{3\ell}{4\pi}\right)^{1/3} = 1.3\ \ell^{1/3} \qquad \text{(III,23)}$$

which is again twice the estimated value in this reference.

In the spirit of (III,21) we expect that $a_\ell(0)^3$ should be linear in ℓ for ℓ large. However, we found that for small ℓ also this approximate empirical formula holds:

$$a_\ell(0) \simeq D[M+N\ell]^{1/3} \qquad \text{(III,24)}$$

where $D = \frac{p_0}{3} = \frac{1}{6}$ is the diffusion constant of monomers. M and N are constant depending on the ratios $\frac{p_i}{p_0}$ but not on ℓ. For $\ell = 1$ to 6 and $\frac{V}{KT} = 1.5$, the constants are obtained graphically as

$$M = 874 \qquad N = 1888 \qquad \text{(III,25)}$$

In the second column of Table (III,i) we calculate $a_\ell(0)$ using (III,24) and (III,25). These values agree to about 2% with those in the first column of the same table which were calculated using canonical average (III,20).

The equation (III,24) hold also for a wide range of temperatures, as can be seen from Table (III,ii) and Fig.(III,i). In this table we give values of $a_\ell(0)$ for various values of γ in the range $-0.8 \le \gamma \le 0.8$ which correspond to the range $-2.2 \le \frac{V}{KT} \le 2.2$. In the last two columns we give values for M and N for each temperature using least squares. In Fig.(III,i) we plot the values in this table in the form $a_\ell(0)^3$ against ℓ, and for each temperature we obtain a straight line with a small intercept as predicted by (III,24). The accuracy of (III,24) is always better than 2% over this range of temperature. As already pointed out earlier, $\frac{V}{KT} \le 0$ simply implies the fact that $p_{-1} < p_0$.

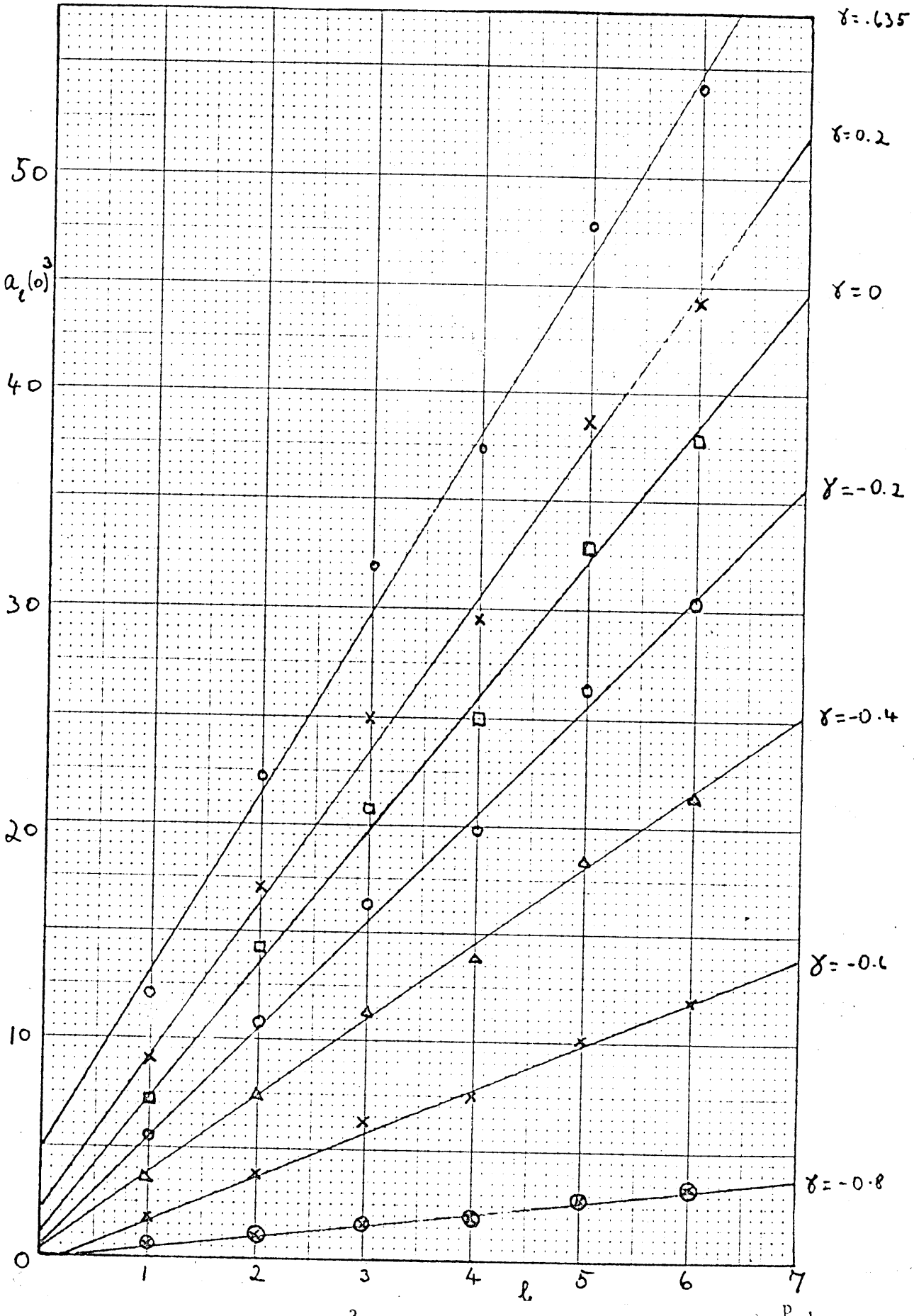

Fig (III,i): Graphs of $a_\ell(0)^3$ against ℓ for the range $-0.8 \leq \gamma \equiv \frac{p_{-1}}{p_0} - 1 \leq 0.8$. The points lie on a straight line with a small intercept, for each value of γ, as predicted by (III,24).

We are now in a position to compare the prediction (III,23) for a spherical cluster with the empirical formula (III,24). For large ℓ, one can neglect M and we can write $a_\ell(0) = D(N\ell)^{1/3}$ with $D = \frac{1}{6}$. For the simulation value $\frac{V}{KT} = 1.5$, we have N = 1888 from (III,25), and so

$$a_\ell(0) = 2.06\ell^{1/3} \qquad \text{(III,26)}$$

This asymptotic form for the kinetic coefficient $a_\ell(0)$ for clusters of size ℓ on a simple cubic lattice is considerably larger than the prediction (III,23) for a spherical cluster.

This is partly due to a temperature effect whereby $a_\ell(0)$ increases with an increase in temperature or equivalently an increase in p_{-1}. This can be seen in Table (III,ii) for the range $-2.2 \le \frac{V}{KT} \le 2.2$ and also in Fig.(III,i). It can be noticed that the estimates (III,22) and (III,23) based on diffusion theory for a spherical cluster depend only on p_0 and does not depend on p_{-1}. To show how $a_\ell(0)$ in Table (III,ii) increases with p_{-1} for fixed p_0, we plot the function $p_0/a_\ell(0)$ against p_0/p_{-1} for fixed ℓ in Fig. (III,ii). We do this for ℓ = 1 to 6 for the range $0.2 \le \frac{p_{-1}}{p_0} < 2$. For each ℓ we obtain a straight line. These straight lines meet one another approximately on this line $\frac{p_0}{p_{-1}} = -1$, and their slopes depend on ℓ. In fact we can write the empirical formula

$$\frac{p_0}{a_\ell(0)} = f(\ell)\left(1 + \frac{p_0}{p_{-1}}\right) + 0.06 \qquad \text{(III,27)}$$

This formula is accurate to better than 1% over the range considered. The equation (III,27) shows an increase of $a_\ell(0)$ with p_{-1}: in fact $\frac{1}{a_\ell(0)}$ is linear in $\frac{1}{p_{-1}}$ for fixed p_0 and fixed ℓ.

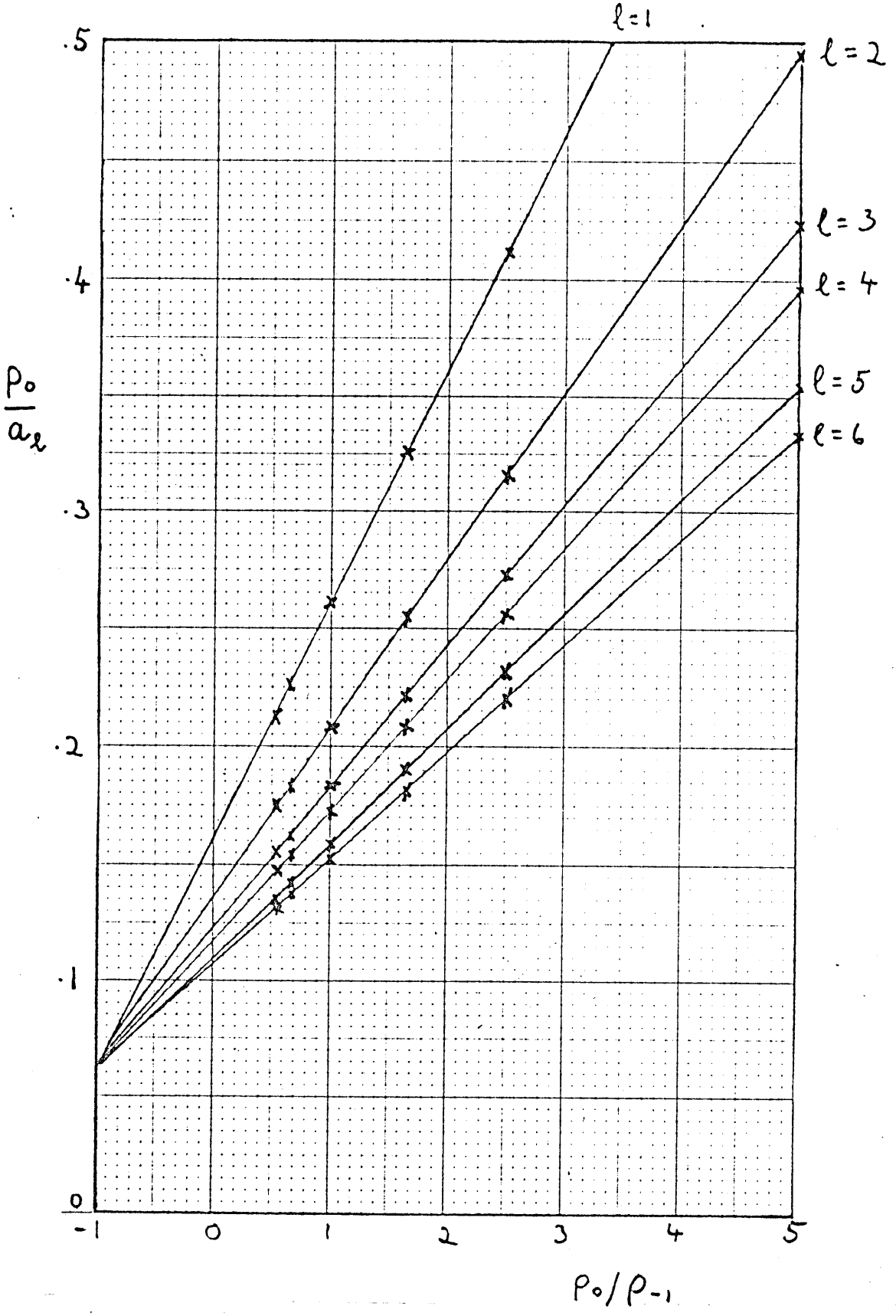

Fig (III,ii): Graphs of $\frac{p_0}{a_\ell(0)}$ against $\frac{p_0}{p_{-1}}$ for $1 \le \ell \le 6$ over the range $0.2 \le \frac{p_{-1}}{p_0} < 2$. The graphs for each integer ℓ are all straight lines meeting on the line $\frac{p_0}{p_{-1}} = -1$.

Table(III,iii) Here we list for various temperatures the individual $a_{\lambda\lambda^+}$ for sizes $\ell = 3$ and $\ell = 4$. For size $\ell = 3$ there are two types of clusters; for $\ell = 4$ there are 7 different shapes of clusters. We also give $a_3(0)$ and $a_4(0)$ calculated in the canonical average (III,20) of the individual $a_{\lambda\lambda^+}$.

$\gamma = \frac{p_{-1}}{p_0} - 1$	$a_{\lambda\lambda^+}$ 	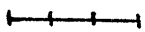	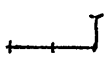				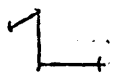	$a_4(0)$ from canonical average (III,20)			$a_3(0)$
-0.8	1.29	1.44	1.39	1.28	1.22	1.08	1.17	1.28	1.25	1.15	1.17
-0.6	1.97	2.19	2.11	1.99	1.91	1.73	1.83	1.97	1.91	1.79	1.81
-0.4	2.40	2.65	2.56	2.46	2.36	2.18	2.27	2.42	2.33	2.22	2.24
-0.2	2.69	2.96	2.86	2.78	2.69	2.50	2.57	2.73	2.62	2.51	2.53
0.0	2.91	3.20	3.09	3.02	2.92	2.73	2.79	2.96	2.83	2.73	2.75
0.2	3.07	3.38	3.25	3.19	3.10	2.90	2.95	3.13	3.00	2.90	2.92
0.4	3.20	3.52	3.39	3.33	3.23	3.02	3.08	3.26	3.13	3.02	3.04
0.6	3.31	3.64	3.49	3.43	3.33	3.12	3.18	3.36	3.23	3.13	3.15
0.8	3.40	3.74	3.58	3.51	3.42	3.20	3.26	3.45	3.32	3.21	3.23

Another reason for the discrepancy between (III,26) and (III,23) is the fact that the more compact a cluster λ is, the smaller is the value $a_{\lambda\lambda^+}$. This is readily seen in Table (III,iii) where we give the values $a_{\lambda\lambda^+}$ for all the cluster λ of sizes 3 and 4. We can take the number of nearest neighbouring sites of a cluster λ, or equivalently the number of sites in N_1, to be a measure of the compactness of λ. It can then be seen that the more compact a cluster λ is, the smaller is the value $a_{\lambda\lambda^+}$ for a given size ℓ. Thus the straight cluster of size 3, ⟝—⟞, has a value $a_{\lambda\lambda^+}$ which is about 3% higher than that for the bent cluster, ⌟ , for γ about .6 ($\frac{V}{KT} \simeq 1.5$). For clusters of size 4, $a_{\lambda\lambda^+}$ for the straight cluster, ⟝——⟞, is about 14% higher than that for the most compact 4-cluster ⊢ . For $\ell = 6$, $a_{\lambda\lambda^+}$ for the straight cluster is 4.12 and $a_{\lambda\lambda^+}$ for  is 3.34 at $\gamma = 0.2$, a discrepancy of about 20%. Conversely, for given size ℓ, clusters of intermediate compactness have intermediate values of $a_{\lambda\lambda^+}$ as can be seen for $\ell = 4$ in Table (III,iii).

Throughout this chapter we have assumed steady state diffusion. This is noticed in some real alloys. Thus, for example, Pedder (1978) reports that the coarsening of this cadmium oxide phase in silver - cadmium alloys is well modelled by a steady state diffusion theory in which the diffusion of cadmium atoms across to the larger cadmium clusters determines the rate of coarsening. In the simulation also, the concentration of the small clusters varies very little with time, so that we can justify our assumption of a steady state in the equation (III,5) and (III,6).

In the numerical solution of the Becker-Döring equations, to be described in Chapter VI, J_ℓ/C_ℓ is found to be less than 10^{-3} for the small clusters, and 10^{-2} for the larger clusters.

Chapter IV: Calculation of $a_1(0)$ and $a_2(0)$ in terms of $\gamma = \frac{p_{-1}}{p_0} - 1$, using the Green's function $G(\underline{r})$.

IV.1 The Green's Function $G(\underline{r})$

In this chapter we will check the S.O.R. calculation for $a_\ell(0)$ in the previous chapter by finding a_1 and a_2 in terms of the parameter $\gamma \equiv \frac{p_{-1}}{p_0} - 1$ using the Green's function $G(\underline{r})$ of the finite difference Laplacian. The coefficients a_1 and a_2 will be obtained as quotients of two polynomials in γ. As in the previous chapter we assume a low density.

As in Chapter III, we have to solve equation (III,5) for $f(\underline{r})$ under boundary conditions such as (III,11) in the presence of cluster C at the origin of coordinates. For sites $\underline{x}$ far from cluster C, the difference equation (III,5) reduces to the finite difference analogue of Laplace's equation, (III,6). We therefore introduce the Green's function $G(\underline{r})$ for the finite difference Laplacian which can be expressed using the difference operator Δ which is defined by

$$\Delta G(\underline{r}) = \sum_{i=1}^{6} [G(\underline{r}+\underline{e}_i) - G(\underline{r})] \qquad \text{(IV,1)}$$

where the sum is over the six neighbours $\underline{r}+\underline{e}_i$ of $\underline{r}$. We can then define G(r) as

$$\begin{aligned} &\Delta G(\underline{r}) = 0 \qquad r \neq 0 \\ &\Delta G(\underline{0}) = 4\pi \qquad \text{(IV,2)} \\ &\text{and } G(\underline{r}) = \frac{1}{r} + o\left(\frac{1}{r^2}\right) \text{ for large } r \end{aligned}$$

where r is the Pythagorean length of the vector $\underline{r}$. Since $G(\underline{r})$ depends only on this magnitude of $\underline{r}$, $G(\underline{r})$ is symmetrical about the origin, and if $\underline{r} = (r_x, r_y, r_z)$, then $G(r_x, r_y, r_z) = G(-r_x, r_y, r_z) = G(r_y, -r_x, -r_z) =$ etc. Also

the equations (IV,2) define a unique G because if there were two G's satisfying (IV,2), the difference $d(\underline{r})$ will satisfy $\Delta d(\underline{r}) = 0$ for all $\underline{r}$ using the linearity of the operation Δ, and also $d(\underline{r}) = 0$ for large $\underline{r}$. The two conditions imply that $d(\underline{r}) = 0$ everywhere and hence $G(\underline{r})$ is unique (Isaacson and Keller, 1966).

We found G numerically using equation (IV,3) and the boundary condition $G(\underline{r}) = \frac{1}{r}$ for $r \in B$ where B is a big boundary which contains the origin. We used an SOR method to solve for G for different cubes of edges 18, 20, 22, and we found that the solution does not depend on the size of the boundary used. In the program to do this, we used the symmetry properties of $G(\underline{r})$. The values of $G(\underline{r})$ for small r are shown in Table (IV,i).

IV.2 To calculate $a_1(0)$ in terms of $\gamma \equiv \frac{P_{-1}}{P_0} - 1$ in the limits of zero density.

To find $a_1(0)$ we consider a monomer ϵ situated at the origin of coordinates of the simple cubic lattice Σ. See Fig.(IV,i). The monomer is denoted by ● in this figure. The set N_1 of nearest neighbours of the cluster ϵ consists of the six vectors e_i, i = 1 to 6, when e_i are the vectors (1,0,0), (-1,0,0) etc. These are denoted by . in Fig.(IV,i), where we give only an x-y section through the origin for clarity. The set N_2 of the second nearest neighbours

Table (IV, i) Table of the Green's function $G(\underline{r})$ and the function $H^i(\underline{r})$ for a_1 from (IV, 5), and the function $G^i(\underline{r})$ for a_2 from (IV, 22), for relevant values of $\underline{r}$.

$\underline{r}$	$G(\underline{r})$	$H^1(\underline{r})$	$H^2(\underline{r})$	$G^1(\underline{r})$	$G^2(\underline{r})$	$G^3(\underline{r})$	$G^4(\underline{r})$
000	3.176						
100	1.081	8.3244	3.2341				
110	0.6935	8.9867	2.8316	.7722	4.3233	4.1485	5.2572
111	0.5476	6.9411	2.5488	.7036	3.7506	3.7276	6.9200
200	0.5389	5.6632	4.8409	1.3369	5.6108	3.2160	3.7968
210	0.4515	5.4166	2.7136	0.9388	6.3294	3.2037	3.7506
120	"			0.6299	3.2037	6.1206	3.7276
211	0.4016						
220	0.3525						
221	0.3287						
222	0.2846						
300	0.3461	3.9952	2.3939	3.3783	3.7552	2.5196	2.8144
310	0.3207						
311	0.3019						
320	0.2773						
400	0.2549						
410	0.2452						
500	0.2022						

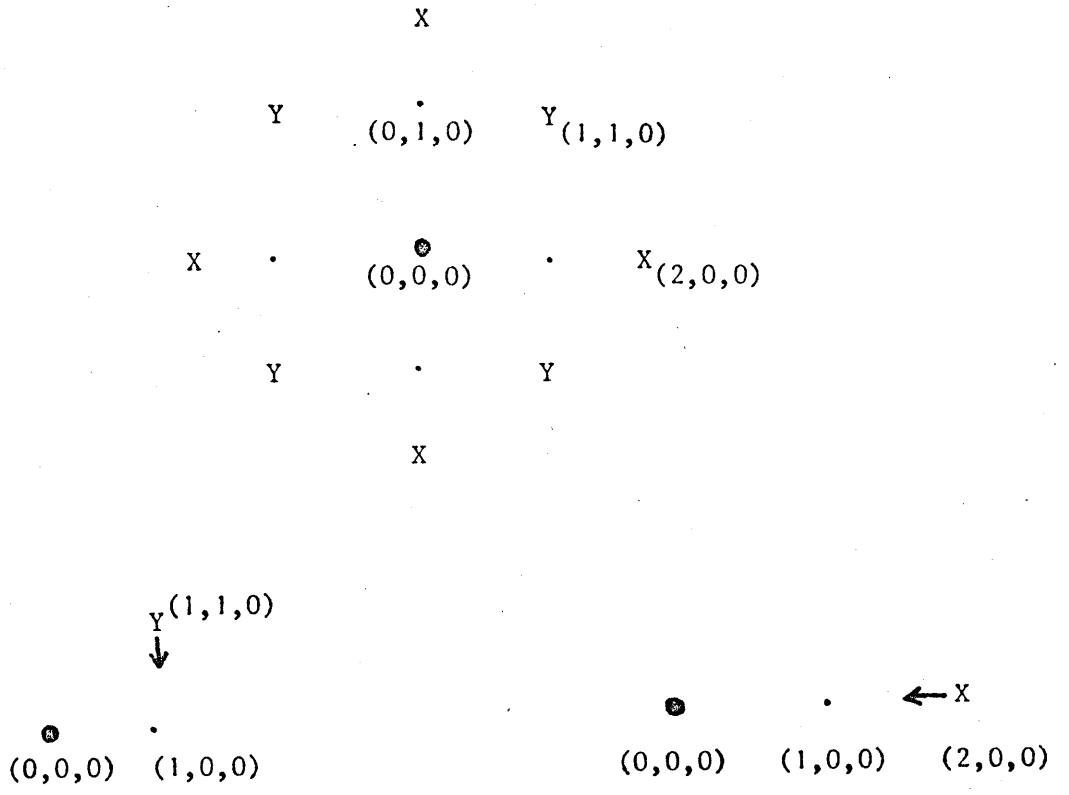

Fig.(IV,i). The first diagram shows a monomer ● at the origin. For clarity we show only the x-y plane. The sites marked • are the nearest neighbours of the central cluster ● , and are the sites such as (1,0,0) (-1,0,0) etc. There are six sites in N_1, the set of nearest neighbours of the central cluster. The set of second nearest neighbours N_2 consists of 18 sites marked X and Y, shown separately in the second and third diagrams. The sites Y are sites like (1,1,0), (-1,1,0), etc of which there are 12 in number. The Y sites are sites like (2,0,0), (0,2,0) etc. and there are 6 of these.

of the monomer $\mathcal{C}$ consists of eighteen lattice sites: 6 sites marked X which are sites such (1,1,0), (-1,1,0) etc., and 12 sites marked Y, which are sites of the form (2,0,0), (-2,0,0) etc. The six sites marked X have the same symmetry relative to the origin, and so do the 12 sites marked Y. These symmetries are shown separately in the second and third diagram in Fig.(IV,i).

The function $f(\underline{r})$ for the monomer case is by definition the probability that site $\underline{r}$ is occupied by a monomer given there is a monomer at the origin. Then $f(\underline{r})$ has to satisfy the difference equation (III,5) as in Chapter III. As in (III,8), the boundary condition for large $\underline{r}$ is $f(\underline{r}) \to C_1$. For sites such as (1,0,0), that is $\underline{r} \in N_1$, $f(\underline{r})$ can be taken to be zero as in (III,11), because by (III,9), f_{100} is proportional to C_2/C_1, rather than C_1. For this problem therefore, we can take $f(\underline{r})$ to satisfy the boundary conditions

$$f(\underline{r}) \to C_1 \qquad \underline{r} \to \infty$$

$$f_{100} = 0$$

This is analogous to equation (III,11). The function $f(\underline{r})$ is thus linear in C_1 as in Chapter III.

Since $f(\underline{r})$ satisfies Laplace's finite difference equation (III,6) for sites $\underline{x} \in \Sigma-(\mathcal{C} \cup N_1 \cup N_2)$ and since $f(\underline{r}) \simeq C_1 - \frac{K}{r}$ for large r, as (III,18), it can be easily checked using the properties (IV,2) of $G(\underline{r})$ that these two properties are automatically satisfied if we write $f(\underline{r})$ as

$$f(\underline{r}) = C_1 + \sum_{\underline{y} \in N_2} G(\underline{r}-\underline{y})g(\underline{y}) + h(\underline{r}) \qquad \text{(IV,3)}$$

where $h(\underline{r}) = 0$ for all $\underline{r}$ not in N_1

In (IV,3), $g(\underline{y})$ are unknown coefficients linear in C_1 and C_2/C_1, and the summation is over the sites $\underline{y}$ in N_2, the set of second nearest neighbours of the cluster $\mathcal{C}$. The problem for finding $f(\underline{r})$ is therefore reduced to finding $g(\underline{y})$ for $\underline{y}\varepsilon N_2$ and $h(\underline{r})$ for $\underline{r}\varepsilon N_1$. Since for $\underline{r}\varepsilon N_2$, $f(\underline{r})$ has to satisfy (III,5), the quantities $g(\underline{y})$ and $h(\underline{r})$ are obtained by considering (IV,3) at the sites $\underline{r}\varepsilon N_2$. This will be done later on in this section.

In equation (IV,3) two coefficients $g(\underline{x})$ and $g(\underline{y})$ are equal if the two vectors $\underline{x}$ and $\underline{y}$ in N_2 have the same symmetry relative to the central cluster. Therefore when the central cluster is a monomer at (0,0,0) as in Fig.(IV,i), the vectors (1,1,0), (1,-1,0), etc have the same symmetry relative to the origin, and so $g(1,1,0) = g(1,-1,0) = \text{etc}$, which value we denote by g_1; similarly $g(2,0,0) = g(0,-2,0) = \text{etc}$. These are denoted by g_2. One can then add together the quantities $G(\underline{r}-\underline{y})$ for those $\underline{y}\varepsilon N_2$ with the same symmetry to simplify the mathematics. For monomers, therefore, we can write (IV,3) as

$$f(\underline{r}) = c_1 + g_1 H^1(\underline{r}) + g_2 H^2(\underline{r}) + h(\underline{r}) \qquad \text{(IV,4)}$$

where $h(\underline{r}) \neq 0 \Leftrightarrow \underline{r} = (1,0,0)$, $(-1,0,0)$ etc., and $H^1(\underline{r})$ and $H^2(\underline{r})$ are linear combinations $\sum_{\underline{y}} G(\underline{r}-\underline{y})$ for those $\underline{y}$ in N_2 having the same symmetry. The functions $H^1(\underline{r})$ and $H^2(\underline{r})$ are therefore defined explicitly as:

$$\begin{aligned} H^1(\underline{r}) = {} & G(\underline{r} - \overline{110}) + G(\underline{r} - \overline{101}) + G(\underline{r} - \overline{0,1,1}) \\ & + G(\underline{r} - \overline{-110}) + G(\underline{r} - \overline{-101}) + G(\underline{r} - \overline{0-11}) \\ & + G(\underline{r} - \overline{-1-10}) + G(\underline{r} - \overline{-10-1}) + G(\underline{r} - \overline{0-1-1}) \end{aligned}$$

and (IV,5)

$$\begin{aligned} H^2(\underline{r}) = {} & G(\underline{r} - \overline{200}) + G(\underline{r} - \overline{020}) + G(\underline{r} - \overline{002}) \\ & + G(\underline{r} - \overline{-200}) + G(\underline{r} - \overline{0-20}) + G(\underline{r} - \overline{00-2}) \end{aligned}$$

In Table (IV,i) we give the values of $H^1(\underline{r})$ and $H^2(\underline{r})$ in the third and fourth columns for relevant values of $\underline{r}$ using the values $G(\underline{r})$ given in the second column of that table.

Using the boundary property $G(\underline{r}) = \frac{1}{r}$ for large r, one can easily relate the constant K defined in (III,15) to the quantities $g(\underline{y})$ in (IV,3) or g_i's in (IV,4). Comparing the coefficients of $\frac{1}{r}$ in the two equations we have the relation

$$K = -\sum_{\underline{y}\in N_2} g(\underline{y}) = -(12g_1 + 6g_2)$$

since $g(\underline{r}) = g_1$ for the twelve vectors (1,1,0), (1,-1,0), etc and $g(\underline{r}) = g_2$ for the six vectors (2,0,0), etc. Equation (III,16) then gives us the relation

$$\frac{J_1}{C_1} = -4\pi\left(\frac{\rho_0}{3}\right)(12g_1 + 6g_2) \qquad \text{(IV,6)}$$

Comparing (IV,6) with (IV,2), since $\frac{J_1}{C_1}$ and g_1 and g_2 are linear in C_1, we then get a_1 as the coefficient of C_1 in the right hand side of (IV,6). We now find g_1 and g_2 in terms of the physical quantities C_1, C_2, p_i, and $\gamma = \frac{p_{-1}}{p_0} - 1$.

The quantities g_1 and g_2 can be obtained by considering the difference equation (III,5) on the sites where it varies from the finite difference analogue of Laplace's equation, namely the sites in N_2 eg. the sites (1,1,0) and (2,0,0). Writing the difference equation (III,5) for (2,0,0) and dividing by $\frac{p_0}{3}$ we obtain

$$f_{300} + 4f_{210} - 5f_{200} + \left[\frac{p_1}{p_0} f_{100} - \frac{p_{-1}}{p_0} f_{200}\right] = 0 \qquad \text{(IV,8)}$$

We now consider the definition of Δ, defined in (IV,1), operating on $f(2,0,0)$ and we then subtract this from (IV,8) thus obtaining

$$\Delta f_{200} = \alpha f_{100} + \gamma f_{200} \qquad \text{(IV,9)}$$

where

$$\alpha = 1 - \frac{p_1}{p_0} \quad \text{and} \quad \gamma = \frac{p_{-1}}{p_0} - 1 \qquad \text{(IV,10)}$$

One can easily find $\Delta f(\underline{r})$ in terms of $\Delta H^1(\underline{r})$ and $\Delta H^2(\underline{r})$. In fact using (IV,5), (IV,2) and the linearity of Δ we have

$$\Delta H^1(1,1,0) = \Delta H^2(2,0,0) = -4\pi$$
$$\text{and } \Delta H^i(\underline{r}) = 0 \qquad \text{otherwise} \qquad \text{(IV,11)}$$

We then apply the operator Δ to (IV,4) for the sites $\underline{r} = (2,0,0)$ and $(1,1,0)$. By the linearity of Δ we obtain

$$\Delta f_{200} = -4\pi g_2 + h_{100}$$
$$\text{and } \Delta f_{110} = -4\pi g_1 + 2h_{100} \qquad \text{(IV,12)}$$

Then substituting for Δf_{200} from (IV,12) into (IV,9) we obtain the relation

$$-4\pi g_1 + h_{100} = \alpha f_{100} + \gamma f_{200} \qquad \text{(IV,13)}$$

Doing a similar analysis for f_{110} we obtain the analogue of (IV,13) as

$$-4\pi g_1 + 2h_{100} = 2\alpha f_{100} + 2\gamma f_{110} \qquad \text{(IV,14)}$$

We can then use the fact that $f_{100} = 0$, and the equation (IV,4) for $\underline{r} = (1,0,0)$, $(1,1,0)$ and (200) to eliminate h_{100}, f_{110} and f_{200} from the two equations (IV,13) and (IV,14) to obtain two simultaneous equations for g_1 and g_2 in terms only of c_1, c_2 γ and α. Doing this procedure respectively on (IV,13) and [(IV,14) - 2×(IV,13)] we obtain:

$$g_2[-4\pi - H^2_{100} - \gamma H^2_{200}] + g_1[-H^1_{100} - \gamma H^1_{200}]$$

$$= c_1(1+\gamma)$$

$$g_2[8\pi - 2\gamma(H^2_{110} - H^2_{200})] - g_1[4\pi + 2\gamma(H^1_{110} - H^1_{200})] = 0$$

In these two equations we then substitute the values of H^i_{xyz} which are given in Table (IV,i) for relevant values of $\underline{r} = (x,y,z)$. We then obtain

$$g_2[-15.8005 - 4.8409\gamma] + g_1[-8.9867 - 5.6632\gamma] = c_1(1+\gamma)$$

$$g_2[25.1327 - 4.0186\gamma] + g_1[-12.5664 - 6.6470\gamma] = 0$$

Solving for g_1 and g_2 we then obtain these formulae:

$$g_1 = \frac{-[c_1(1+\gamma)] \times [2.0093\gamma+4\pi]}{203.88 + 170.82\gamma + 27.468\gamma^2}$$

$$g_2 = \frac{-[c_1(1+\gamma)] \times [3.3235\gamma+2\pi]}{203.88 + 170.82\gamma + 27.468\gamma^2} \qquad \text{(IV,15)}$$

We can then substitute these equations into (IV,6) for J_1/C_1 and we then have the equation

$$\frac{J_1}{C_1} = \frac{3.873(1+0.233\gamma)}{1 + 0.833\gamma + 0.1347\gamma^2} p_{-1} c_1 \qquad \text{(IV,16)}$$

The coefficient of C_1 in this equation then gives us $a_1(0)$ as the ratio of two polynomials in $\gamma = \frac{p_{-1}}{p_0} - 1$:

$$a_1(0) = \frac{3.873(1+0.233\gamma)\ p_{-1}}{1 + 0.833\gamma + 0.1347\gamma^2} \qquad \text{(IV,17)}$$

To check (IV,17) we shall calculate $\frac{\partial c_2}{\partial t}$, and a_1 will be the coefficient of c_1^2 in this formula. Considering the various ways in which a particle can go to or move from (1,0,0) in one move, and remembering that by symmetry $f_{110} = f_{1-10} = f_{101} =$ etc, and that $p(\underline{x},\underline{y}) = \frac{p_i}{3}$, we have

$$\frac{\partial c_2}{\partial t} = C_1 \times 6 \frac{\partial f_{100}}{\partial t}$$

$$= C_1 \times 6\{(\frac{p_{-1}}{3})(f_{200}+4f_{110}) - 5(\frac{p_{+1}}{3})f_{100}\} \qquad \text{(IV,18)}$$

where the factor 6 occurs because a monomer has six neighbouring sites at which a dimer can form. Then substituting (IV,4) into (IV,18) we obtain for $f_{100} = 0 = c_2$,

$$\frac{\partial c_2}{\partial t} = 2p_{-1}[5c_1 + \overline{H^1_{200}+4H^1_{110}}g_1 + \overline{H^2_{200}+4H^2_{110}}g_2]c_1$$

$$= 2_{p-1}[5c_1 + 41.61g_1 + 16.167g_2]c_1 \qquad \text{(IV,19)}$$

on using the values of H^i from Table (IV,i). One can then substitute the equation (IV,15) for g_1 and g_2, using (II,1), (II,2) with $c_2 = c_3 = 0$, and again we arrive at the equation (IV,16), and hence the same value for a_1 as in (IV,17). This also serves as a numerical check for a_1.

IV.3 To calculate $a_2(0)$ in terms of $\gamma = \frac{p_{-1}}{p_0} - 1$ in the limit of zero density.

To find $a_2(0)$ we have to solve (III,5) for $f(\underline{r})$, but this time we have a dimer as the central cluster. We assume the dimer is situated at (0,0,0) and (1,0,0). See Fig.(IV,ii). The dimer is denoted by ●——● . The sites adjacent to the dimer are denoted by • and are ten in all. The set of second nearest neighbours N_2 contain 26 sites in all and they fall under four separate symmetries relative to the central dimer. These four

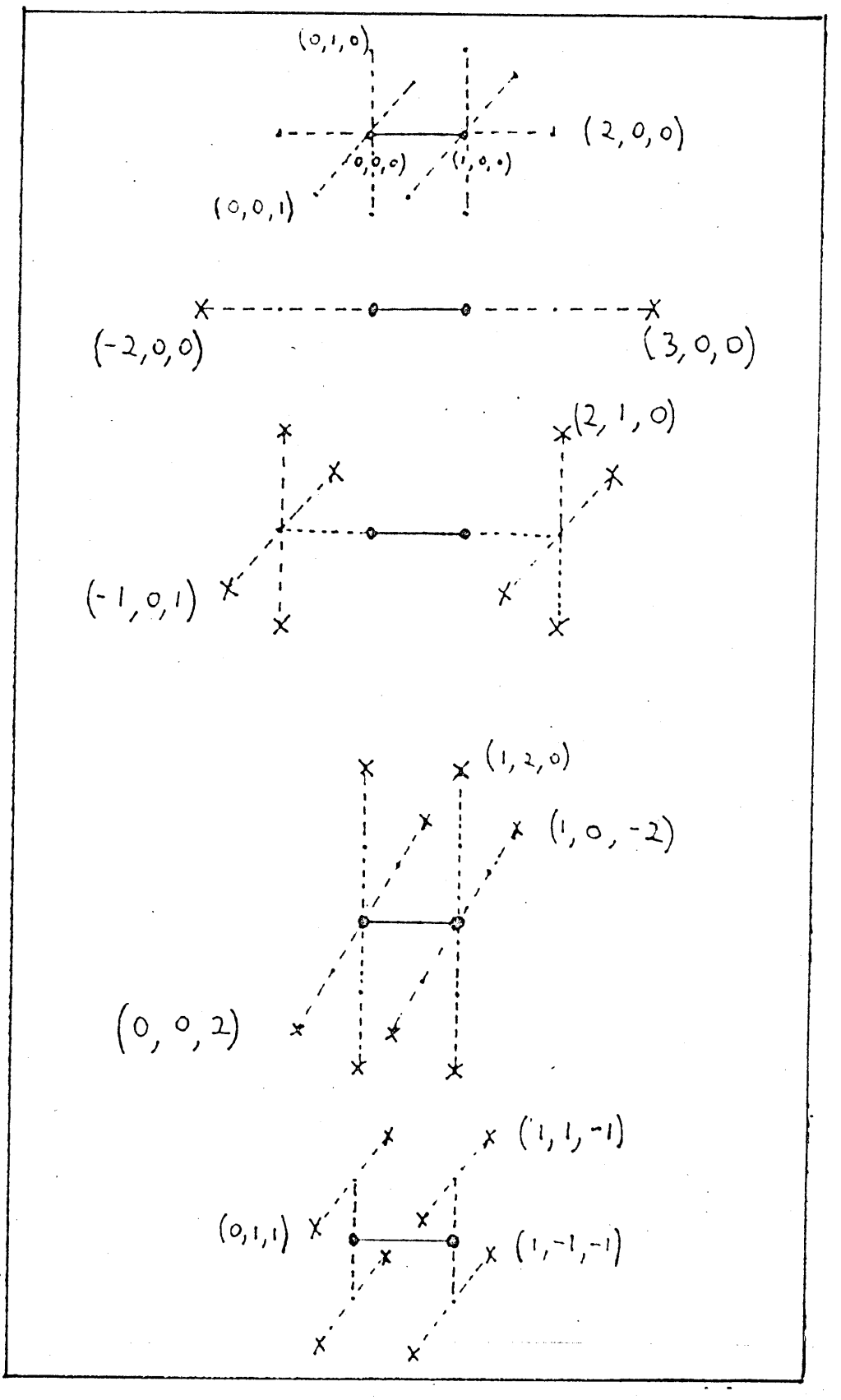

Fig (IV,ii) Illustration showing a dimer at (0,0,0) and (1,0,0) and its ten nearest neighbours. We also show the four symmetries of the second nearest neighbours with respect to the central dimer.

symmetries are shown separately in four diagrams in Fig.(IV,ii) and are denoted by X. The first equivalence class contains two sites : (-2,o,o) and (3,o,o). This is the axial symmetry. The other three equivalence classes each contain 8 sites. Vectors such as (2,1,o),(1,2,o) and (o,1,1) belong to each of these three equivalence classes.

The function $f(\underline{r})$ which satisfies (III,5) for the dimer case has to satisfy also certain boundary conditions which are different from the monomer case. For large r, the boundary condition is unchanged, so $f(\underline{r}) \to c_1$ for large $\underline{r}$. For $\underline{r} \epsilon N_1$, however, that is for sites r like (2,0,0) and (1,1,0), $f(\underline{r})$ is proportional to C_3/C_2 and in a way similar to (III,11), we can formally require $f(\underline{r}) = 0$ for sites $\underline{r}$ such as (2,0,0) and (1,1,0). The boundary conditions then are

$$f(\underline{r}) \to C_1 \text{ for } \underline{r} \text{ large}; \quad f(\underline{r}) = 0 \text{ for } \underline{r} \epsilon N_1 \qquad \text{(IV,20)}$$

The function $f(\underline{r})$ is then linear in C_1.

As in the monomer case, $f(\underline{r})$ for the dimer case has to satisfy certain symmetry properties. It is easy to observe from the first diagram in Fig.(IV,ii) that symmetry about the plane $x = \frac{1}{2}$, and symmetry about the x-axis lead to the equations

$$f(x+1, y, z) = f(-x, y, z) \quad \forall_{x>0}$$

and $f(x,y,z) = f(x,-y,z) = f(x,z,y) = \text{etc.}$

To solve for $f(\underline{r})$ in the dimer case we can write analogously to (IV,3) and (IV,4) the formula

$$f(\underline{r}) = C_1 + \sum_{i=1}^{4} g_i G^i(\underline{r}) + h(\underline{r}) \qquad \text{(IV,21)}$$

where the summation is over the four symmetries of the sites in N_2,

g_i depend on c_1, c_3/c_2, p_i but are independent of r, $h(\underline{r}) \neq 0 \Leftrightarrow \underline{r} \propto N_1$ i.e. if $\underline{r}$ is a nearest neighbouring site of a dimer. The quantities $G^i(\underline{r})$ are linear combinations $\Sigma^i_{\underline{n}\in N_2} G(\underline{r}-\underline{n})$ where the sum Σ^i is over the vectors $\underline{n}$ in N_2 having the same symmetry i. Explicitly the $G^i(\underline{r})$ for the four symmetries i=1 to 4, shown respectively in the last four diagrams in Fig. (IV,ii), are given by

$$G^1(\underline{r}) = G(\underline{r} - \overline{300}) + G(\underline{r} - \overline{-200})$$

$$\begin{aligned} G^2(\underline{r}) = {} & G(\underline{r} - \overline{210}) + G(\underline{r} - \overline{-110}) \\ & + G(\underline{r} - \overline{-1-10}) + G(\underline{r} - \overline{2-10}) \\ & + G(\underline{r} - \overline{-10-1}) + G(\underline{r} - \overline{-101}) \\ & + G(\underline{r} - \overline{201}) + G(\underline{r} - \overline{20-1}) \end{aligned}$$

$$\begin{aligned} G^3(\underline{r}) = {} & G(\underline{r} - \overline{020}) + G(\underline{r} - \overline{120}) \\ & + G(\underline{r} - \overline{0-20}) + G(\underline{r} - \overline{1-20}) \\ & + G(\underline{r} - \overline{002}) + G(\underline{r} - \overline{102}) \\ & + G(\underline{r} - \overline{00-2}) + G(\underline{r} - \overline{10-2}) \end{aligned}$$

$$\begin{aligned} G^4(\underline{r}) = {} & G(\underline{r} - \overline{011}) + G(\underline{r} - \overline{111}) \\ & + G(\underline{r} - \overline{01-1}) + G(\underline{r} - \overline{11-1}) \\ & + G(\underline{r} - \overline{0-11}) + G(\underline{r} - \overline{1-11}) \\ & + G(\underline{r} - \overline{0-1-1}) + G(\underline{r} - \overline{1-1-1}) \end{aligned}$$

(IV,22)

The $G^i(\underline{r})$ are given in Table (IV,i) for relevant values of $\underline{r}$. It is easy to show using the definition of G and G^i, and the linearity of the operation Δ that

$$\Delta G^1_{300} = \Delta G^2_{210} = \Delta G^3_{120} = \Delta G^4_{111} = -4\pi$$

(IV,23)

$$\Delta G^i(\underline{r}) = 0 \quad \text{for } \underline{r} \text{ not in the same equivalence class as any of } (3,0,0),(2,1,0),(1,2,0),(1,1,1).$$

Using the boundary property $G(\underline{r}) = \frac{1}{r}$ for large r, one can easily relate the constant K in (III,15) to the quantities g_i in (IV,21). In the same way as the derivation of (IV,6) we have

$$\frac{J_2}{C_2} = -4\pi(\frac{p_0}{3})(2g_1 + 8g_2 + 8g_3 + 8g_4) \qquad \text{(IV,24)}$$

In this equation the coefficient of g_i in the degeneracy of each symmetry and $\frac{p_0}{3}$ is the value of $p(\underline{x},\underline{y})$ far from the central dimer in the limit of zero density. The coefficients g_i are linear in C_1, and the coefficient of C_1 in the right hand side of (IV,24) then gives a_2.

To find g_i, we proceed as for a_1. We write the equation (III,5) for the sites P in N_2. From this we then subtract the corresponding identity for $\Delta f(\underline{r})$ given by (IV,1). Using (IV,23) and the linearity of Δ we arrive at the equations

$$\Delta f_{120} = -4\pi g_3 + h_{110} = \alpha f_{110} + \gamma f_{120} \qquad \text{(a)}$$

$$\Delta f_{300} = -4\pi g_1 + h_{200} = \alpha f_{200} + \gamma f_{300} \qquad \text{(b)}$$

$$\Delta f_{210} = -4\pi g_2 + h_{110}+h_{200} = \alpha(f_{110}+f_{200}) + 2\gamma f_{210} \qquad \text{(c)}$$

$$\Delta f_{111} = -4\pi g_4 + 2h_{110} = 2\alpha f_{110} + 2\gamma f_{111} \qquad \text{(d)}$$

The quantities h_{200} and h_{110} can be eliminated by using equations (IV,21) and the second boundary condition in (IV,20) for sites $\underline{r}$ in N_1. We then have

$$0 = f_{110} = C_1 + \sum_1^4 g_i G^i_{110} + h_{110} \qquad \text{(e)}$$

and

$$0 = f_{200} = C_1 + \sum_1^4 g_i G^i_{200} + h_{200} \qquad \text{(f)}$$

In the simultaneous equations (a)-(d), we can eliminate f_r and h_r

using (IV,21) , (e) and (f)。 The coefficients of g_i will then depend only on C_1 , γ,α and the G^i's。 Having done these eliminations and substitutions, we take linear combinations as follows for simplicity:

$$
\begin{aligned}
&2\times(a)-(d): && -4\pi(2g_3-g_4) &&= 2\gamma\sum_1^4 g_i(G^i_{120}-G^i_{111})\\
&(a)+(b)-(c): && -4\pi(g_3+g_1-g_2) &&= \gamma\sum_1^4 g_i(G^i_{120}+G^i_{300}-2G^i_{210})\\
&(a)-(b) && 4\pi(g_1-g_3) + \sum_1^4 g_i\left[(G^i_{200}-G^i_{110})+\gamma(G^i_{300}-G^i_{120})\right] &&= 0\\
&(b) && 4\pi g_1 + \sum_1^4 g_i(G^i_{200}+\gamma G^i_{300}) &&= -C_1(1+\gamma)
\end{aligned}
\qquad \text{(IV,25)}
$$

When we substitute the values of $G^i(r)$ into (IV,25) and write the equations in matrix form, we have

$$
\begin{bmatrix}
-0.737\gamma & -0.5469\gamma & 4\pi+2.393\gamma & -2\pi-3.1924\gamma\\
4\pi+2.1306\gamma & -4\pi-5.6999\gamma & 4\pi+2.2328\gamma & 0.9592\gamma\\
13.1308+2.748\gamma & 1.2875+0.5515\gamma & -13.499+3.60185\gamma & -1.4586-0.9132\gamma\\
13.903+3.3783\gamma & 5.6108+3.7552\gamma & 3.216+2.5196\gamma & 3.7986+2.8144\gamma
\end{bmatrix}
\begin{bmatrix} g_1\\ g_2\\ g_3\\ g_4 \end{bmatrix}
=
\begin{bmatrix} 0\\ 0\\ 0\\ A \end{bmatrix}
\qquad \text{(IV,26)}
$$

with $A = -C_1(1+\gamma)$

The g_i's are then found by Cramer's rule in terms of the parameter γ. Denoting the Cramer determinant by det we have for g_i and det the equations

$$
\begin{aligned}
\det &= 628.901(66.795+103.330\gamma+55.777\gamma^2+12.539\gamma^3+\gamma^4) \\
\det xg_1 &= 72.312(16.520+20.662\gamma+8.121\gamma^2+\gamma^3)A \\
\det xg_2 &= 42.841(54.471+46.806\gamma+12.257\gamma^2+\gamma^3)A \\
\det xg_3 &= 53.810(21.153+24.861\gamma+9.079\gamma^2+\gamma^3)A \\
\det xg_4 &= 31.331(72.675+55.395\gamma+13.179\gamma^2+\gamma^3)A
\end{aligned}
\qquad \text{(IV,27)}
$$

We can then use equation (IV,24) and (V,27) to give us J_2/C_2 in terms of α,γ and c_1:

$$\frac{J_2}{C_2} = \frac{4.825(1+0.901\gamma+0.260\gamma^2+0.024\gamma^3)}{1+1.547\gamma+0.835\gamma^2+0.187\gamma^3+0.015\gamma^4} p_{-1}c_1 \qquad \text{(IV,28)}$$

where again the detailed balance condition is satisfied. The coefficient of c_1 is a_2 which is then given by

$$a_2 = \frac{4.825(1+0.901\gamma+0.260\gamma^2+0.024\gamma^3)p_{-1}}{1+1.547\gamma+0.835\gamma^2+0.187\gamma^3+0.015\gamma^4} \qquad \text{(IV,29)}$$

We can check (IV,29) by calculating $\frac{\partial c_3}{\partial t}$, and a_2 is then the coefficient of c_1c_2 in this formula. We can again assume that the ratios of the concentration of various 3-sized clusters of different shapes and orientation are the same as at equilibrium. Since given a dimer at (0,0,0) and (1,0,0), a cluster of size 3 can be formed by absorbing a monomer at one of the 8 sites isomorphic to (1,1,0) or at one of the two sites (2,0,0) or (-1,0,0), we can write

$$C_3 = C_2[8f_{110} + 2f_{200}]$$

We can then find the derivative of c_3 with respect to time by considering how a monomer can go to or move from (1,1,0) and (2,0,0). We use the symmetry of f in the dimer case, and the form for $f(\underline{r})$ given in (IV,21), and the fact that $p(\underline{x},\underline{y}) = \frac{p_i}{3}$ to obtain:

$$\frac{\partial c_3}{\partial t} = \beta c_2\left[\frac{p_{-1}}{3}(2f_{111}+f_{120}+f_{210}) - 4p_1 f_{110}\right]$$

$$+\alpha c_2\left[\frac{p_{-1}}{3}(f_{300}+4f_{210}) - 5p_1 f_{200}\right]$$

$$= 2c_2\left[7p_{-1}C_1 + \sum_{i=1}^{4}(8\overline{G^i_{111}+G^i_{210}}+4G^i_{120}+G^i_{300})g_i\right]$$

$$+ \text{terms proportional to } c_3$$

$$= 2c_2[7p_{-1}c_1+19.0371g_1+97.21g_2+82.452g_3+103.09g_4]$$

where we have substituted the relevant value of $G^i(\underline{r})$ from Table (IV,i). From (IV,27) we can then substitute for g_i into the above expression for $\frac{\partial c_3}{\partial t}$ and we obtain the same formula as (IV,28). This therefore gives the same expression for $a_2(0)$ as (IV,29).

Table (IV,ii) The Kinetic coefficients $a_1(0)$ and $a_2(0)$ in the limit of zero density calculated by the Green's function method, and compared with S.O.R. results from previous chapters. A closed formula for $a_1(0)$ and $a_2(0)$ are given in equations (IV,17) and (IV,29).

$\gamma = \frac{p_{-1}}{p_0} - 1$	a_1		a_2	
	from Green's function (IV,17)	from S.O.R. (III,20)	from Green's function (IV,29)	from S.O.R. (III,20)
-0.8	0.76	0.76	1.01	1.01
-0.6	1.22	1.22	1.58	1.58
-0.4	1.54	1.54	1.96	1.96
-0.2	1.76	1.76	2.22	2.22
0.0	1.94	1.94	2.41	2.42
0.2	2.07	2.08	2.57	2.57
0.4	2.19	2.19	2.69	2.69
0.6	2.28	2.28	2.78	2.79
0.8	2.36	2.36	2.87	2.88
1.0	2.42	2.43	2.94	2.95
1.2	2.48	2.48	3.00	3.01
1.4	2.53	2.54	3.06	3.06
1.6	2.58	2.58	3.10	3.11
1.8	2.62	2.62	3.15	3.15
2.0	2.65	2.66	3.18	3.19
2.2	2.69	2.69	3.22	3.23
2.4	2.72	2.72	3.25	3.26
2.6	2.74	2.75	3.28	3.29
2.8	2.77	2.77	3.30	3.31
3.0	2.79	2.80	3.33	3.34

We can now check numerically $a_1(0)$ and $a_2(0)$ given by (IV,17) and (IV,29) with the numerical values of a_1 and a_2 obtained from the canonical average (III,20). This is done in Table (IV,ii) for $-1 \leq \gamma \leq 3$. It can be noticed that the accuracy is better than 1% in all cases over this range of parameter γ. This serves as a numerical check for a_1 and a_2.

It can be noticed from (IV,27) and (IV,29) that a_1 and a_2 depend only on p_0 and p_{-1} and do not depend on p_1. Physically the reason for this is that a_ℓ depends on the rate at which monomers diffuse towards the central cluster at large distances from the origin: this rate is proportional to p_0. Also a_ℓ depends on p_{-1} which is a measure of the attraction between the central cluster and a monomer. Conversely a_ℓ does not depend on p_1 because this is a measure of the rate at which clusters break up. It can also be seen in the mathematical analysis for $\frac{\partial c_{\ell+1}}{\partial t}$ in this chapter that p_1 always multiplies $f(\underline{r})$ for $\underline{r} \epsilon N_1$ which is proportional to $C_{\lambda+}/C_\lambda$ rather than c_1 and so $a_\ell(0)$, the coefficient of c_1 in this quantity, does not depend on p_1.

Chapter V Comparison of the Differential Equations with the Simulation of a Quenched Alloy at the same value of ℓ^*.

In this chapter we compare the numerical solution of the differential equation described in Chapter II with concentrations of various sized clusters in the simulation of a quenched alloy. This simulation was first described in Sur et al (1977); it was described also in Penrose et al (1978).

V.1 Numerical computation of differential equations

The system of differential equations used is that given in equations (II,1), (II,2) and (II,3). We take $a_\ell(0)$ for $\ell \geq 7$ to be given by the extrapolation formula $a_\ell(0) = \frac{1}{6}[874+1888\ell]^{1/3}$ which is given in (III,24) and (III,25). For the partition functions Q_ℓ for $\ell \geq 11$, we use the equation (I,7) with $w_s = 0.010526$ and $c = 2.415$. The quantities $b_\ell(0)$ are then given by the equations (II,8). The parameter $\mu(\ell^*)$ in (II,7) and (II,8) which describes the variation of a_ℓ and b_ℓ when the density of clusters is non-zero, is taken equal to 1, for numerical convenience. The factor $\mu(\ell^*)$ will be estimated empirically in the next section and we will find $\mu(\ell^*)$ theoretically in the next chapter.

The initial concentrations in the differential equations were taken to be the equilibrium distribution at infinite temperatures as in the simulation. These initial values are shown for density $\rho = 0.075$ in Table (I,ii). Since the lattice gas in the simulation was quenched to $T = 0.59T_c$ where T_c is the critical temperature, the coefficients $a_\ell(0)$, $b_\ell(0)$ and Q_ℓ in our differential equations are all evaluated at this temperature which is equivalent to $\frac{V}{KT} = 1.5$, or $y = 4.482$. In the differential equations as in the

simulation therefore the temperature changes instantaneously from $T = \infty$ at zero time to $T = 0.59T_c$, or equivalently $\frac{V}{KT} = 1.5$, thereafter, and the temperature is held constant at this value.

For numerical integration we used a Runge-Kutta procedure. We took a system of equations with maximum cluster size $L = 800$, ie $c_\ell = 0$ for $\ell > 800$. Equation (II,9) gives the differential equation satisfied by the concentration of clusters of maximum size L. This was enough over the time range considered in the simulations since the biggest cluster contained about 600 particles. We then computed the solution of the differential equations for $\rho = 0.075$ for $L = 800$ and $L = 1600$, and found that the value of c_{600} differed by not more than 10% over the same time interval as will be considered in this chapter. Also the number of clusters larger than 600 was at most only 1% of the total number of clusters larger than 20 for this interval of time. For our computer runs we therefore settled on $L = 800$. We computed the differential equations for the three densities $\rho = 0.05$, 0.075 and 0.10 all at temperatures $T = 0.59T_c$.

V.2 Empirical estimate for $\mu(\ell^*)$

The differential equations were computed with $\mu(\ell^*) = 1$ in (II,7) and (II,8). We take equation (I,9) to be our definition of ℓ^* with $W_s = 0.010527$ and $C = 2.415$ for $\frac{V}{KT} = 1.5$, and with $w = c_1/(1-\rho)^3$ from (I,6). We denote ℓ^* in the simulation and in the differential equations by ℓ^*_{sim} and ℓ^*_{de}. We will compare the simulation at time t with the differential equations at time t_{de} where

$$\ell^*_{sim}(t) = \ell^*_{de}(t_{de}) \qquad (V,1)$$

that is we will compare them when the value of ℓ^* is the same in both.

Since the W-formula (I,6) was used in the detailed balance condition (II,4) for $\frac{b_{\ell+1}}{a_\ell}$, and since $\frac{J_\ell}{c_\ell}$ in (II,2) is very small except for the earliest time, we expect that ℓ^*, or W, determines via (I,6) the distribution of clusters in the differential equations also. This is borne out by Table (I,iii), where for each value of ℓ^*, we give the corresponding distribution predicted by the differential equations at this value of ℓ^*, for $\rho = 0.10$ and $T = 0.59T_c$. For ℓ^*_{de}, we took W to be $c_1/(1-\rho)^3$ in (I,9). From Table (I,iii), we see that $\rho_{10} = \sum_1^{10} \ell c_\ell$ for the differential equations and from the W formula (I,6) agree to about 1% after $t = 1000$. Our method of comparison at the same ℓ^* based on (V,1) will therefore ensure that the comparison is made when the total number of particles in the small clusters, and hence also in the large clusters, is the same in both the differential equations and in the simulation. Also ℓ^* is expected to be linear in t_{de} (Penrose et al 1978), so that it as good a variable as time as an independent variable for this problem.

The importance of (V,1) lies also in the fact that we can obtain an 'empirical' value for $\mu(\ell^*)$ by finding the relation between the simulation time t, and t_{de}. Indeed since $\mu(\ell^*) = 1$ in the differential equations, we can write the Becker Döring equations in Section (II,1) as

$$\frac{d\underline{c}}{dt} = \mu(\ell^*) f(\underline{c}) \quad \text{and} \quad \frac{d\underline{c}}{dt_{de}} = f(\underline{c})$$

where $\underline{c} = (c_1, c_2, \ldots)$ and $f(\underline{c})$ is independent of $\mu(\ell^*)$. From these two equations therefore

$$\frac{dt_{de}}{dt} = \mu(\ell^*) \quad \text{or else} \quad t = \int_0^{t_{de}} \frac{dt_{de}}{\mu(\ell^*)} \qquad (V,2)$$

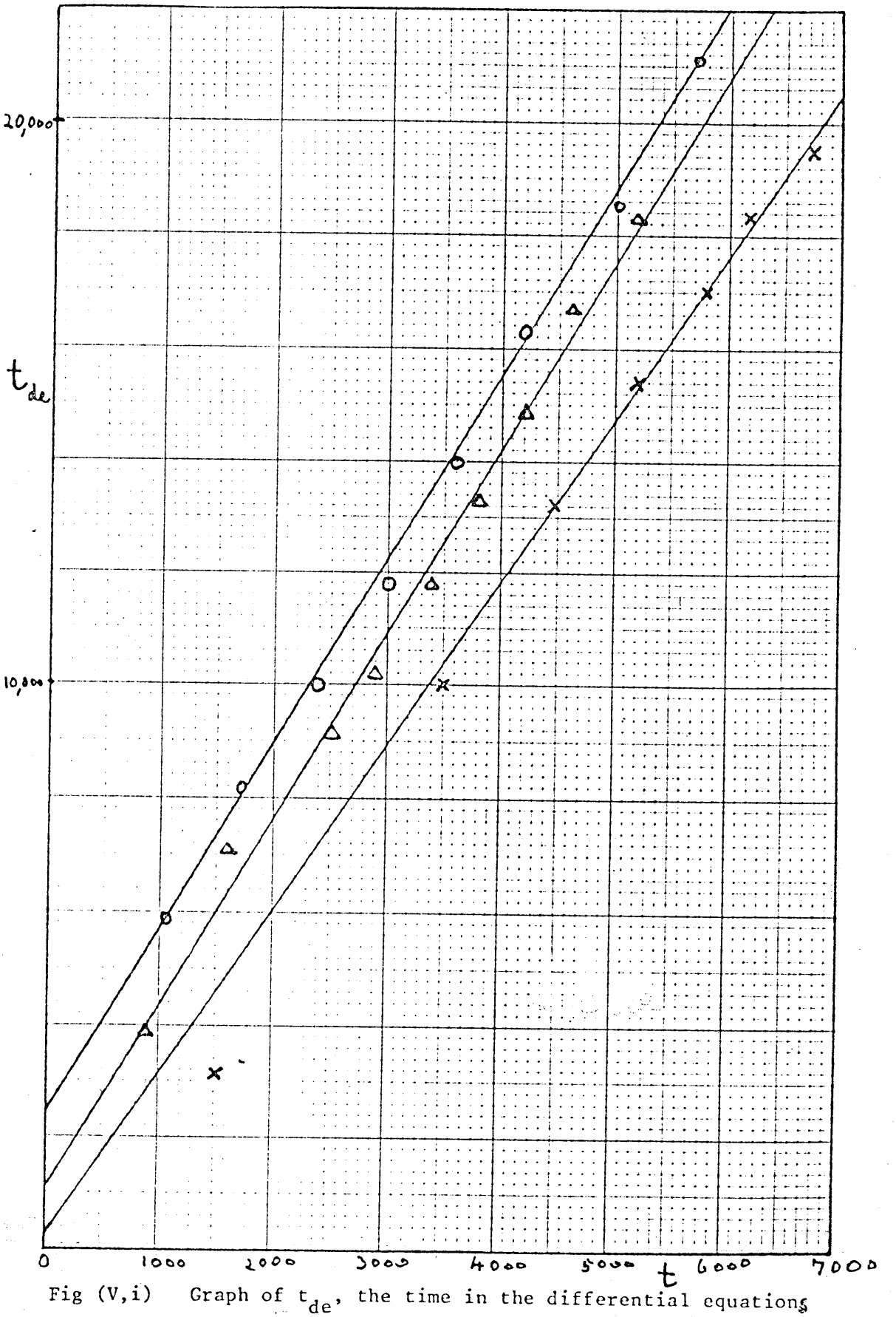

Fig (V,i) Graph of t_{de}, the time in the differential equations with coefficient $a_\ell(0)$, against simulation time t, when the value of ℓ^* is the same in the simulation and the differential equations. The slope of this graph gives an empirical estimate for $\mu(\ell^*)$. It is seen that $\mu(\ell^*)$ is practically constant for $t > 1000$.

Densities ρ = 0.05, 0.075, 0.10

Equation (V,2) gives us the relation between t, t_{de}, and $\mu(\ell^*)$. In Fig.(V,i), we plot t_{de} against t for the three densities ρ = 0.05, 0.075, 0.10. The pairs of values t and t_{de} for given ℓ^* increased approximately linearly from about 20 to 200 for these densities. The graphs of t_{de} against t are approximately linear except for the earlier times (t<1000) for the lower densities.

$$t_{de} = \mu(\ell^*)(t+t_0) \qquad (V,3)$$

$$\mu(\ell^*) = \begin{matrix} 2.89 \\ 3.30 \\ 3.23 \end{matrix} \qquad t_0 = \begin{matrix} 0 \\ 400 \\ 800 \end{matrix} \qquad \text{for} \quad \begin{matrix} \rho = 0.05 \\ \rho = 0.075 \\ \rho = 0.10 \end{matrix}$$

Thus, except for the earlier times, $\mu(\ell^*)$ is approximately constant over the time range considered and is approximately equal to 3.0 for these densities. The equations also have an intercept which increases with density. For ρ =0.075 and 0.10, ℓ^* increases very rapidly with time initially over a period $t \simeq t_0$, from $\ell^* \simeq 2$ to a certain value, $\ell^* \simeq 30$, and then increases more slowly after that. In the next chapter, we will calculate $\mu(\ell^*)$ and the quantities ℓ^*_{de} and ℓ^*_{sim} will then be compared together as a function of t.

V.3 Comparison of the concentrations of large clusters in the differential equations and the simulation at the same ℓ^*.

We now compare c_ℓ for $\ell \geq 20$ in the differential equations and the simulation at the same value of ℓ^* as explained in the previous section. We do this for the densities ρ = 0.05, 0.075, 0.10.

We drew histograms of the simulation concentrations of various values of ℓ^* in the available range $0 \leq \ell^* \leq 210$, which is equivalent to the simulation time range $0 \leq t \leq 6000$ for these three densities.

To estimate c_ℓ from the simulation we define g_ℓ as the total number of clusters of size ℓ or larger:

$$g_\ell = \sum_{\ell}^{\infty} c_\ell \qquad (V,4)$$

Then we take c_ℓ in the histograms for the simulation concentrations to be defined by

$$c_{\ell+\frac{1}{2}(h-1)} = \frac{-g_{\ell+h} + g_\ell}{h} \qquad (V,5)$$

where h is chosen to be the least value so that c_ℓ does not fluctuate too rapidly with ℓ. In fact we find that h is about $\frac{1}{2}\ell^*$.

The histograms for the simulation concentrations c_ℓ for $\ell \geq 20$ are given in Fig.(V,ii) for the three densities $\rho = 0.05$, 0.075, and 0.10 respectively. In each diagram we also give the concentrations c_ℓ predicted by the differential equations at the same value of ℓ^* as in the simulation.

Both the histograms and the solution of the differential equations are monotonic decreasing with ℓ for earlier simulation times $0 \leq t \leq 1000$, or equivalently for $\ell^* \leq 40$. Gradually however a point of inflexion appears at about $t = 1800$ for density $\rho = 0.075$ and at about $t = 1000$ for $\rho = 010$. Near this point of inflexion eventually, a small maximum and minimum start appearing at about $t = 2800$ and $t = 1800$ for densities 0.075 and 0.10 respectively. The minimum and maximum become more pronounced with time and they signify the separation of the particles into two phases. The differential equations are quite successful in predicting the times or rather the value of ℓ^* at which the point of inflexion first appears in the simulation.

Fig (V,ii): Comparison of C_ℓ for the simulation and the differential equations for $0 \leq t \leq 7000$. Densities $\rho = 0.05, 0.075, 0.10$. Note that the ℓ-axis does not start from the origin because C_ℓ is very large for small ℓ.

1. Density $\rho = 0.05$

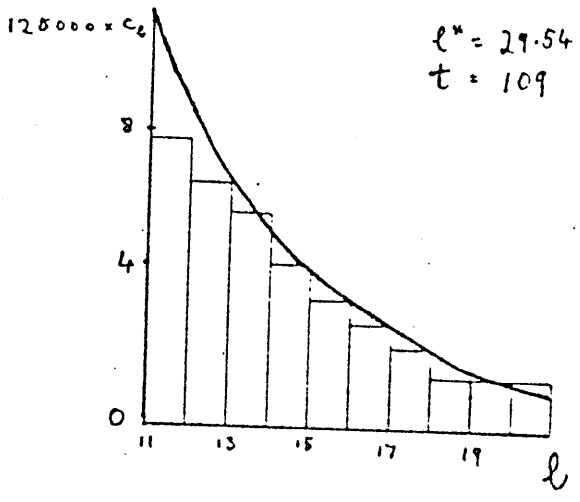

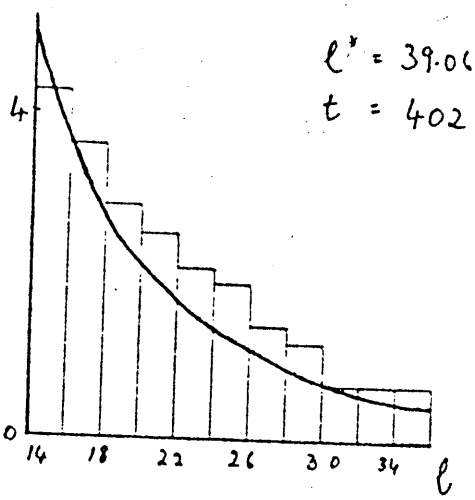

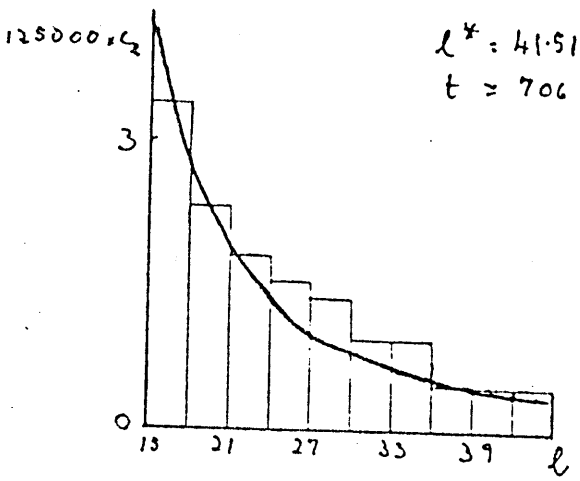

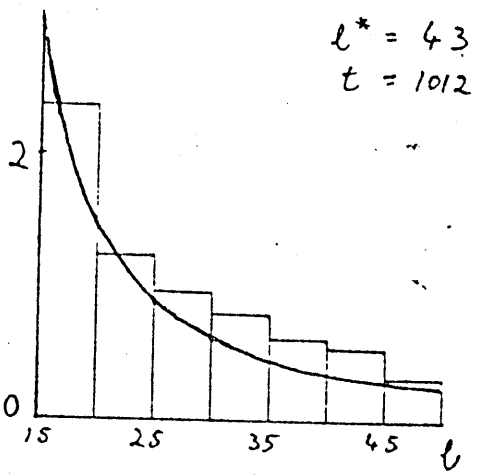

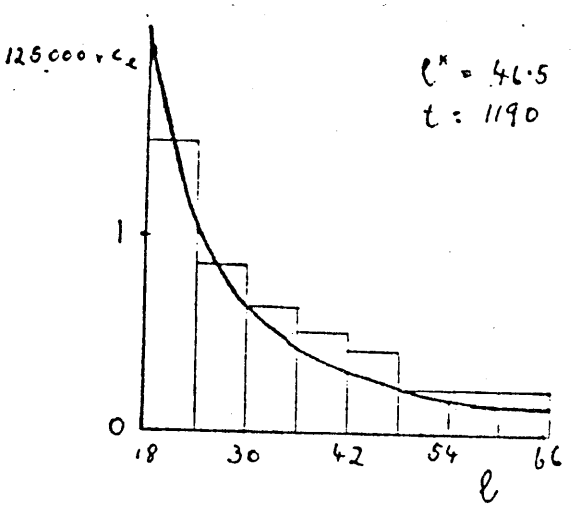

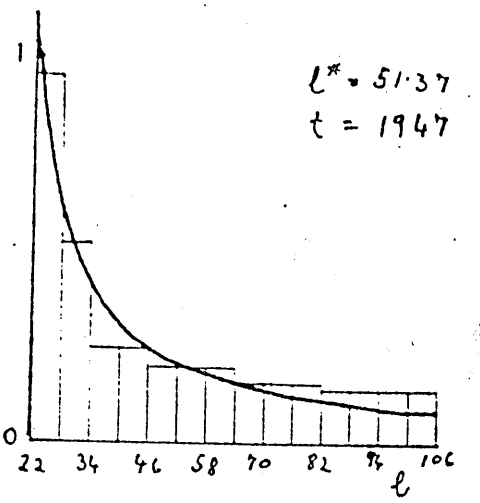

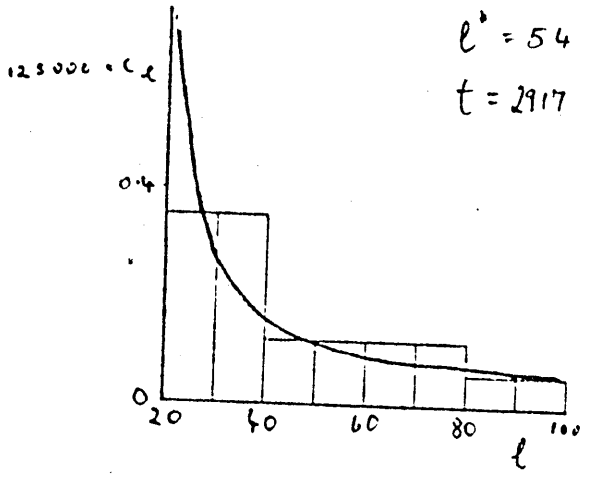

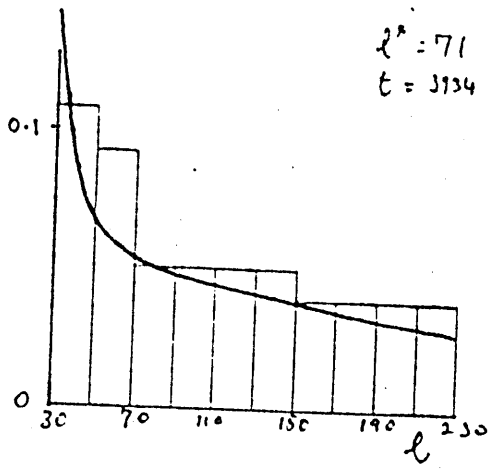

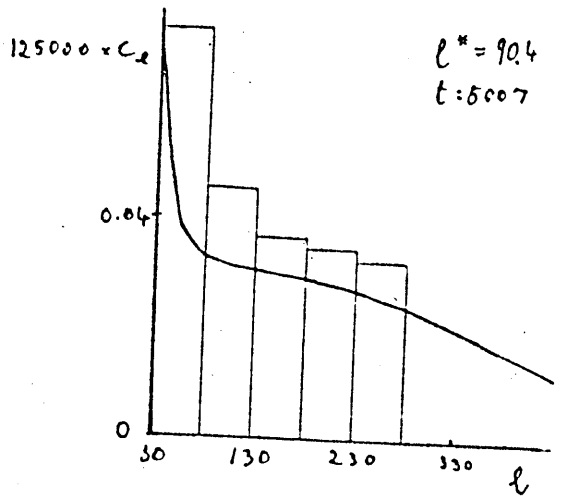

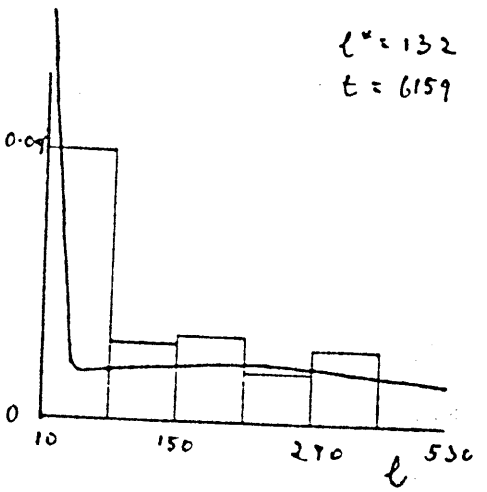

2. Density $\rho = 0.075$

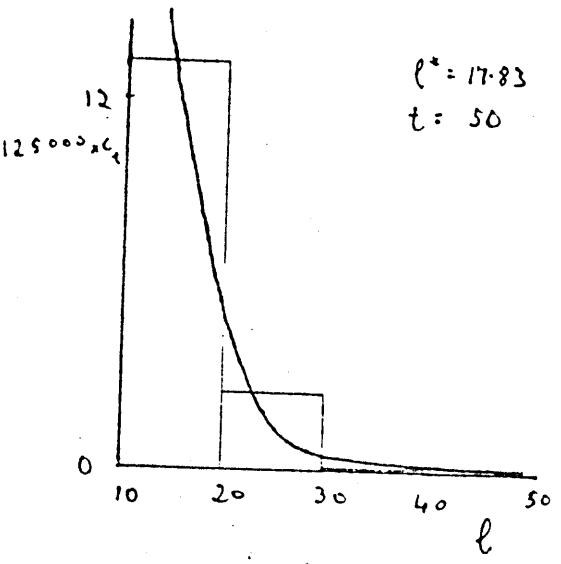

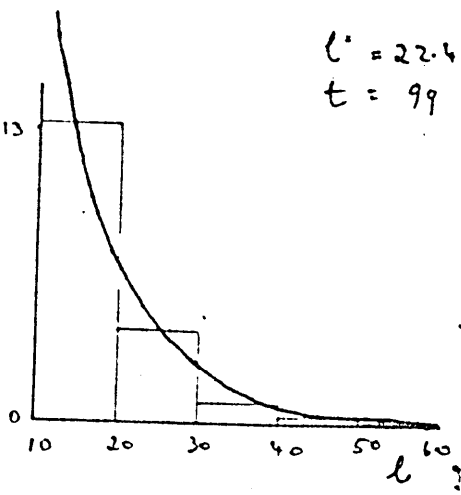

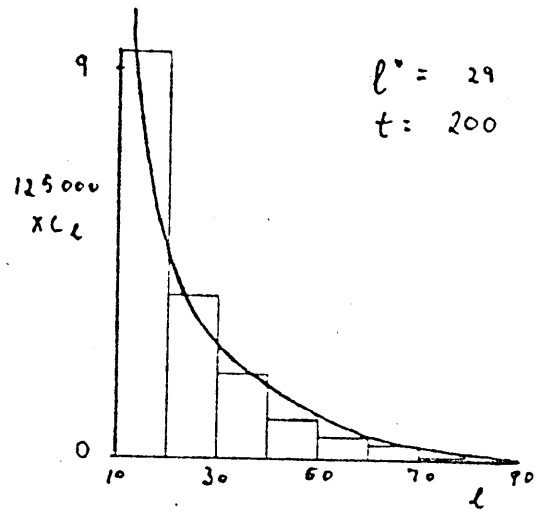
9
125000
XC ℓ
0
10
30
60
70
90
ℓ
ℓ* = 29
t = 200

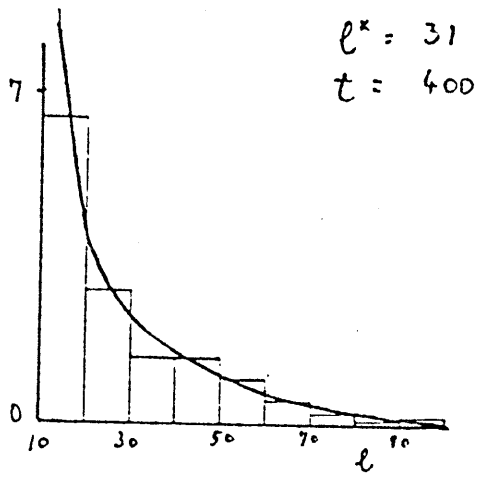
7
0
10
30
50
70
90
ℓ
ℓ* = 31
t = 400

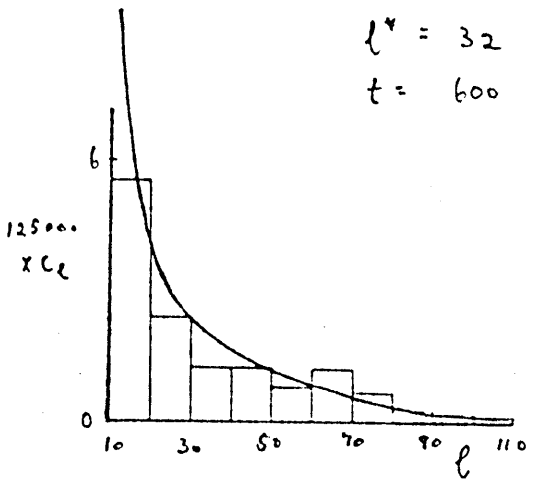
6
125000
XC ℓ
0
10
30
50
70
90
110
ℓ
ℓ* = 32
t = 600

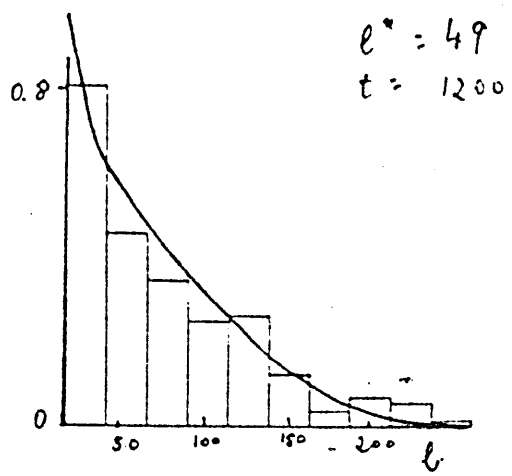
0.8
0
50
100
150
200
ℓ
ℓ* = 49
t = 1200

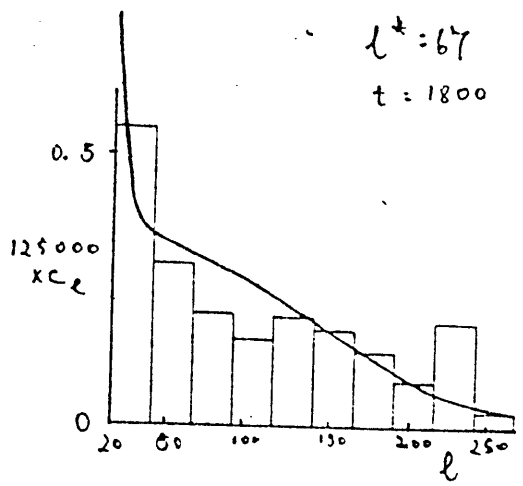
0.5
125000
XC ℓ
0
20
60
100
150
200
250
ℓ
ℓ* = 67
t = 1800

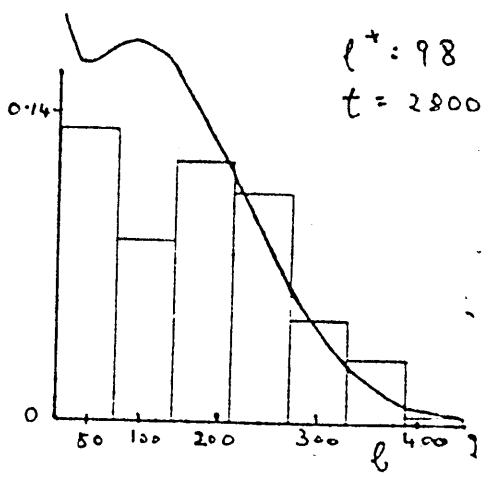
0.14
0
50
100
200
300
400
ℓ
ℓ* = 98
t = 2800

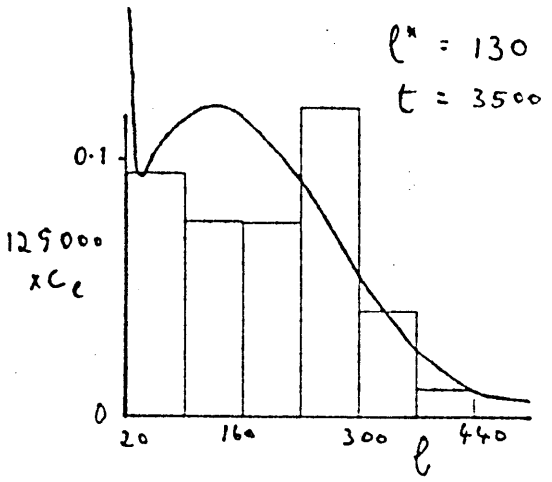

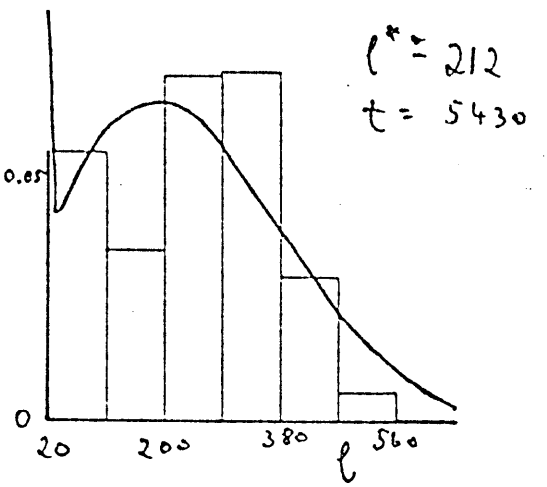

3. Density $\rho = 0.10$

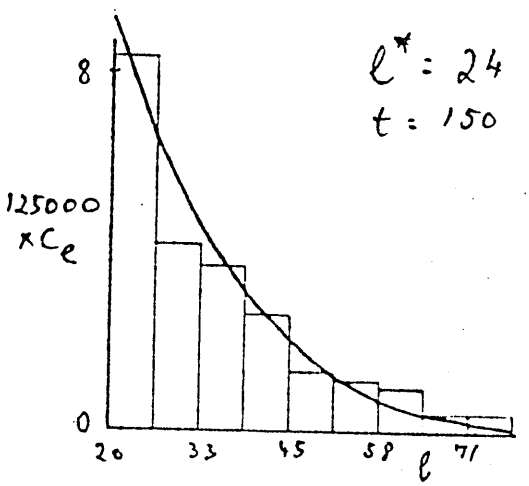

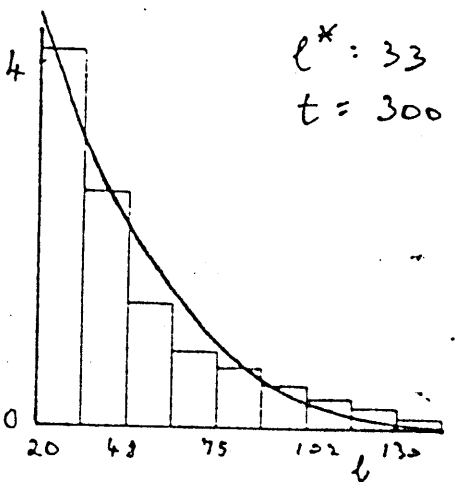

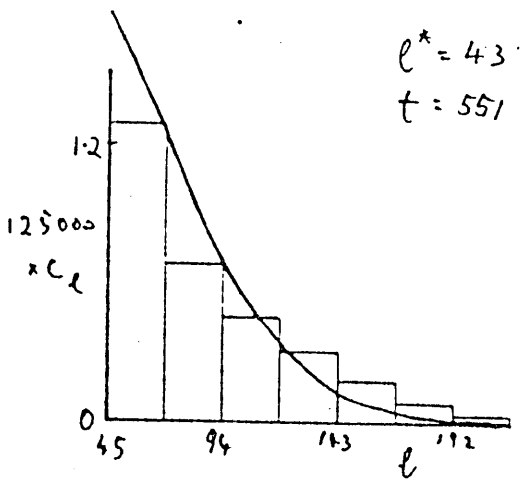

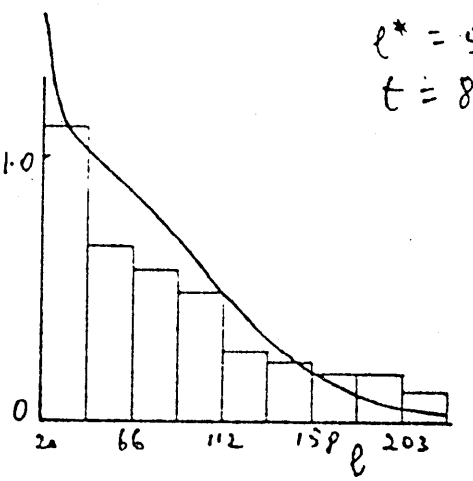

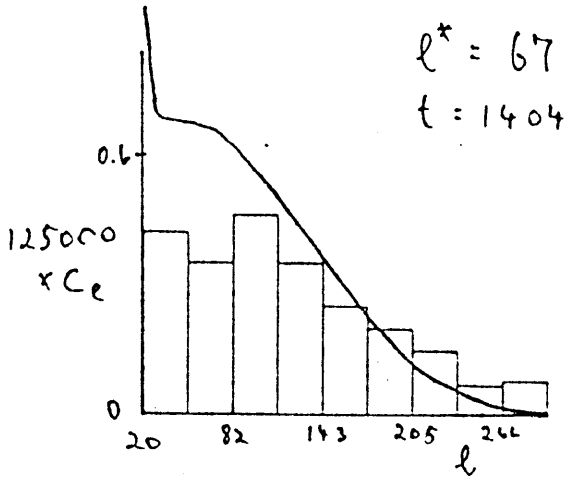
$\ell^* = 67$
$t = 1404$
0.6
125000 x C_ℓ
0
20
82
143
205
266
ℓ

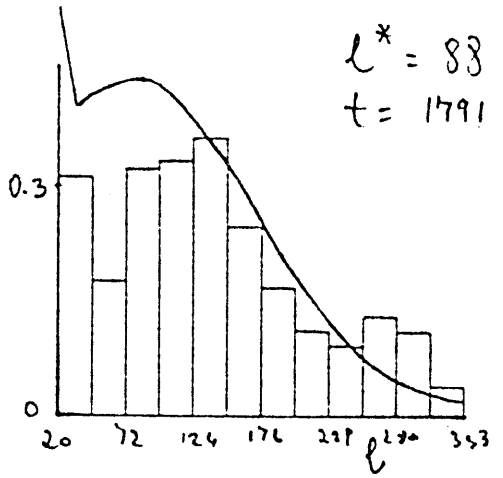
$\ell^* = 88$
$t = 1791$
0.3
0
20
72
124
176
228
280
343
ℓ

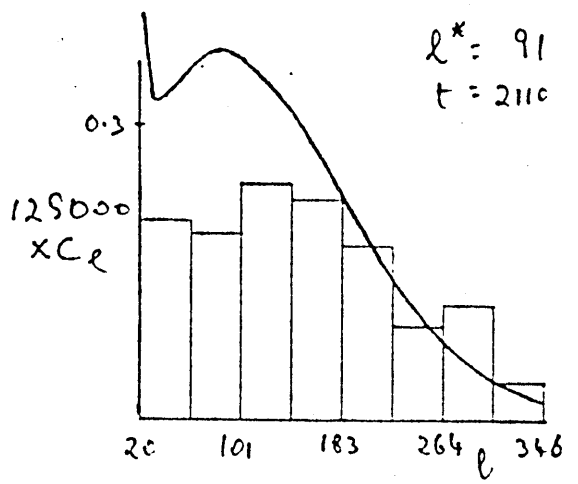
$\ell^* = 91$
$t = 2110$
0.3
125000 x C_ℓ
20
101
183
264
346
ℓ

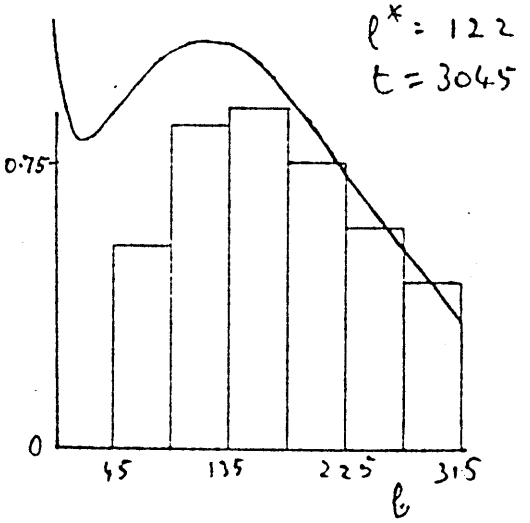
$\ell^* = 122$
$t = 3045$
0.75
0
45
135
225
315
ℓ

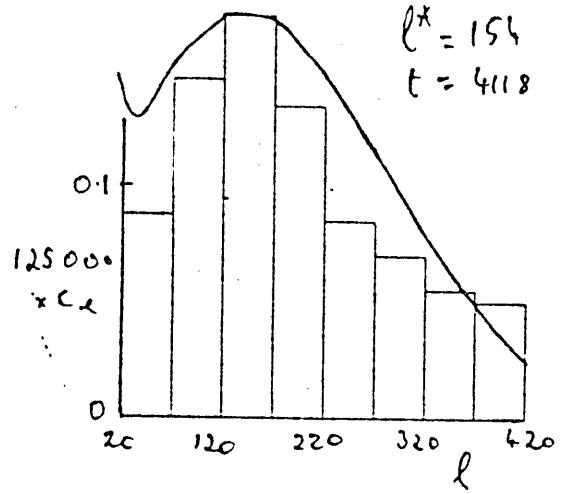
$\ell^* = 154$
$t = 4118$
0.1
125000 x C_ℓ
0
20
120
220
320
420
ℓ

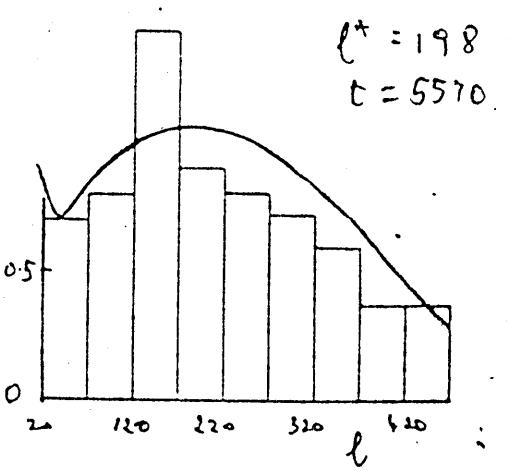
$\ell^* = 198$
$t = 5570$
0.5
0
20
120
220
320
420
ℓ

For earlier times, when C_ℓ for the differential equations and the simulation are monotonic decreasing in ℓ, the differential equations are quite close to the histogram ($\sim$ 10%) on inspecting the relevant diagrams in Fig.(V,ii).

For $\rho = 0.05$, however, the maximum and minimum never quite appears in the time range considered, although there seems to be a broad point of inflexion in the simulation after about $t = 5000$. Again this is successfully predicted by the differential equations although it predicts c_ℓ to be slightly lower than that in the simulation for $t = 5000$.

It is interesting to see how well the differential equations predict the position of the local maximum and minimum in the $(c_\ell - \ell)$ histograms and also the concentrations at these two points. In Table (V,i) we give ℓ_{max} and ℓ_{min}, which we define as that value of ℓ for which c_ℓ is a local maximum and minimum respectively. We also give $c_{\ell max}$ and $c_{\ell min}$ which are the concentrations of the local maximum and minimum respectively. We compare these quantities for the simulation and the differential equations atthe same ℓ^* and for densities $\rho = 0.075$ and 0.10. For the simulation we give the range of values of ℓ for which c_ℓ is a local maximum or a local minimum in the histogram.

On inspecting Table (V,i) we found that when the maximum and minimum first appear , the differential equations tend to underestimate ℓ_{max} and ℓ_{min} and overestimate $c_{\ell max}$ and $c_{\ell min}$. In the case $\rho = 0.10$, for later times when the maxima and minima are more pronounced the differential equations are more accurate. The quantities ℓ_{max} and ℓ_{min} for $\rho = 0.10$ all lie within the corresponding range for the simulation at these later times. Towards

Table (V,i): Position of local maxima and minima in c_ℓ-ℓ curve and concentrations at their two points for both differential equation and simulation for densities $\rho = 0.075$ and 0.10.

$\rho = 0.075$

ℓ^*	sim time t		ℓ_{min}	$C_{\ell min}$	ℓ_{max}	$C_{\ell max}$
98	2800	sim	80-140	.086	140-200	.123
		de same ℓ^*	42	.163	97	.178
130	3500	sim	90-235	.075	235-305	.119
		de same ℓ^*	34	.092	130	.121
211	5430	sim	110-200	.034	200-390	.068
		de same ℓ^*	31	.040	200	.062

$\rho = 0.10$

ℓ^*	sim time t		ℓ_{min}	$C_{\ell min}$	ℓ_{max}	$C_{\ell max}$
90	1949	simulation	20-103	.26	103-145	.30
		de same ℓ^*	33	.4	82	.44
91	2110	simulation	20-100	.2	101-142	.25
		de same ℓ^*	32	.33	84	.38
120	3045	simulation	20-90	.11	90-180	.18
		de same ℓ^*	29	.17	130	.22
180	4118	simulation	20-70	.09	120-170	.175
		de same ℓ^*	32	.12	145	.18
198	5570	simulation	20-70	.07	120-220	.12
		de same ℓ^*	32	.07	190	.11

the end of the time range considered ($t \simeq 5000$), the differential equation concentrations at the maximum and minimum, $C_{\ell max}$ and $C_{\ell min}$, are accurate to about 18% for $\rho = 0.075$ and to 5% for $\rho = 0.10$. One can also notice that ℓ_{max} increases with time and is roughly equal to ℓ^* in the differential equations and the simulation.

For $\rho = 0.10$, ℓ_{min} decreases with time for both differential equations and simulation. This is not the case for ℓ_{min} for $\rho = 0.075$. For this density, ℓ_{min} decreases with time for the differential equations, whereas in the simulation, $\ell_{min} \simeq \ell^*$ and increases with time. This increase in ℓ_{min} with time is probably only a transient feature in the simulation. Histograms for real alloys (Ardell and Nicholson, 1966) do not show such a local minimum for c_ℓ for asymptotic times. The concentrations c_ℓ for the differential equations will be compared with histograms of real alloys in Chapter VII.

For $\ell > \ell_{max}$, c_ℓ for the differential equations is monotonic decreasing in ℓ. This is also true of the simulation when the maximum and minimum are more pronounced, that is after about $t = 2200$ for 0.10 density, and after $t \simeq 2800$ for density 0.075. In this region again, the differential equation c_ℓ-ℓ curve, is quite near to the histogram. However, we will discuss the large clusters in more detail in Chapter VII.

Chapter VI: Calculation of $\mu(\ell)^*$: comparison of ℓ^*_{sim} and ℓ^*_{de} at the same value of simulation time t.

In the previous chapter we compared the concentration c_ℓ predicted by the simulation and the differential equations, when the value of ℓ^* is the same in both, ie when equation (V,1) holds. To complete the comparison, therefore, we have to compare $\ell^*_{sim}(t)$ and $\ell^*_{de}(t)$ together as a function of t. Since $\mu(\ell^*)$ was put equal to 1 in the differential equations, ℓ^*_{de} was given in terms of t_{de} in (V,1). To find ℓ^*_{de} in terms of t rather than t_{de}, we use (V,2) which relates to to t_{de} and $\mu(\ell^*)$. We therefore turn our attention to calculate $\mu(\ell^*)$.

The quantity $\mu(\ell^*)$ was defined in (II,7) as $\mu(\ell^*) = a_\ell / a_\ell(0)$, namely the ratio of the coefficient a_ℓ when the supersaturation is W, to $a_\ell(0)$, the value of a_ℓ in the limit of zero density. The quantities ℓ^*, W and the concentrations of the small clusters C_ℓ are related by (I,6) and (I,9). To find $\mu(\ell^*)$ for any ℓ^*, we use equation (III,I7), where we interpret Po/3 to be the diffusion constant in the limit of zero density, as shown in (III,22). Taking an average such as (III,20) over all translationally inequivalent clusters λ of size ℓ, we can write (III,I7) for any density as $a_\ell = 4\pi D(\ell^*) K_\ell$, where K_ℓ is the average of K for the clusters of size ℓ. Since K, defined in (III,I5), and hence K_ℓ, is independent of density, we then have $a_\ell / a_\ell(0) = D(\ell^*)/D = 6D(\ell^*)$ using (III,22). Therefore,

$$\mu(\ell^*) = 6D(\ell^*). \qquad \text{(VI,1)}$$

The quantity $\mu(\ell^*)$ has been obtained analytically (Penrose, unpublished) on the Bethe lattice, a lattice with constant coordination number q but with no polygons. On the Bethe lattice, the equilibrium or steady state concentrations of the

small clusters, which gives ℓ^*, and $D(\ell^*)$, can be found exactly in terms of a certain parameter ξ. Besides we will show that the equilibrium properties of the lattice gas on the Bethe lattice with coordination number $q = 6$ are practically identical quantitatively to the properties of the lattice gas on the simple cubic lattice. The steady state concentrations of the small clusters on the two lattices also agree to a considerable extent. I am very grateful to my supervisor Professor Oliver Penrose, for showing me most of the results in the next three sections.

VI.1 Statistical mechanics of a lattice gas on the Bethe lattice

We now consider a lattice gas with fugacity z on a Bethe lattice with coordination number q. In the following for brevity, we denote an empty site by o, and an occupied site by •.

Given a large finite Bethe lattice, we can then denote by $\Xi(o\!-\!\!\times)$ as the grand partition function of the lattice gas given that a particular site on the boundary is empty, and we denote by $\Xi(\bullet\!-\!\!\times)$, the grand partition function given that this site is occupied. Since this particle is on the boundary, its coordination number is 1, namely it has only 1 nearest neighbour. Similarly in $\Xi(\bullet\!-\!\!\bullet\!-\!\!\times)$ both sites are given occupied, and so on.

When the fugacity is z we can define θ to be

$$\theta = \frac{\Xi(\bullet\!-\!\!\times)}{z\Xi(o\!-\!\!\times)}$$

Since in $o\!-\!\!\times$, the site adjacent to the left hand one can only be either full or empty, we can write

$$\Xi(\text{ 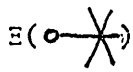 }) = \Xi(\text{ 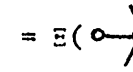 }) + \Xi(\text{ 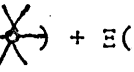 })$$

$$= \Xi(\text{ 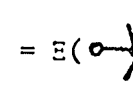 })\left[1 + \frac{\Xi(\text{ 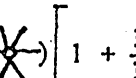 })}{\Xi(\text{})}\right]$$

$$= \Xi(\text{ 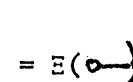 })[1 + z\theta^{q-1}] \qquad \text{(VI,3)}$$

because the (q-1) branches coming out of the right hand site are statistically independent of each other since we are using the Bethe lattice. Similarly for 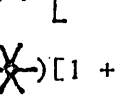 we can write

$$\Xi(\text{}) = \Xi(\text{ 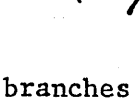 }) + \Xi(\text{ 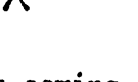 })$$

$$= \Xi(\text{ 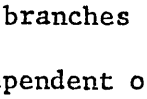 })\left[\frac{\Xi(\text{ 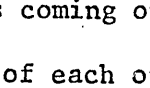 })}{\Xi(\text{})} + \frac{\Xi(\text{})}{\Xi(\text{})}\right]$$

$$= \Xi(\text{ 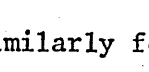 })\left[z + z^2 y\theta^{q-1}\right] \qquad \text{(VI,4)}$$

where $y = exp\left(\frac{V}{KT}\right)$ accounts for the fact that there is an attraction V between the two full sites appearing in the terms $\Xi(\text{ 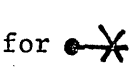 })$.

If we define parameter ξ to be

$$\xi = z\ \theta^{q-1} \qquad \text{(VI,5)}$$

we can divide (VI,4) by (VI,3) and using (VI,2) and (VI,5) we obtain the relation

$$\theta = \frac{1 + zy\theta^{q-1}}{1 + z\theta^{q-1}} = \frac{1 + y\xi}{1+\xi} \qquad \text{(VI,6)}$$

We will now relate θ and ξ to the density ρ of the lattice gas on the Bethe lattice. We use the fact that the density is equal to the probability that a given site is full, whereas $(1-\rho)$ is equal to the probability that it is empty

$$\frac{\rho}{1-\rho} = \frac{\Xi(\text{ 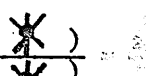 })}{\Xi(\text{})}$$

$$= z\theta^q = \theta\xi \qquad \text{(VI,7)}$$

where the last two equalities follow from (VI,4) and (VI,5).

VI.2 Equilibrium distribution of small clusters on the Bethe lattice.

The equilibrium distribution of the small clusters on the Bethe lattice can be calculated in terms of the quantities z, ρ and ξ introduced in the previous section.

We first find c_1, the equilibrium or steady state concentration of monomers. The probability that the origin 0 is empty is $1-\rho$. The probability that a neighbouring site x is empty given 0 is empty is given by $\Xi($  $)/(\Xi($ $)+\Xi($ $))$ $= 1/(1+\xi)$ using equation (VI,1). Then the probability of finding 0 and its q neighbours all empty () is given by $(1-\rho)\,(\frac{1}{1+\xi})^q$. The concentration of monomers at fugacity z is then given (Lebowitz and Penrose 1977) by

$$c_1 = z(1-\rho)\,(\frac{1}{1+\xi})^q \qquad \text{(VI,8)}$$

Similarly one can derive the steady state concentrations c_ℓ of ℓ-clusters on the Bethe lattice with coordination number q. As for the monomer case we have to find the probability that the sites on the cluster and its nearest neighbours are empty. We denote the set of sites on an ℓ-cluster and all its nearest neighbours by S_ℓ. If one increases ℓ by 1, the number of sites in $S_{\ell+1}$ is $(q-1)$ more than in S_ℓ. It can then be easily shown by induction that the probability that S_ℓ is empty is equal to $(1-\rho)\,(1+\xi)^{-[(q-1)\ell+1]}$. This is true for $\ell=1$, as for the monomer case. Assuming it is true for an integer ℓ,

$$P\{S_{\ell+1} \text{ is empty}\} =$$

$$= P\{S_\ell \text{ is empty}\} \times P\{\text{the}(q-1) \text{ extra sites in } S_{\ell+1} \text{ are empty/ given } S_\ell \text{ is empty}\}.$$

$$= (1-\rho)\frac{1}{(1+\xi)^{\ell(q-1)+1}} \times \frac{1}{(1+\xi)^{q-1}} = (1-\rho)\frac{1}{(1+\xi)^{(\ell+1)(q-1)+1}}$$

Therefore such a formula is true for all ℓ. The concentration c_ℓ at equilibrium is therefore equal to (Lebowitz and Penrose, 1977) $z^\ell \times p\{S_\ell \text{ is empty}\}$ × the partition function of ℓ-clusters in the given lattice. Therefore the equilibrium or steady state concentrations of ℓ-clusters c_ℓ on the Bethe lattice with coordination number q:

$$c_\ell = \left[\frac{q(q-1)[\ell(q-1)-1]!}{(\ell-1)![\ell(q-2)+2]!}\ y^{\ell-1}\right]\left(\frac{1-\rho}{1+\xi}\right)\left[\frac{z}{(1+\xi)^{q-1}}\right]^\ell \qquad \text{(VI,9)}$$

The first term in square brackets is the partition function for the ℓ-clusters on the Bethe lattice: the term involving factorials is equal to (Fisher and Essam 1961) the number of inequivalent ℓ-clusters on the Bethe lattice, and $y^{\ell-1}$ is the Boltzmann factor for the ℓ-clusters, since these have $\ell-1$ bonds on the Bethe lattice. The equation (VI,9) corresponds to the approximate equation (I,6) for the equilibrium or steady state concentrations c_ℓ on the cubic lattice.

We can now calculate the parameters ρ and c_ℓ for ℓ = 1 to 10 for the Bethe lattice with q = 6, and compare them with the equilibrium parameters of the simple cubic lattice. For coexistence of the two phases by the theory of the Ising model, the fugacity z satisfies the relation

$$z = y^{-q/2} = y^{-3} \qquad \text{(VI,10)}$$

We can then solve for θ using the first relation in (VI,6) and then find ρ and ξ using (VI,7) and c_ℓ using (VI,9). We also define the percolation W_S as in (I,8) by

$$W_s = \frac{c_1}{(1-\rho)^3} \qquad \text{(VI,11)}$$

The quantity ρ found in this way is the coexistence density for the Bethe lattice, and is analogous to (I,9) which is the corresponding expression for the simple cubic lattice. In Table (VI,i) we give ρ, c_ℓ and W_s for three different temperatures. We also give observed values for ρ, c_ℓ and W_s on the simple cubic lattice for simulations of a lattice gas (Kalos et al 1978).

The predictions of (VI,8), (VI,9) are very close to the observed c_ℓ on the simple cubic lattice for the lower temperature given by $\frac{V}{KT} = 1.5$. And also $\sum_1^{10} \ell c_\ell$ agrees to $\frac{1}{2}\%$ with the corresponding value observed in the simulation. Also since W_s is very well predicted for this temperature we can define ℓ^* exactly as for the simple cubic lattice with $W_s = 0.010526$ and $C = 2.415$ in equation (I,8) for $\frac{V}{KT} = 1.5$.

For the higher temperature, however, the theory for the Bethe lattice underestimates c_ℓ for $\ell \geq 2$. This is because in (VI,9) the last term raised to the ℓ'th power is $\frac{z}{(1+\xi)^{q-1}} = c_1 \frac{(1+\xi)}{1-\rho} = \frac{c_1}{(1-\rho)^2}$, whereas the corresponding term in (I,6) is $W = \frac{c_1}{(1-\rho)^3}$, thus leading to a higher concentration c_ℓ for the simple cubic lattice for the larger values of ρ. The disparity becomes more serious for higher temperatures or equivalently densities.

Table (VI,i): Equilibrium parameters for the Bethe lattice with coordination number q = 6. These are compared with corresponding values obtained from a simulation of a lattice gas on the simple cubic lattice (Kalos et al, 1978).

$\frac{V}{KT}$	1.5		1.0926		0.99438	
$\bar{z}$	0.011109		0.03771		0.050163	
	Bethe	simple cubic	Bethe	simple cubic	Bethe	simple cubic
θ	1.0483		1.1275		1.1710	
ξ	0.014064		0.06871		0.11148	
ρ	0.01453	0.0146	0.072	0.075	0.116	0.127
C_1	0.010066	0.010126	0.02349	0.023370	0.023735	0.023002
W_s	0.010519	0.010526	0.0294	0.029837	0.0344	0.035247
C_2	0.001402	0.001382	0.005684	0.005944	0.005745	0.006060
C_3	0.000326	0.000328	0.002292	0.002582	0.002317	0.002673
C_4	0.000096	0.000102	0.001171	0.001388	0.001184	0.001621
C_5	0.000032	0.000035	0.000686	0.000870	0.000694	0.000940
C_6	0.000012	0.000013	0.000440	0.000549	0.000445	0.000716
C_7	0.000005	0.000006	0.000300	0.000395	0.000304	0.000525
C_8	0.000002	0.000002	0.000215	0.000278	0.000217	0.000459
C_9	0.000001	0	0.000159	0.000210	0.000161	0.000336
C_{10}	0	0	0.000122	0.000163	0.000123	0.000294
$\sum_1^{10} \ell c_\ell$	.014524	.014593	0.058959	.064709	0.059595	0.071932

VI.3 The diffusion constant on the Bethe lattice as a function of ξ.

We consider two adjacent sites α and β on the Bethe lattice with q = 6 with respective fugacities z_α and z_β, and local monomer concentrations c_α and c_β. If $j_{\alpha\beta}$ is the probability per unit time that particles go from α to β, we can write down the definition of the diffusion constants D_z and D_c as

$$j_{\alpha\beta} = D_z(z_\alpha - z_\beta) = D_{c_1}(c_\alpha - c_\beta) \quad . \tag{VI,12}$$

If one lets $z_\alpha \to z_\beta$, and $c_\alpha \to c_\beta$ in this equation, we then have that

$$D_c = D_z \frac{dz}{dc_1} \tag{VI,13}$$

where $\frac{dz}{dc_1}$ is the variation of fugacity with c_1 the concentration of monomers. The quantity $\frac{dz}{dc_1}$ can be obtained by logarithmic differentiation of ξ, z, ρ, θ, and c_1 in equations (VI,3) to (VI,8). This gives us

$$\frac{dz}{dc_1} = \left(\frac{z}{c_1}\right)\left(\frac{1+6\xi - 4y\xi + y\xi^2}{1-\rho - 4y\xi - 2y\xi\rho - 5y\xi^2 - \rho y\xi^2}\right) \tag{VI,14}$$

The two equations (VI,13) and (VI,14) give us D_c the quantity we are interested in, provided we know D_z. We therefore calculate this quantity.

We take a general case when r neighbours of α, and s are occupied and each of α and β neighbours of β can be occupied or unoccupied. Denoting an occupied site by • , and an unoccupied site by o, the probablities of the four cases illustrated here:

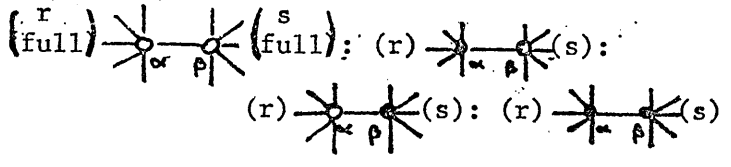

(VI,15)

are respectively in the ratio

$$\xi_\alpha^r \xi_\beta^s \; : \; z_\alpha y^r \xi_\alpha^r \xi_\beta^s \; : \; z_\beta y^s \xi_\alpha^r \xi_\beta^s : \; z_\alpha z_\beta y^{r+s+1} \xi_\alpha^r \xi_\beta^s \qquad \text{(VI,16)}$$

The transition probabilities per unit time for a particle to go from site α to β or viceversa for these four cases are given by

$$0, \; \frac{1}{3}\rho_{r-s}, \; \frac{1}{3}\rho_{s-r}, \; 0 \qquad \text{(VI,17)}$$

respectively where

$$\rho_{r-s} = \frac{1}{y^{r-s}+1} \qquad \text{(VI,18)}$$

using (I,1), (I,2) and (I,3). To find the absolute probabilities of (VI,15), we add the four probabilities in (VI,16), for all r and s between 0 and q-1 = 5. It is easy to show, using the binomial theorem that this normalization constant is equal to

$$(1+\xi_\alpha)^{q-1}(1+\xi_\beta)^{q-1} + z_\alpha(1+y\xi_\alpha)^{q-1}(1+\xi_\beta)^{q-1}$$

$$+ z_\beta(1+\xi_\alpha)^{q-1}(1+y\xi_\beta)^{q-1} + yz_\alpha z_\beta\left[(1+y\xi_\alpha)(1+y\xi_\beta)\right]^{q-1}$$

Using (VI,6) and (VI,5) on this expression, we obtain the normalization constant as

$$(1+\xi_\alpha)^{q-1}(1+\xi_\beta)^{q-1}(1+\xi_\alpha+\xi_\beta+y\xi_\alpha\xi_\beta) \qquad \text{(VI,19)}$$

The absolute probabilities for the configurations in (VI,15) are then given by (VI,16)/(VI,19). Remembering that there are $\binom{q-1}{r} \times \binom{q-1}{s}$ configuration for each case in (VI,15), we can express $j_{\alpha\beta}$ using (VI,16), (VI,17) and (VI,19) as

$$j_{\alpha\beta} = \frac{\sum_r \sum_s \binom{q-1}{r}\binom{q-1}{s}\xi_\alpha^r \xi_\beta^s (z_\alpha y^r \rho_{r-s} - z_\beta y^s \rho_{s-r})}{(1+\xi_\alpha)^{q-1}(1+\xi_\beta)^{q-1}(1+\xi_\alpha+\xi_\beta+y\xi_\alpha\xi_\beta)} \qquad \text{(VI,20)}$$

Since from equation (I,1), $y^r \rho_{r-s} = y^s \rho_{s-r}$, we use the first equality in (VI,12) and let $\xi_\alpha \to \xi_\beta$ thus obtaining the diffusion

constant D_z as

$$D_z = \frac{\sum_r \sum_s \binom{q-1}{r}\binom{q-1}{s} \xi^{r+s} y^r \rho_{r-s}}{(1+\xi)^{2q-2}(1+2\xi+y\xi^2)} \qquad \text{(VI,21)}$$

For $\frac{V}{KT} = 1.5$, or equivalently $y = 4.4816$, (VI,21) becomes

$$D_z = \frac{0.5 + 8.176\xi + 75.07\xi^2 + 386.19\xi^3 + 1441.2\xi^4 + 3508\xi^5}{3(1+\xi)^{10}(1+2\xi + 4.4816\xi^2)} \qquad \text{(VI,22)}$$

which gives D_z as a function of ξ. As $\xi \to 0$, $D_z \to \frac{1}{6}$ from (VI,22), $\rho \to 0$ from (VI,5) and (VI,7), and so $\frac{dz}{dc_1} \to 1$ using (VI,8) and (VI,14). The equation (VI,13) then implies that

$$D_c \to \frac{1}{6} \quad \text{as } \xi \to 0 \qquad \text{(VI,23)}$$

which agrees with (III,22). This also implies that $\mu(\ell^*) = 6D_c$, as predicted by (VI,1).

In Table (VI,ii) we give for various values of ξ, corresponding quantities $\theta, \rho, z, c_1, W, \frac{dz}{dc}, D_z$ and $6D_c$, which we calculate from equations (VI,6), (VI,7), (VI,8), (VI,11), (VI,14), (VI,22) and (VI,13) respectively. We also list ℓ^* which can be obtained from c_1 via (I,9) with $W = c_1/(1-\rho)^3$ where ρ in Table (VI,ii) is interpreted as the total number of particles in the small clusters during steady state. We plot $\mu(\ell^*)$ against ℓ^* in Fig. (VI,i). This graph shows that $6D_c$ is very large for small ℓ^*, but quickly decreases to about 2 for $\ell^* \simeq 50$. Then $\mu(\ell^*)$ decreases very slowly to 1 as $\ell^* \to \infty$, or equivalently as $W \to W_s$.

Table (VI,ii): Parameters on the Bethe lattice calculated in terms of ξ, at steady state for the temperature corresponding to y = 4.4816. In particular we give c_1, ℓ^*, and $\mu(\ell^*)=6D_c$

ξ	θ	ρ	z	c_1	W	ℓ^*	$\frac{dz}{dc}$	D_z	$6D_c$
.005	1.01732	.00506	.004588	.00443	.00450		1.0766	.1704	1.101
.01	1.03447	.01024	.008441	.00787	.00812		1.170	.1744	1.224
.015	1.05145	.01553	.01167	.01051	.01101	151271	1.287	.1786	1.379
.02	1.06827	.02092	.014375	.01250	.01332	755.1	1.440	.1829	1.581
.025	1.08492	.02641	.01663	.01396	.01513	170.4	1.651	.1875	1.858
.03	1.10141	.03199	.01851	.01501	.01654	77.5	1.966	.1922	2.267
.035	1.11774	.03765	.02005	.01571	.01762	48.0	2.494	.1971	2.950
.04	1.13391	.04339	.02134	.01613	.01843	35.3	3.589	.2021	4.352
.045	1.14993	.04920	.02238	.01634	.01901	28.9	7.344	.2073	9.135
.05	1.16580	.05508	.02322	.01637	.01941	25.4	-28.5	.2127	-36.34

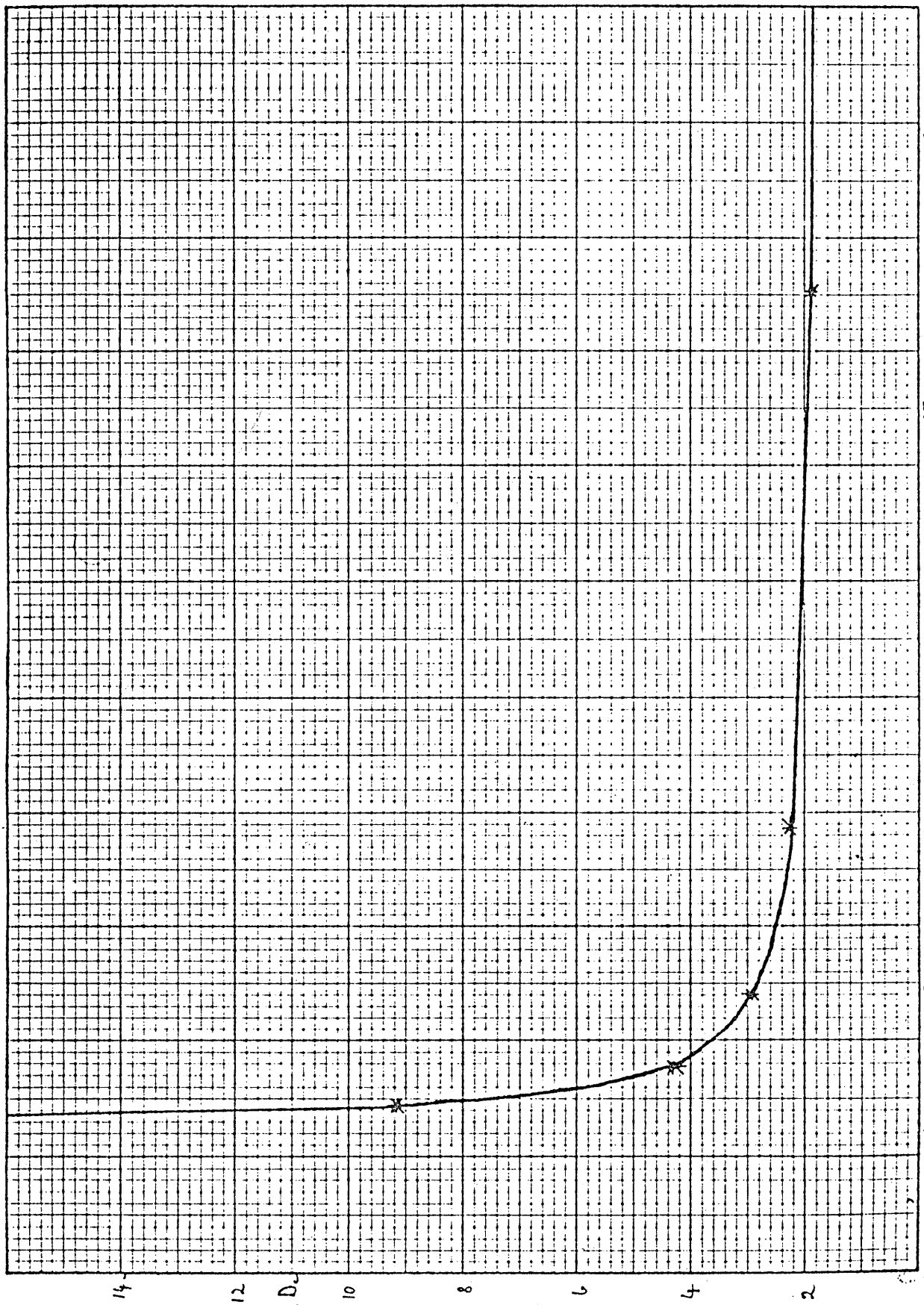

Fig (VI,i): Graph of $\mu(\ell^*)$ against ℓ^* . The quantity $\mu(\ell^*)$ is effectively constant and approximately equal to 2 in the range $50 \leq \ell^* \leq 200$.

Since D_z is always positive, D_c has the same sign as $\frac{dz}{dc_1}$ from (VI,13). Whenever ξ is such that the denominator of (VI,14) becomes zero, $\frac{dz}{dc_1}$ and D_c becomes infinite, and as ξ decreases, then quantities change sign. This is evident from the last two lines in Table (VI,ii) and also in Fig.(VI,i). From then we see that D_c is negative for $\ell^* < 26$, infinite at $\ell^* \simeq 26$, and positive for $\ell^* > 26$.

This confirms the predictions of Cahn (1961,1962) that in the early stages of the time evolution of quenched alloys, the diffusion constant is negative for the earliest times when the supersaturations is high or ℓ^* small. This phenomenon was termed spinodal decomposition, and has been observed experimentally for short times in liquid mixtures (Huang et al, 1974) and in alloys such as the B_2O_3 - PbO - Al_2O_3 system (Zarzycki and Naudin, 1969), where the spinodal mechanism gives way to Ostwald ripening or coarsening, within a few minutes after the quench. The infinite value of D_c therefore corresponds to a crossover between spinodal decomposition for higher values of ξ to coarsening for the smaller values, or equivalently from small to large values of ℓ^*.

VI.4 Comparison of ℓ^*_{DE} and ℓ^*_{sim} at the same value of simulation time t.

Since we know $\mu(\ell^*)$ as a function of c_1, or equivalently ℓ^*, we can find the simulation time t corresponding to the differential equation time t_{de} using equation (V,2). We plot a graph of $\frac{1}{6D_c}$ against t_{de} for the densities ρ = 0.05, 0.075, 0.10 in Fig. (VI,ii). The area bounded by this graph, the ordinate t_{de}, and the t_{de} axis then gives the required simulation time t corresponding to t_{de}. This graph is done by first noting the value of ℓ^*_{de} at t_{de} from the computer solution of the differential equation, ℓ^* being defined by (I,9) with $W = c_1(1-\rho)^{-3}$, where ρ is the overall density. We then find the value of $\frac{1}{6D_c}$ at $\ell^* = \ell_{de}$ from Fig.(VI,i). In Table (VI,iii) we give for these three densities t_{de}, $\ell^*_{de}(t_{de})$, the simulation time t corresponding to t_{de}, and $\ell^*_{sim}(t)$. We then plot these values of ℓ^*_{de} and ℓ^*_{sim} on the same graph against simulation time t. This is done in the figures Fig. (VI,iii), Fig. (VI,iv) and Fig. (VI,v) for the three densities ρ = 0.05, 0.075 and 0.10 respectively.

The integration (V,2) for the simulation time t was done graphically from Fig (VI,ii). For negative values of D_c we took $1/6D_c$ to be zero because D_c is very large when it is negative. Also D_c is negative only for a very short time initially.

Table (VI,iii): Comparison of ℓ^*_{DE} and ℓ^*_{sim} corresponding to the same simulation time t.

ρ	t_{DE}	$\ell^*_{DE}(t_{DE})$	t	$\ell^*_{sim}(t)$
0.05	3150	39	560	43
	6300	47	1440	47
	9500	57	2520	52
	12600	73	3800	68
	15800	104	5200	100
	18900	153	6740	156
0.075	3400	37	290	30
	6800	59	1340	55
	10200	99	2800	98
	13600	144	4430	164
	17100	185	6180	204
0.10	3700	38	315	35
	7400	72	1565	75
	11100	112	3195	124
	14800	146	4985	175
	18500	180	6885	230
	20300	198	7876	235

Figs.(VI,iii), (VI,iv), (VI,v): Graph of ℓ^* and ℓ^*_{de} against simultation time t for densities ρ = 0.05, 0.075, 0.10 respectively.

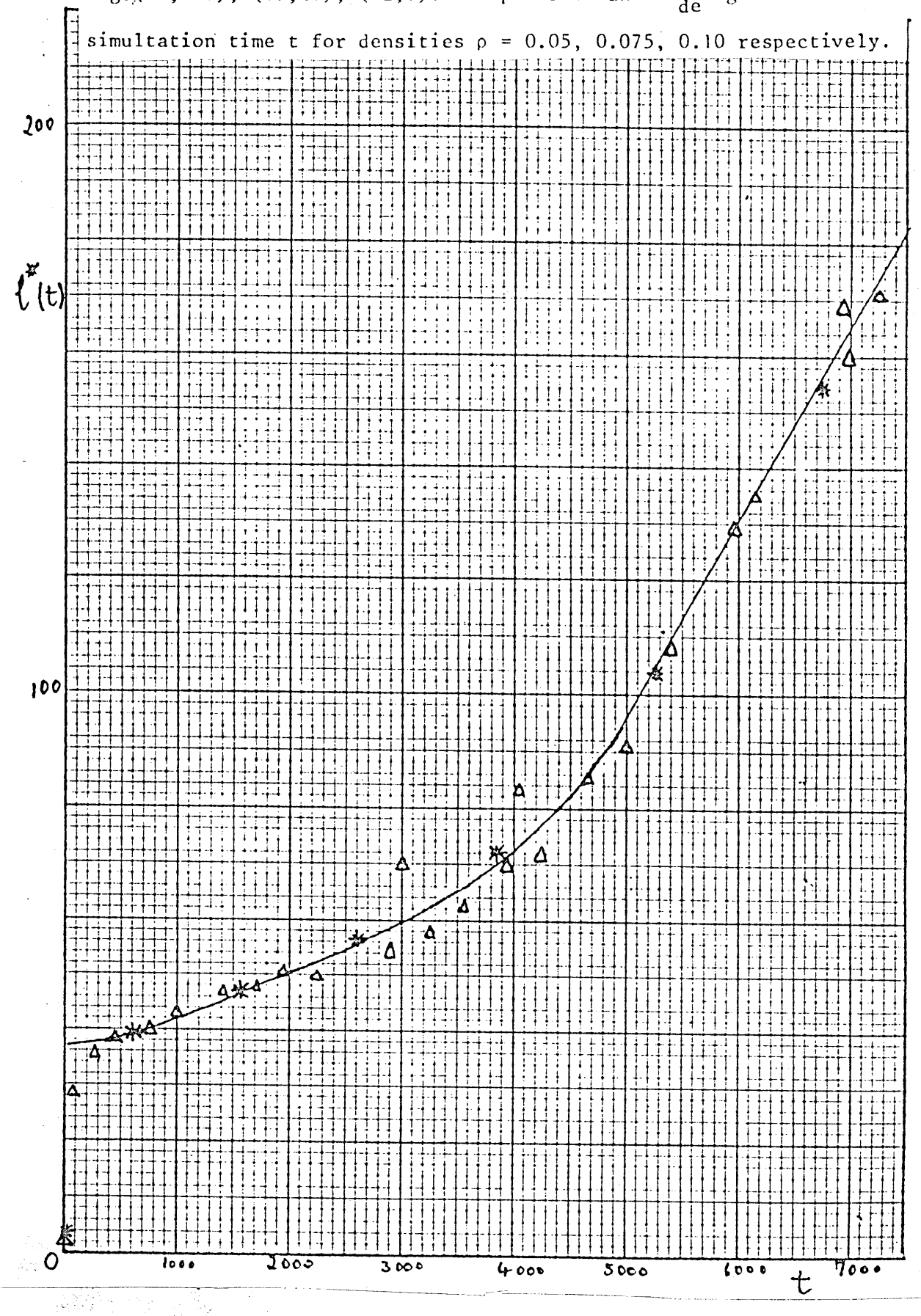

Fig(VI,iii): Graph of ℓ^* and ℓ^*_{de} against simulation time t for density ρ = 0.05. $\Delta = \ell^*$; $* = \ell^*_{de}$.

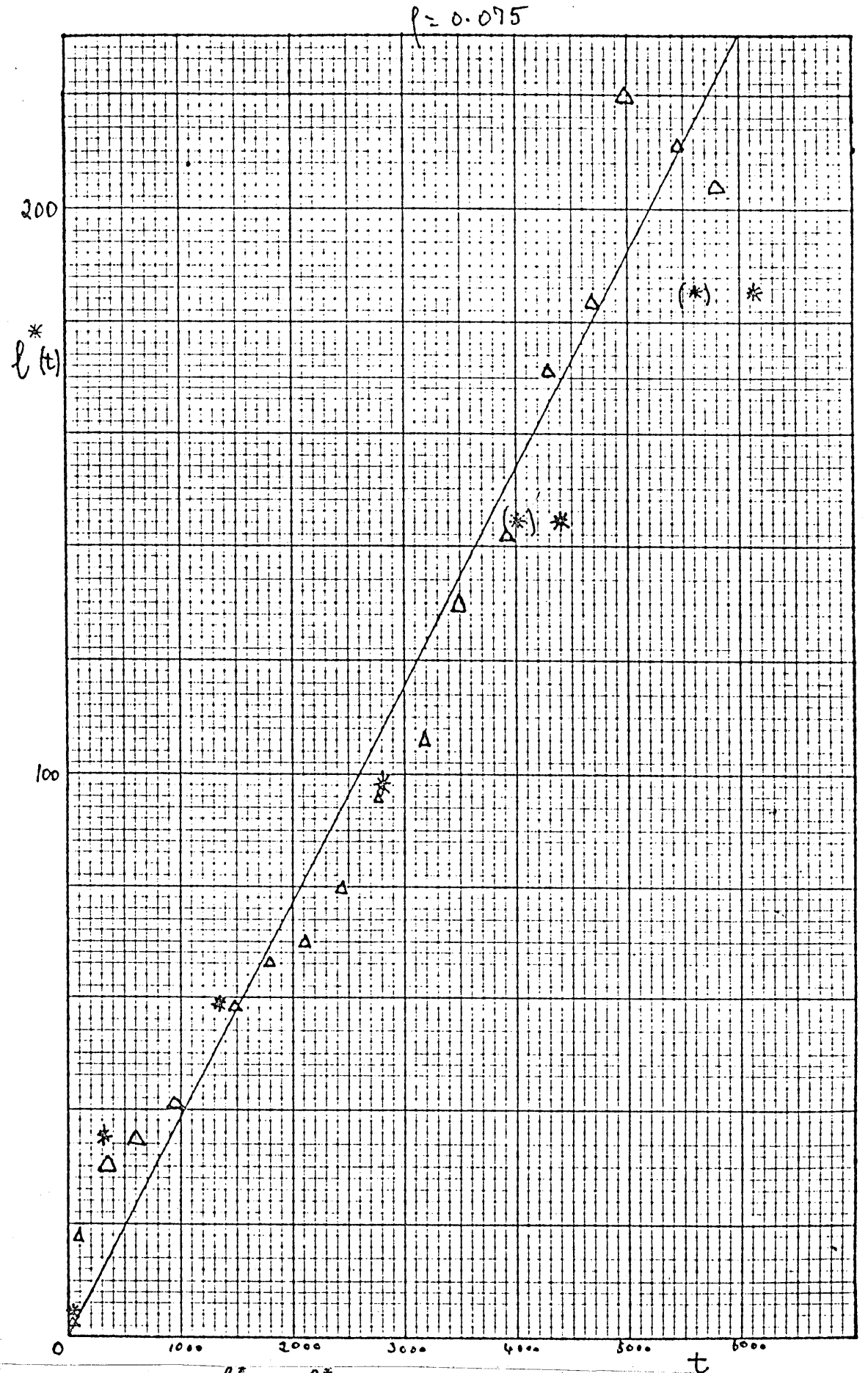

Fig (VI,iv): Graph of ℓ^* and ℓ^*_{de} against simulation time t for density ρ =0.075.
$\Delta = \ell^*$; $* = \ell^*_{de}$.

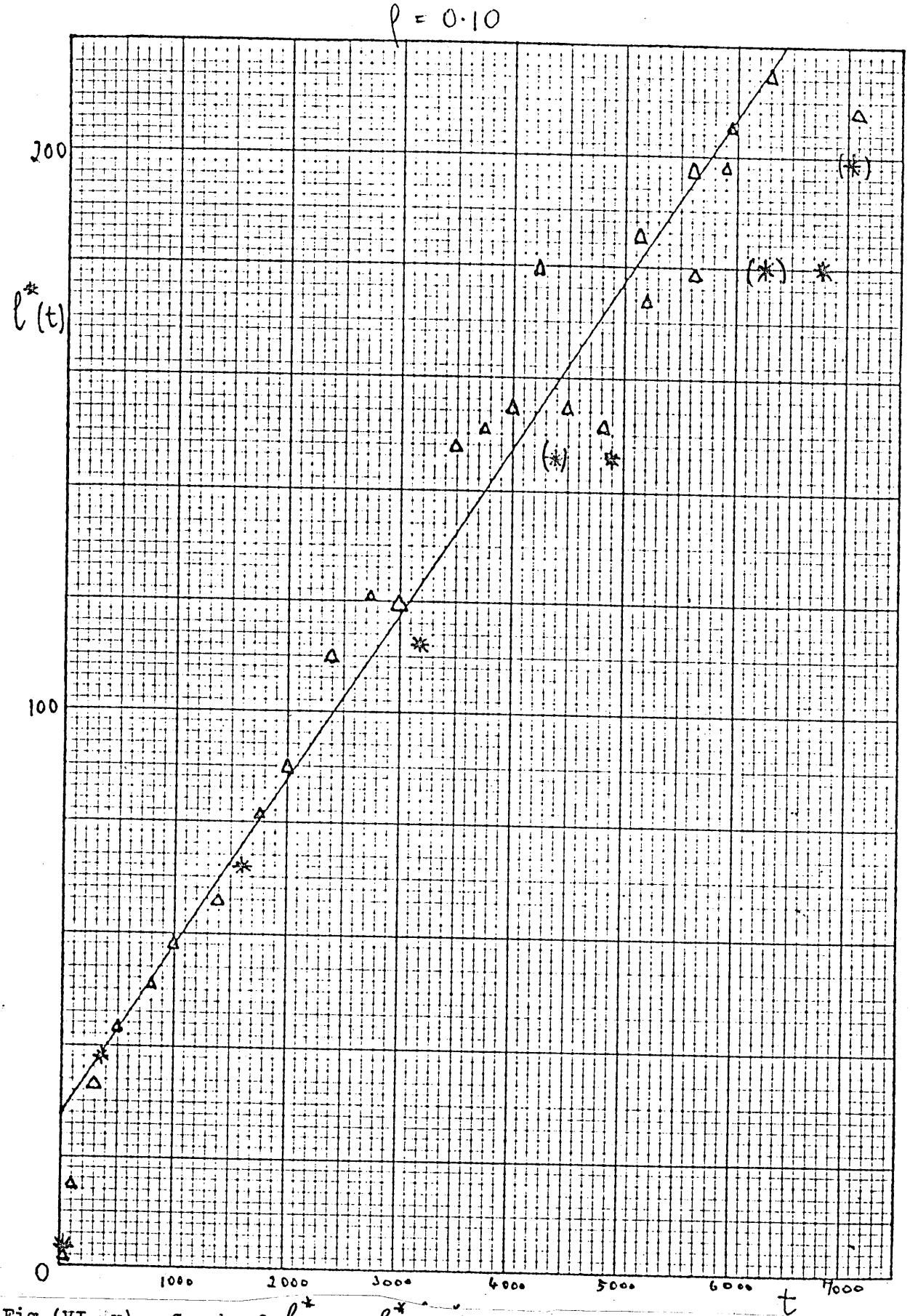

Fig (VI, v): Graph of l^* and l^*_{de} against simulation time t for density ρ =0.1
$\Delta = l^*$; $* = l^*_{de}$.

It can be seen for all the densities, that ℓ^*_{de} and ℓ^*_{sim} increases very quickly from 2 to about 30 over the simulation time range $0 \leq t \leq 300$. Then ℓ^* increases more slowly after that, and reaches 200 at about $t = 6000$.

This very large increase in ℓ^* initially seems to be related to the fact that the diffusion constant D_c is infinite at about $\ell^* = 30$, and then changes sign and becomes positive for large values of ℓ^*. We therefore have spinodal decomposition over the range $0 \leq t \leq 300$ for all the three densities and after that there is a crossover to the slower coarsening mechanism with positive D_c.

For $\rho = 0.05$, $\ell^*_{de}(t)$ and $\ell^*_{sim}(t)$ agree very well with each other over the whole time range considered $0 \leq t \leq 7000$, as can be seen from Table (VI,iii) and Fig.(VI,iii). It can be seen that both $\ell^*_{de}(t)$ and ℓ^*_{sim} grow slowly at first over the range $300 \leq t \leq 4000$. After that ℓ^* is approximately linear in t for $t \geq 4000$. In fact for this range we can write:

$$\ell^*(t) = -81 + 0.35t \qquad t \geq 4000, \quad \rho = 0.05 \qquad \text{(VI,24)}$$

For the two higher densities, however ℓ^*_{sim} and ℓ^*_{de} agree very well together for $0 \leq t \leq 5000$, and are both approximately linear over the whole time range considered $0 \leq t \leq 7000$. In fact we can write to an accuracy of 5%, the linear relations

$$\left.\begin{aligned} \ell^*_{sim}(t) &\simeq 0.038t \\ \ell^*_{de}(t) &\simeq 20 + 0.028t \end{aligned}\right\} \quad \text{for } \rho = 0.075 \qquad \text{(VI,25)}$$

and similarly

$$\left.\begin{aligned} \ell^*_{sim}(t) &\simeq 0.031t \\ \ell^*_{de}(t) &\simeq 34 + 0.024t \end{aligned}\right\} \quad \text{for } \rho = 0.10 \qquad \text{(VI,26)}$$

In the theory of coarsening, it has been assumed (Lifshitz and Slyozov, 1961) that $\ell^*(t_{de})$ should be linear in t_{de} asymptotically. Since t is related to t_{de} via $\mu(\ell^*)$ in (V,2) and since $\mu(\ell^*)$ is approximately constant from Fig. (V,i) and Fig. (VI,i) over most of the considered time range we expect $\ell^*(t)$ to be linear in t also for large t. The three equations (VI,24), (VI,25), (VI,26) therefore show that the Lifshitz Slyozov assumption is valid also at early times.

A possible reason for the observed discrepancy in ℓ^* is that, for fixed c_1, c_ℓ for the Bethe lattice is of the order $(1-p)^\ell$ smaller than c_ℓ for the simple cubic lattice, as we pointed out towards the end of Section VI.3. To take this into account, we can then use p_{20} instead of c_1 for calculating ℓ^*_{de} and ℓ^*_{sim}. We can then consider $6D_c$ as a function of p_{20}. Doing this leads to improved values of ℓ^*_{de} for the larger times for p =0.075 and 0.10. These values are shown in brackets in Fig. (VI,iv) and Fig. (VI,v).

One must recall that the effect of coagulation of large clusters increases the higher the density. It has been estimated (Penrose et al, 1978) that coagulation between large clusters increases the number of particles in the large clusters by about one quarter times the number of particles per site in the large clusters. This phenomenon becomes more important for higher densities (Lebowitz et al, 1976).

To obtain an average value of $\mu(\ell^*)$ as predicted by this theory, we plot t against t_{de} as given in Table (VI,iii)。 This graph is given in Fig。 (VI,vi)。 From this we see that this curve is approximately linear, and hence $\mu(\ell^*)$ is approximately constant. In fact we can write this formula analogous to (V,3).

$$t_{de} = \mu(\ell^*)(t+t_0) \qquad \text{(VI,27)}$$

$\mu(\ell^*) \simeq 2.5$ and $t_0 \simeq 1400$ for $\rho = 0.05, 0.075, 0.10$

As in (V,3), $\mu(\ell^*)$ is again approximately constant over $0 \leq t \leq 7000$. The slope is smaller, and the intercept bigger in this case than in (V,3)。 The intercept t_0 arises because of the presence of spinodal decomposition since ℓ^* increases very rapidly in this regime。

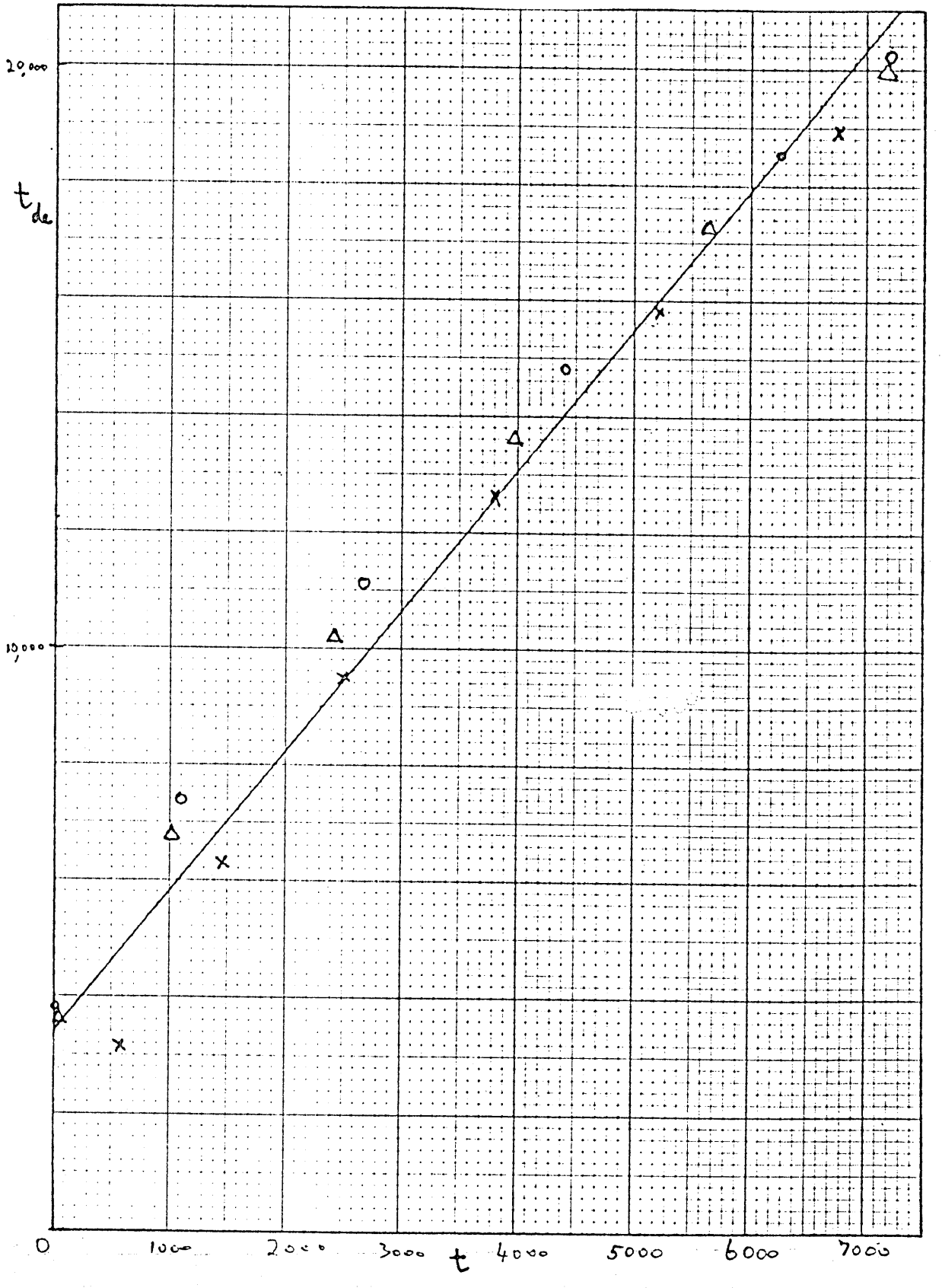

Fig (VI,vi): Graph of t_{de} against t as predicted by the theory in this chapter for densities ρ = 0.05, 0.075, 0.10. The lines are approximately straight and their slopes are equal to $\mu(\ell^*)$. Compare this graph with that in Fig (V,i).

The main conclusions we draw from this chapter therefore are that $\ell^*_{de}(t)$ and $\ell^*_{sim}(t)$ are quite close to one another for $0 \leq t \leq 7000$, for the densities $\rho = 0.05, 0.075, 0.10$.

Also the quantity $\mu(\ell^*)$ can be approximately assumed to be constant over this time range, except perhaps for the very earliest times, in the regime of spinodal decomposition. Also $\ell^*_{de}(t)$ and $\ell^*_{sim}(t)$ are both approximately linear in t for $\rho = 0.075$ and 0.10 for the whole time range considered, and also for $\rho = 0.05$ for $t \geq 4000$. This implies that the Lifshitz-Slyozov coarsening mechanism starts early, soon after spinodal decomposition has taken place.

Chapter VII Comparison of the Becker-Döring Equations with the Lifshitz-Slyozov Theory and with Real Alloys.

The purpose of this chapter is to compare the predictions of our differential equations with those of the theory of Lifshitz and Slyozov (1961) and with the cluster distribution observed in real alloys such as NiAl (Ardell and Nicholson, 1966).

VII.1 Reduction of the Becker-Döring equations to (I,12)

It has been shown (Penrose et al, 1978) that the Becker-Döring equations as described in Chapter II, can be reduced to an equation similar to (I,12) which describes the rate of growth of droplets of size ℓ with time. For large ℓ and t, we can assume that the scale of variation of c_ℓ is ℓ^*, so that $1 - \frac{c_{\ell-1}}{c_\ell}$ has the order of magnitude $1/\ell^*$. If we assume ℓ^* itself is large, we can approximate the Becker-Döring equations by the partial differential equation (op. cit.)

$$\frac{\partial c(\ell,t)}{\partial t} = -A \frac{\partial}{\partial \ell}\left[\left(\frac{\ell}{\ell^*}\right)^{1/3} - 1\right] c(\ell,t) \qquad \text{(VII,1)}$$

where A is the coefficient of $\left(\frac{\ell}{\ell^*}\right)^{1/3}$ in the quantity $a_\ell c_\ell c_1$ as calculated from (II,7) and the asymptotic formula (III,24) and (III,25) for $a_\ell(0)$ to find a_ℓ, and write c_1 in terms of ℓ^* using $W = c_1/(1-\rho)^3$ in (I,9). Then A is given explicitly as

$$A = \mu(\ell^*)\left(\frac{p_0}{3} N^{1/3}\right) W_s (1-\rho)^3 \qquad \text{(VII,2)}$$

with N given by (III,24).

Since $\mu(\ell^*)$ was shown to be approximately constant over most of the time range in both simulation and differential equations in Fig. (V,1) and Fig. (VI,vi) we can consider A to be constant.

In (VII,1) we assume that $c(\ell,t)$ is a smooth function of continuous variables, chosen that $c(\ell,t) = c_\ell(t)$ when ℓ is an integer.

Equation (VII,i) is valid only when ℓ and ℓ^* are both large. For small ℓ, however, we know that the small clusters obey the steady state distribution (I,6). We can therefore introduce a size L so that clusters larger than this size are considered to be large and to obey (VII,1), whereas clusters smaller than this size are considered small and obey (I,6). The conservation of mass condition can then can be written as

$$\rho_L(W) + \int_L^\infty \ell c(\ell,t)d\ell = \rho = \text{constant} \qquad \text{(VII,3)}$$

where $\rho_L(W)$ was defined in (I,8). The value of L therefore should satisfy the inequalities $1 << L << \ell^*$. The latter inequality follows because the steady state formula (I,6) does not apply to clusters larger than ℓ^*. Then $\rho_L(W)$ signifies the number of particles in the small clusters at supersaturation W, which can be expressed in terms of ℓ^* from (I,9). In the integral in (VI,3), $c(\ell,t)$ is given by (VII,1). The quantity ℓ^* therefore controls both $\rho_L(W)$ and the integral in (VII,3). Lifshitz and Slyozov treat ℓ as a continuous variable from the beginning and do not distinguish between W and the density of the vapour, $\rho_L(W)$. Instead of (VII,3), therefore, they take the simpler equation

$$W + \int_0^\infty \ell c(\ell,t)d\ell = \rho$$

The quantity ℓ^* was found in Chapters V and VI to be linear in both the simulation and the differential equations, so that we can write in general

$$\ell^* = K(t+t_1) \qquad \text{(VII,4)}$$

where K and t_1 are constants independent of time. Since ℓ^* is such an important quantity in this theory, we change variables from t to ℓ^* in (VII,1) as was done in Penrose (1978). Using

(VII,4), (VII,1) can be solved by the method of characteristics after this further substitution

$$g(\ell,\ell^*) = \int_{\ell}^{\infty} c(\lambda,\ell^*)d\lambda \qquad \text{(VII,5)}$$

The function $g(\ell,\ell^*)$ stands for the total number of clusters per lattice site larger than ℓ at a certain value of ℓ^*. The new equation can then be written

$$\frac{\partial g}{\partial \ell^*} + \frac{A}{K}\frac{\partial}{\partial \ell}\left[\left(\frac{\ell}{\ell^*}\right)^{1/3} - 1\right] g(\ell,\ell^*) = 0 \qquad \text{(VII,6)}$$

The characteristics of (VII,6) are the solutions of

$$\frac{d\ell}{d\ell^*} = \frac{A}{K}\left[\left(\frac{\ell}{\ell^*}\right)^{1/3} - 1\right] \qquad \text{(VII,7)}$$

This formula is identical to (I,12) with $\bar{\ell} \equiv \ell^*$ and $A \equiv 4\pi D\alpha$. From (VII,7), treating ℓ^* as linearly increasing in t, clusters of size greater than ℓ^* tend to grow, whereas clusters smaller than ℓ^* tend to shrink. The solution f of (VII,7), denoting the natural log by ln, is

$$f = \ell n(\ell^*) + \phi\left(\frac{\ell}{\ell^*}\right) = \text{constant} \qquad \text{(VII,8)}$$

where

$$\phi(x) = \int_0^x \frac{dy}{y + \frac{A}{K}(1-y^{1/3})} \qquad \text{(VII,9)}$$

The general solution of (VII,6) is therefore

$$g(\ell,\ell^*) = \Psi\left(\ell n(\ell^*) + \phi\left(\frac{\ell}{\ell^*}\right)\right) \qquad \text{(VII,10)}$$

where Ψ is an arbitrary function.

VII.2 Comparison of A, K, A/K for simulation and differential equations

We can check the validity of (VII,18) by plotting $g(\ell,\ell^*)$ against the argument $f = \ell n(\ell^*) + \phi(\frac{\ell}{\ell^*})$. We do this in Fig. (VII,i) for $\rho = 0.075$ for $200 > \ell^* > 50$. If (VII,18) is correct, plots of $g(\ell,\ell^*)$ against this argument for various values of ℓ^*, on time t, will all lie on one curve. This is indeed the case when one takes A/K to be 4.00 the value obtained in the 'table' method described in Penrose et al (1978). In Fig. (VII,i) we give these plots for our differential equations, and also for the simulation for various values of ℓ^*. On the same axis, we also plot Ψ from Table VII in the same paper. We must bear in mind, however, that the function ϕ is not defined the same as ours and in fact it can be shown that our argument $\ell n(\ell^*) + \phi(\frac{\ell}{\ell^*})$ is equal to the argument in this cited paper, $\ell n(t) + \phi(\frac{\ell}{t})$, diminished by 3.33. As is to be expected, this curve is an average of the coordinates for the simulation. The differential equation curve is always very near this curve, the error being at worst 15%.

We now compare the quantities A, K, and A/K with the same quantities obtained from the simulation. Taking a mean value of $\mu(\ell^*)$ to be about 2.5 from (VI,27) in the expression (VII,2) for A, and using the value K = 0.028 given in (VI,25) for the differential equations for density $\rho = 0.075$, will give

$$A = 0.11, \quad K = 0.028, \quad A/K = 3.94 \qquad \text{(VII,11)}$$

as compared with the simulation values (op cit)

$$A = 0.15, \quad K = 0.038, \quad A/K = 3.97 \qquad \text{(VII,12)}$$

Therefore A and K are underestimated by 25% by the differential equations. This is because when ℓ^* is linear in t, A and K are

Fig(VII,i): Graph of $g(\ell,\ell^*)$ against the argument $f = \ell n(\ell^*) + \phi(\frac{\ell}{\ell^*})$ for differential equations and simulation for various values of ℓ^*. The constant A/K is taken to be be 4.0. This is a 'universal' curve independent of the value of ℓ^*. Density $\rho = 0.075$.

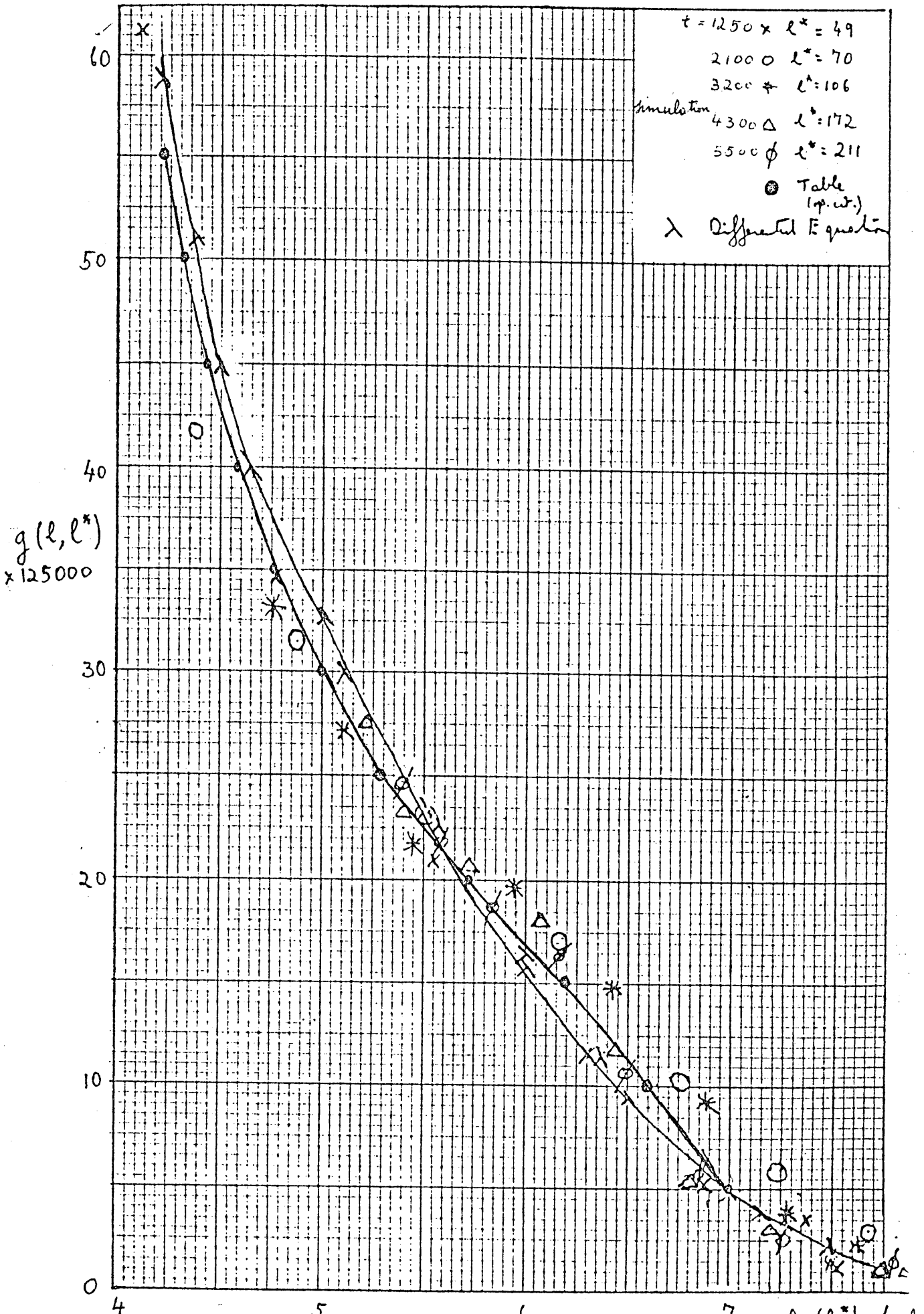

Fig. (VII, i) Graph of $g(\ell, \ell^*)$ against $\ln(\ell^*) + \phi(\frac{\ell}{\ell^*})$ for differential equation and simulation for various values of ℓ^*. The constant A/K is taken to be 4·0.

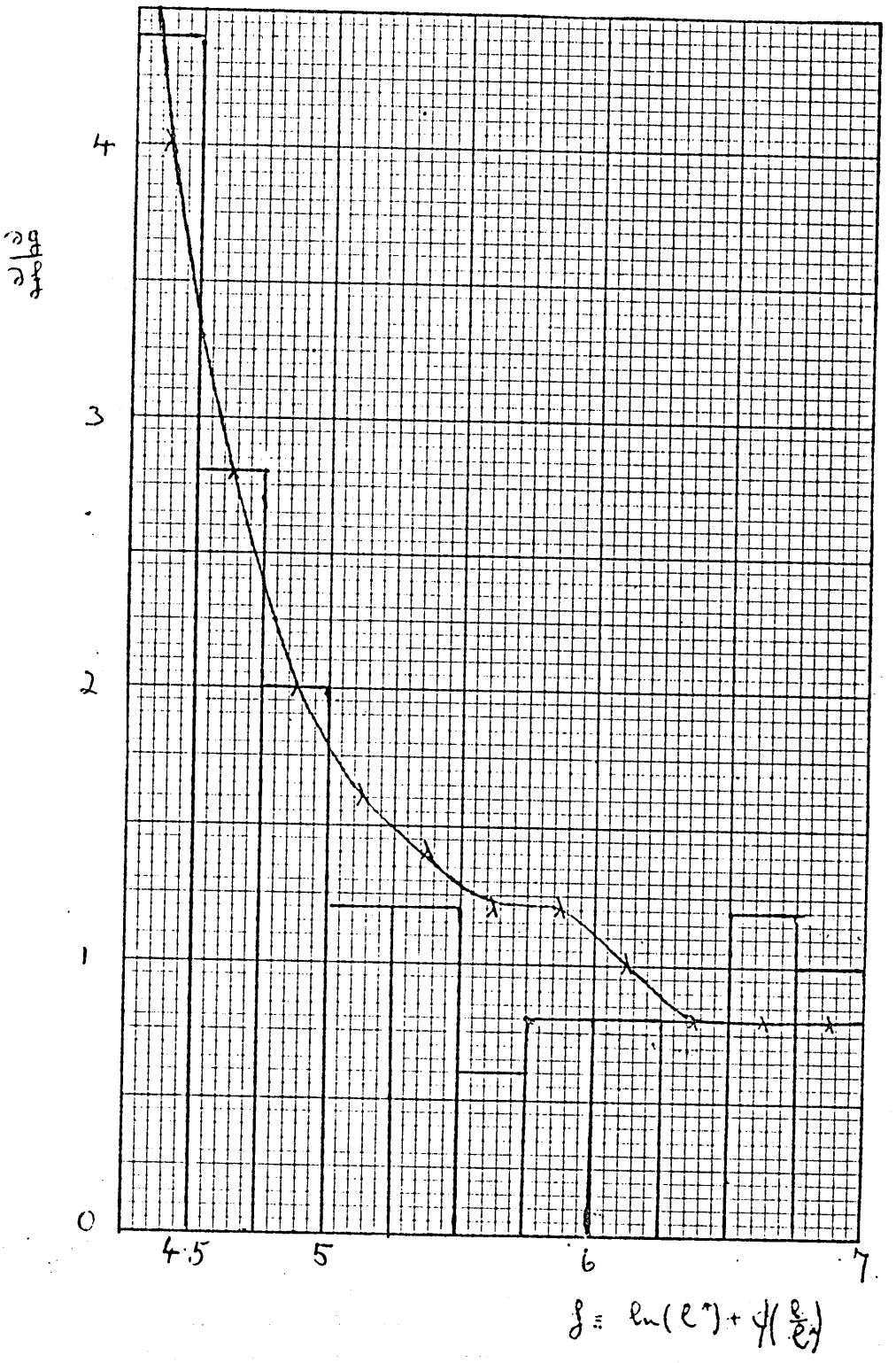

Fig(VII,ii): Graph of the slope of the previous figure against f, for simulation and differential equations. For a given value of A/K, the concentration C_ℓ are proportional to the ordinates in this figure. Density $\rho = 0.075$.

both proportional to $\mu(\ell^*)$ which is underestimated by the same amount as can be seen from (VII,27) and (V,3). However A/K, which is independent of $\mu(\ell^*)$, and is a dimensionless constant, is very well predicted by the differential equations, as evidenced by Fig. (VII,i). As we shall see, A/K characterizes the shape of the cluster size distribution.

It can be seen from Fig. (VII,i) that there are certain consistent differences between the simulation curve and the differential equation curve. The simulation curve has a point of inflexion at $f = \ell n(\ell^*) + \phi(\frac{\ell}{\ell^*}) \simeq 5.8$ and the two curves intersect at this point approximately. The slopes are appreciably different at this point of inflexion. The slope of these curves are important because the concentrations c_ℓ at a certain value of ℓ^* can be obtained from differentiating (VII,5):

$$C(\ell,\ell^*) = -\frac{\partial}{\partial \ell} g(\ell,\ell^*) = -\frac{\partial g}{\partial f}\frac{\partial f}{\partial \ell}$$

$$= \frac{\partial g}{\partial f} \frac{1}{\ell + \frac{A}{K}\ell^* - \frac{A}{K}\ell^{*2/3}\ell^{1/3}} \qquad \text{(VII,13)}$$

Equation (VII,13) implies that since $\frac{A}{K}$ is the same in both simulation and differential equations $c_\ell \equiv C(\ell,\ell^*)$ is proportional to $\frac{\partial g}{\partial f}$, which is the slope of the curves in Fig. (VII,i). We therefore find the slopes of this simulation and the differential equation curves in Fig. (VII,1) and plot them against $f = \ell n(\ell^*) + \phi(\frac{\ell}{\ell^*})$ in Fig. (VII,ii). This graph gives us a summary of how well the differential equations predict c_ℓ for the simulation, when the value of ℓ^* is the same in both. It can be seen from Fig. (VII,ii) that the agreement is reasonably good, apart from the significant minimum in the simulation curve, which we plot as a histogram. This minimum features also in

the simulation histograms for $\rho = 0.075$ in the relevant diagrams in Fig. (V, ii).

The function Ψ in (VII,10) can be found explicitly as a function of the argument $f \equiv \ell n(\ell^*) + \phi(\frac{\ell}{\ell^*})$. This is done in a way similar to that employed in Penrose et al (1978) but using ℓ^* instead of t. Essentially this implies treating $\rho-\rho_L(W)$ in (VII,3) as a function of ℓ^* using the steady state distribution of small clusters (I,6) and equation (I,8) which gives W in terms of ℓ^*. Thus $\rho-\rho_L(W)$ can be accurately approximated by a polynomial in $\frac{1}{\ell^{*1/3}}$. For $\rho = 0.075$ this polynomial is analogous to equation (41) in this cited work and is given by

$$\left[\rho-\rho_{20}(W)\right] = 0.06316 - \frac{0.02859}{\ell^{*1/3}} - \frac{0.18686}{\ell^{*2/3}} \qquad \text{(VII,14)}$$

The integral in the conservation of mass condition (VII,3) can be integrated by parts using the fact that $c_\ell = -\frac{\partial g_\ell}{\partial \ell}$. In fact it can be shown that to an accuracy of $\frac{1}{\ell^*}$, we can write (Penrose et al, 1978) (VII,3) as

$$\rho-\rho_L(W) = \int_0^\infty \Psi(\ell n(\ell^*) + \phi(\tfrac{\ell}{\ell^*}))d\ell \qquad \text{(VII,15)}$$

Since $\rho-\rho_L(W)$ approaches the constant $\rho-\rho_L(W_s)$ for large time, it can be argued that the integral on the right is approximately independent of t, and hence that $\Psi(f)$ is approximately proportional to e^{-f}. For the times considered, however, ρ_{20} is still varying appreciably and so one assumes that $\Psi(f)$ is given approximately by (Penrose et al, 1978)

$$\Psi(f) = C_0 e^{-f} - C_1 e^{-4f/3} - C_2 e^{-5f/3} \qquad \text{(VII,16)}$$

Substituting (VII,14) in the left hand side of (VII,15), and (VII,16) in the right hand side one can obtain the constants

C_0, C_1 and C_2 as

$$C_0 = \frac{.06316}{\int_0^\infty e^{-\phi(x)}dx}$$

$$C_1 = \frac{.02859}{\int_0^\infty e^{-4/3\phi(x)}dx} \qquad \text{(VII,17)}$$

$$C_2 = \frac{.18686}{\int_0^\infty e^{-5/3\phi(x)}dx}$$

We integrated $e^{-\phi(x)}$ by Simpson's rule using (VII,9) with $A/K = 4$. The range from 0 to ∞ in (VII,17) was replaced by the range $0 \leq x = \frac{\ell}{\ell^*} < 5$, because there were no clusters of size $\ell > 5\ell^*$. We then obtain for $\Psi(f)$ the formula

$$g(\ell,\ell^*) = \Psi(f) = 0.05134\,e^{-f} - 0.02947\,e^{-4f/3} - 0.2307\,e^{-5f/3} \qquad \text{(VII,18)}$$

This holds approximately for both simulation and differential equations because $\frac{A}{K}$ is the same in both. In Table (VII,i), we compare the prediction of (VII,22) with the simulation values for g given in Table VII (op. cit), remembering that x as defined in this table is equal to f + 3.33. The agreement is better than 15% over most of the range of x or f.

Table (VII,i): Comparison of (VII,18) with simulation values of g obtained from Table VII from Penrose et al (1978)

x	$12500\ \Psi_{sim}$ from Table VII (op.cit)	$f = x-3.33$	$125000\ \Psi(z)$ from (VII,18)
7.54	55	4.21	56
7.65	50	4.32	52.2
7.76	45	4.43	48.5
7.91	40	4.58	43.6
8.09	35	4.76	38.2
8.32	30	4.99	31.9
8.61	25	5.28	25.1
9.04	20	5.71	17.3
9.51	15	6.18	11.4
9.92	10	6.59	7.8
10.31	5	6.98	5.38

VII.3 Comparison of the cluster size distribution predicted by our equations with that of real alloys.

In this section, we compare the predictions of the Becker-Döring equations and of the Lifshitz-Slyozov theory with the cluster distribution in real alloys. (Ardell and Nicholson 1966, Pedder 1978).

It was found in the previous section that the dimensionless constant A/K is very well predicted by the differential equations and that its value is about 4.0. This differs from the value predicted by Lifshitz and Slyozov. They predict that the denominator in (VII,9) must have a double zero which implies that A/K is 6.75. This is appreciably greater than the value of A/K predicted by the differential equations and observed in the simulation.

The time independent cluster size distribution for several Ni-Aℓ alloys was extensively studied by Ardell and Nicholson (1966). The abscissa in their histograms is taken to be $(\frac{\ell}{\ell^*})^{1/3}$ and the area under the curve is proportional to the total number of clusters. In Fig.(VII,iii), therefore, we plot $\ell^{*1/3}\ \ell^{2/3}\ c_\ell$ against $(\frac{\ell}{\ell^*})^{1/3}$ for the differential equations at density $\rho = 0.075$ for various values of ℓ^*. The area under such a graph also gives the total number of clusters. Since we are now more interested in the shape of the distribution rather than the actual concentrations c_ℓ, we adjust the scales so that all ordinates at $\ell = \ell^*$ in Fig.(VII,iii) are equal to 1. On the same graph we also plot histograms of several Ni-Aℓ alloys (Ardell and Nicholson, 1966). We also plot the Lifshitz-Slyozov distribution with A/K = 6.75. This has an explicit

Fig(VII,iii): Graph of $\ell^{*1/3}\ell^{2/3}c_\ell$ against $(\frac{\ell}{\ell^*})^{\frac{1}{3}}$ for our differential equations and for Ni Al alloys(Ardell and Nicholson, 1966). The predictions of Lifshitz and Slyozov are also given. The ordinates at $\ell = \ell^*$ are all scaled down to 1.

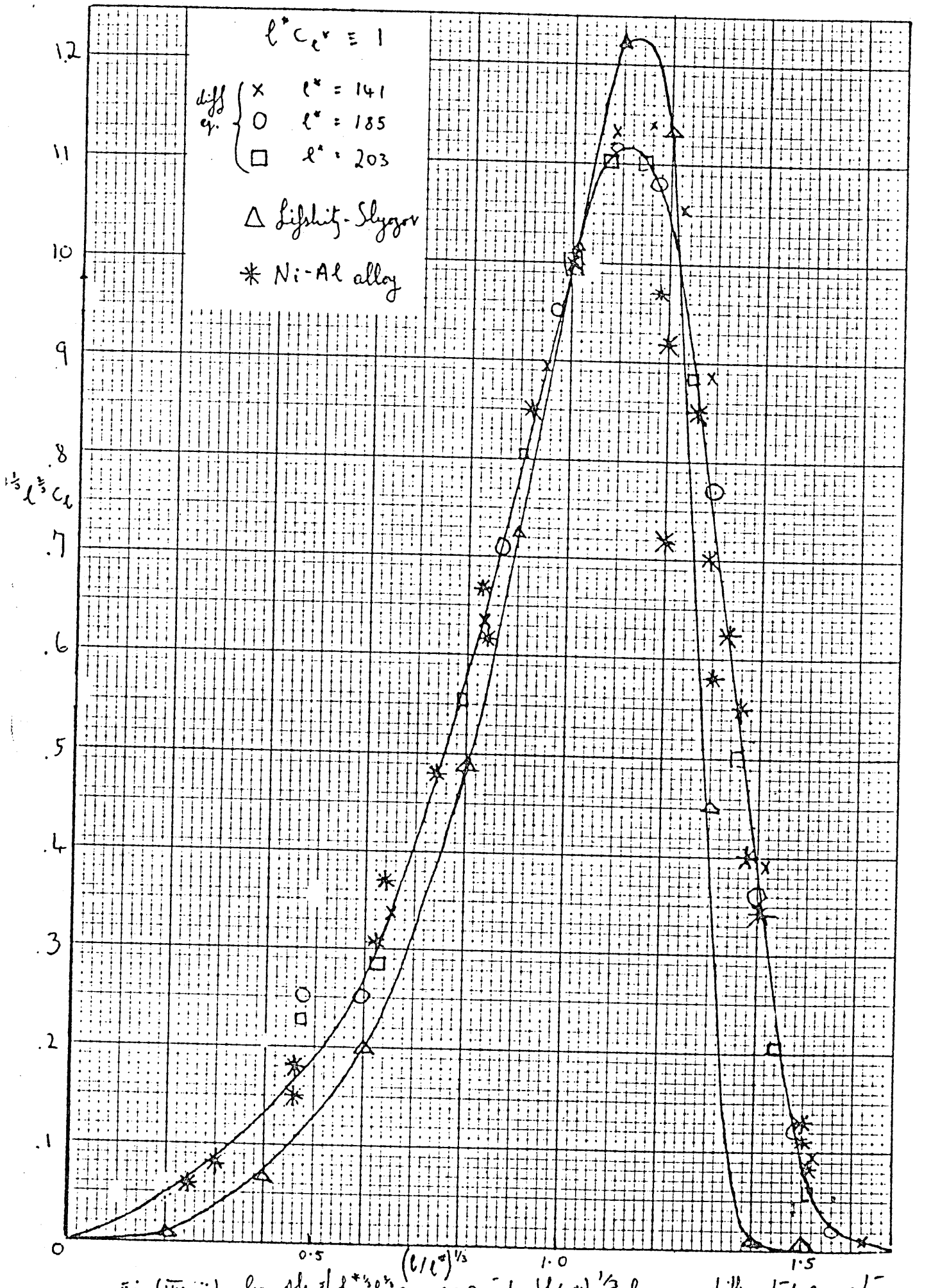

Fig (VII ;iii) Graphs of $l^{*\frac{1}{3}} l^{\frac{1}{3}} c_l$ against $(l/l^*)^{1/3}$ for our differential equation and for Ni-Al alloy. The predictions of Lifshitz + Slyozov are also quoted. All ordinate N $l = l^*$ are taken equal to 1.

formula (Wagner, 1961, and Ardell, 1969). If $r = (\frac{\ell}{\ell^*})^{1/3}$, then the Lifshitz-Slyozov distribution d(r) is given explicitly by

$$d(r) \alpha r^2 (\frac{3}{3+r})^{7/3} (\frac{\frac{3}{2}}{\frac{3}{2}-r})^{11/3} \exp(\frac{-r}{\frac{3}{2}-r}) \text{ for } r \leq \frac{3}{2}$$

$$0 \qquad \text{for } r \geq \frac{3}{2} \qquad \text{(VII,19)}$$

We also require d(r) to be equal to 1 for $\ell = \ell^*$, for the purpose of direct comparison with the other curves.

The normalized distributions of the alloy and our differential equations are broader and have a lower peak than the Lifshitz Slyozov distribution which goes to zero at $(\frac{\ell}{\ell^*})^{1/3} = 1.5$ and is already very small at $(\frac{\ell}{\ell^*})^{1/3} = 1.4$. On the other hand the differential equations and the alloy go to zero at about 1.7. Our distribution also seems to be quite accurate for $\ell < \ell^*$. Fig.(VII,iii) shows that the smaller A/K is, the broader the distribution is.

Ardell and Nicholson (1966) also predict that the quantity $\frac{d\ell^*}{dt}$ should be independent of the density ρ at fixed temperatures. Indeed this is shown to be approximately true for the differential equation for densities $\rho = 0.075$ and 0.10 and for the simulation at the same densities. See Fig.(VII,iv) and F9g.(VI,v). This phenomeon is also observed in Ni Aℓ alloys and also in the coarsening of copper in an α-Fe matrix. (Speich and Oriani, 1965). However, the rate of coarsening is heavily dependent on temperature. In practice, the diffusion

constant D or $\frac{p_0}{3}$ is heavily dependent on temperature. In fact D satisfies Arrhenius law, that is $\ln(D)$ is proportional to $\frac{1}{T}$ in many systems including Cd-Ag (Pedder, 1979), Mn-Mg (Smith, 1967) and Si-Ni alloys (Ardell, 1969 and Rastogi, unpublished quoted in Ardell).

References

Abraham F.F. (1969) J.Chem. Phys. 51, 1632.

Abraham F.F. (1974) "Homogeneous Nucleation Theory" in the Series Advances in Theoretical Chemistry (Academic Press, New York, and London).

Ardell A.J. (1969) "The Mechanics of Phase Transitions in Crystalline Solids" Institute of Metals Monograph Series vol.33. London Page 111.

Ardell A.J. and Nicholson R.B. (1966) J. Phys. Chem. Solids 27, 1793.

Bauer S. H., Wilcox C.F. and Russo S. (1978) J. Phys. Chem. 82, 59.

Becker R. and Döring W. (1935) Ann. Der Phys. 24, 719-752.

Binder K. and Stauffer D. (1974) Phys. Rev. Lett. 33, 1006.

Binder K. and Stauffer D. (1976) Adv. Phys. 25, 346.

Cahn J.W. (1961) Acta Metall. 9, 795.

Cahn J.W. (1962) Acta Metall. 10, 179.

Chandrasekhar S. (1954) "Stochastic Processes in Physics and Astronomy" in "Noise and Stochastic Processes" ed. Wax (Dover Publications, New York).

Courtney W.G. (1962) J. Chem. Phys. 51, 1632.

Fisher M.E. (1967) J. Appl. Phys. 38, 981..

Fisher M. and Essam J.W. (1961) J.Math. Phys. 2, 609.

Frenkel J. (1946) "Kinetic Theory of Liquids", Dover, New York.

Glauber R. (1963) J. Math. Phys. 4, 294.

Greenwood G.W. (1969) Page 103 (See Ardell A.J., 1969)

Huang J.S. Goldburg W.I., and Bjerkaas A.W. (1974) Phys. Rev. Lett. 32, 921.

Huang J.S. and Goldburg W.I. (1976) Bull. Am. Phys. Soc., 21, no.1, 55.

Isaacson and Keller S. (1966) "Elements of Numerical Methods" Wiley, New York.

Ising E. (1925) Z. Phys. 31, 253.

Kalos M. H., Lebowitz J. L., Penrose O. and Sur A. (1978) J. Stat. Phys., 18, 39

Kawasaki K. (1966) Phys. Rev. 145, 224.

Kawasaki K. (1972) in Domb and Green "Phase Transitions and Critical Phenomena" vol.2, Academic Press, New York.

Lebowitz J.L and Kalos M. Scripta Met. 10, 9.

Lebowitz J.L. and Penrose O. (1977) J.Stat. Phys. 16, 321.

Lifshitz I.M. and Slyozov V.V. (1961) J. Phys. Chem. Solids, 19, 35.

Lothe J. and Pound G.M. (1962) J. Chem. Phys. 36, 2080.

Marro J., Bortz A. B., Kalos M. H. and Lebowitz J. L. (1975) Phys. Rev. B12,2000.

Mirold P. and Binder K. (1977) Acta Metall. 25, 1435.

Pedder D.J. (1978) Metall. T.A., 9, 659.

Penrose O., Lebowitz J.L., Marro J., Kalos M.H., and Sur A., (1978) J. Stat. Phys., 19,243

Penrose O. and Lebowitz J.L. (1979) "Towards a rigorous theory of metastability" in Studies in Statistical Mechanics VII, edited by Montroll and Lebowitz (North Holland).

Penrose O. (1978) Sections Notes in Physics, 84. L. Garrido ed. "Stochastic Processes in Nonequilibrium Systems" (Springer, Berlin)

Rastogi (1969) unpublished research, quoted in Ardell A.J. (1969)

Reiss H. (1974) "The Replacement Free Energy in Nucleation Theory" in Nucleation II, Zettlemoyer A.C. ed. (M. Dekker, New York).

Smith A.F. (1969) Acta Met, 15, 1867.

Smoluchowski M. (1916) Phys. Z. 17, 385.

Speich G.R. and Oriani R.A. (1965) Trans. AIME, 233, 623.

Sur A., Lebowitz J.L., Marro J., and Kalos M. H. (1977) Phys. Rev. B15,535.

Sykes M. (1976) Private communication to O. Penrose

Wagner C. (1961) Z. Electrochem. 65, 581.

Zarzycki and Naudin (1969) J. of Non-Cryst Solids I, 215-234.